TAMPEREEN TEKNILLINEN YLIOPISTO
TAMPERE UNIVERSITY OF TECHNOLOGY

MIKAEL RITAMÄKI

EFFECTS OF THERMAL AGING ON POLYMER THIN FILM INSULATIONS FOR CAPACITOR APPLICATIONS

Master of Science Thesis

Examiner: Research Manager Kari Lahti
Examiner and topic approved by the Council of the Faculty of Computing and Electrical Engineering on 8th October 2014

ABSTRACT

TAMPERE UNIVERSITY OF TECHNOLOGY
Master's Degree Programme in Electrical Engineering
RITAMÄKI, MIKAEL: Effects of Thermal Aging on Polymer Thin Film Insulations for Capacitor Applications
Master of Science Thesis, 117 pages, 2 Appendix pages
December 2014
Major: Power Systems and Market
Examiner: Research Manager Kari Lahti
Keywords: Polymer, aging, degradation, modeling, thermal stress, capacitor, metallized film capacitor, BOPP, nanocomposite, dielectric strength, self-healing

Modern high power density, high reliability and low loss film capacitors are based on bi-axially oriented polymer thin film insulation systems, with graceful aging properties due to the use of self-healing metallized electrodes. There is however a growing need for more compact units offering even higher energy densities, which can be reached by increasing the rated voltages or the relative permittivity of the dielectric. Recent trends to tailor these dielectric properties include approaches such as polymer nanocomposites and chain-end functionalized polymers. Since capacitor lifetimes span to over 30 years, the aging properties of new materials need to be verified to assure there is no untimely reduction in reliability. While the assessment of short-term dielectric properties is relatively straightforward, one of the main scientific challenges is that there is virtually neither knowledge nor literature about the aging behaviour of these novel dielectrics.

The main objectives of this thesis were to conduct a comprehensive literature review on polymer thin film insulation systems and to conduct a thermal aging experiment to evaluate the aging behaviour of BOPP and PP-based silica nanocomposite thin films. The literature review in which the physiochemical, morphological and electrical properties, in addition to aging and degradation mechanisms and life and reliability models are discussed is divided in Chapters 2-4. The experiment utilized a 1008-hour thermal step stress cycle with temperatures from 50°C to 110°C. A purpose-tailored oven provided an inert aging environment, and aging progression was evaluated with novel MultiBreak breakdown performance characterization measurement system, both of which are discussed in Chapter 5.

The results from the aging experiment suggest that the aging of pure PP –materials occurs locally, whereas the aging of PP-based nanosilica takes place evenly in polymer-nanoparticle interface. Interfacial aging manifests as an increased scatter in breakdown voltages, whereas local aging is characterized by a formation of a distinct defect population, which was measured starting from 50…70°C. The presence of a defect population decreased the lower 5% breakdown probabilities considerably. The defect subpopulation seemingly disappeared after 90…100°C, which indicate an unknown and different mechanism may operate at higher temperatures. Morphological changes and antioxidant conversion were suggested as possible explanations, but further research is needed to confirm the issue.

Based on the possibility of different mechanisms it is suggested that accelerated aging experiments for pure PP materials should be conducted near the rated operating temperature range, at a maximum temperature of 60…65°C, whereas nanocomposite aging may be evaluated using higher temperatures. Also, the possibility of utilizing controlled heat treatments and the role of processing parameters should be thoroughly evaluated, as they are seen as possible ways to improve the properties of PP thin films.

TIIVISTELMÄ

TAMPEREEN TEKNILLINEN YLIOPISTO
Sähkötekniikan koulutusohjelma
RITAMÄKI, MIKAEL: Lämpöikäännytyksen vaikutukset kondensaattorikäyttöön suunniteltuihin ohutkalvoeristyksiin
Diplomityö, 117 sivua, 2 liitesivua
Joulukuu 2014
Pääaine: Sähköverkot ja -markkinat
Tarkastaja: Tutkimuspäällikkö Kari Lahti
Avainsanat: polymeeri, ikääntyminen, mallintaminen, lämpörasitus, kondensaattori, metalloitu ohutkalvokondensaattori, BOPP, nanokomposiitti, läpilyöntilujuus, itseparaneminen

Ohutkalvoeristyksiä käytetään kondensaattorisovelluksissa, joissa vaaditaan luotettavuutta, korkeaa energiatiheyttä ja pieniä häviöitä. Itseparanevia metalloituja ohutkalvoeristyksiä käyttäen kondensaattorit saadaan ikääntymään hallitusti. Uudet sovelluskohteet ovat luoneet tarpeen ohutkalvokondensaattoreiden energiatiheyden parantamiselle, mihin voidaan päästä kentänvoimakkuutta tai suhteellista permittiviteettiä nostamalla. Parannusta on haettu uusien materiaalien, kuten nanokomposiittien sekä valmistusprosessin parametrien säädön avulla. Kondensaattoreilta vaaditaan usein luotettavaa yli 30 vuoden elinikää, ja uusien materiaalin ikääntymiskäytös täytyy tuntea ennenaikaisen ikääntymisen varalta. Vaikka lyhytaikaisten ominaisuuksien määrittäminen onkin verraten yksinkertaista, tiedon puute uusien eristemateriaalien ikääntymiskäytöksestä on yksi alan haasteista.

Diplomityön tavoitteena oli laatia kattava kirjallisuusselvitys polymeeriohutkalvoeristysjärjestelmistä ja kokeellisesti vertailla perinteisen BOPP-kalvon ja PP-silika nanokomposiitin ikääntymiskäytöstä lämpörasituksessa. Kappaleisiin 2–4 jakautuva kirjallisuusselvitys käsittelee polymeerien kemiallisia, fyysisiä ja sähköisiä ominaisuuksia, joiden pohjalta siirrytään tarkastelemaan kondensaattorisovelluksissa merkittäviä ikääntymismekanismeja sekä niiden vaikutusten mallintamista. Kokeellisessa osuudessa ohutkalvoja ikäännytettiin 1008 tuntia suojakaasussa ja askeleittain korotetussa 50…110 °C lämpötilassa. Ikääntymistä kartoitettiin läpilyöntikäytöksen muutoksien avulla, uutta MultiBreak-mittausmenetelmää hyödyntäen.

Puhtaassa PP-kalvossa mitattiin 50…70 °C lämpörasituksesta lähtien pääjakaumasta poikkeava defektipopulaatio, mitä kirjallisuusselvityksen pohjalta pidettiin merkkinä paikallisiin epäideaalisuuskohtiin keskittyvästä ikääntymisestä. PP-silikassa vastaavaa kehitystä ei havaittu, mikä nähtiin merkkinä erilaisesta, polymeeri-nanopartikkelien vuorovaikutusalueessa tapahtuvasta ikääntymisestä. Puhtaissa PP-kalvoissa esiintynyt heikkojen pisteiden jakauma katosi 90…100 °C jälkeen, minkä tulkittiin viittaavan erilliseen, vain korkeilla lämpötiloilla toimivaan mekanismiin. Aiheuttajaksi esitettiin rakenteellisia muutoksia tai antioksidanttien kulumista, mutta aihe vaatii lisätutkimusta.

Tutkimustulosten pohjalta esitetään, että puhtaiden PP-ohutkalvojen ikääntymiskäytöstä reaalimaailman sovelluksissa pitää tarkastella enintään 60…65 °C lämpötiloissa, kun taas nanosilika–materiaalien ikääntymistä voidaan kiihdyttää ainakin 110 °C:ssa. Lisäksi hallittu lämpökäsittely ja lämpöön liittyvien prosessointiparametrien säätö pitää nähdä mahdollisina keinoina parantaa nykyisten PP-kalvojen läpilyöntikestoisuutta.

PREFACE

This Master of Science Thesis was done for the Department of Electrical Engineering at Tampere University of Technology during the year 2014. The thesis explored the aging behavior polymer thin films.

First of all, I want to address my gratitude to Adjunct Professor and Research Manager Kari Lahti for the extremely interesting M.Sc. and B.Sc. thesis topics and for all his feedback and guidance during the writing process. The B.Sc. thesis, related to ceramic insulations, sparked my interest in dielectric materials, a topic which I was thankfully able to continue in my M.Sc. studies.

Thereafter, I want to thank M.Sc. and researcher Ilkka Rytöluoto for introducing the novel MultiBreak test method and for his indispensable help and advice during the course of this thesis. I also want to thank M.Sc. and researcher Minna Niittymäki for all the advice related to practical issues.

I also want to express my gratitude to Senior Lab.Tech Pentti Kivinen, Senior Lab.Tech. Hannu Nieminen, Lab.Tech. Pekka Nousiainen, and Lab.Tech. Mikko Kunnari for constructing the test oven and for their aid whenever technical issues arose. I also want to thank Lab.Tech. Bengt-Olof Holmström for lending the precision low-flow gas regulator.

I also want to thank all the people at the Department of Electrical Energy Engineering for providing an enjoyable working atmosphere. Finally, I want to thank everyone who thinks their contribution should be recognized in this chapter.

TABLE OF CONTENTS

TERMS AND DEFINITIONS

A	Area
AC	Alternating current
BB	Beta binomial based estimation of confidence bounds
C	Capacitance [F]
cdf	Cumulative density function
d	Distance
D	Electric displacement
DAC	Digital-to-analog converter
DAQ	Data acquisition system
DC	Direct current
DF	Dissipation factor
DFT	Density functional theory
DUT	Device under test
E	Electric field
E	Energy
EMI	Electromagnetic interference
ESL	Equivalent series inductance
ESR	Equivalent series resistance
f	Frequency [Hz]
FM	Fisher information matrix based estimation of confidence bounds
FTIR	Fourier transform infrared spectroscopy
HPLC	High performance liquid chromatigraphy
HV	High voltage, >1000V_{RMS} AC, >1500V DC
HVPS	High voltage power supply
i	Current (as a function of time) [A]
L	Inductance [H]
l	Length
Line frequency	50Hz (Europe) / 60Hz (US)
LV	Low voltage
LV	Low voltage, 50-1000V_{RMS} AC, 120-1500V DC
MD	Molecular dynamics
MLE	Maximum likelihood estimation
MV	Medium Voltage
NANOPOWER	Novel Polymer Nanocomposites for Power Capacitors
P	Active power [W]
P	Polarization
PD	Partial discharge
PET	Polyethylene terephthalate
PF	Packing factor

POM	Polyacetal
PP	Polypropylene
PS	Polystyrene (Styrox)
PVC	Poly(vinyl chloride)
PVD	Physical vapour deposition
Q	Charge [C] / Q factor / Reactive power [VAr]
Quenching	Rapid cooling
Redox	Reduction and oxidation (–reactions)
RF	Radio frequency (approx. 3kHz-300GHz)
RMS	Root-mean-square
RRX	Linear recursion on X
RRY	Linear recursion on Y
R_s	Sheet resistance [Ω/square]
Schooping	Electrode deposition process
sq	Square
SRF	Self-resonant frequency
T	Temperature [K/°C]
t	Time / thickness
tan δ	Loss tangent
u	Voltage (as a function of time) [V]
U	Voltage [V]
VAr	Volt ampere reactive
W	Watt
w	Width
wt-%	Weight percent
XLPE	Cross-linked polyethylene
ε	Total permittivity
ε'	Real permittivity
ε''	Imaginary permittivity
ε_0	Vacuum permittivity, $\varepsilon_0 = 8.85 \times 10^{-12}\,\mathrm{Fm}^{-1}$
ε_r	Relative permittivity
ρ	Density
τ	Time constant/relaxation time
ω	Angular frequency [rad/s]

1. INTRODUCTION

Polymer insulations are utilized in a broad range of electric systems, such as undersea and underground power cables, film capacitors, overhead power line insulators and in various other kind of insulations, for example in bushings and surge arresters. Insulating polymers have high breakdown strength, low dielectric losses and they operate reliably even when subjected to electrical, thermal, chemical and mechanical stresses. The service life of polymer insulations is long, in many applications spanning to over 30 years.

Despite their already advantageous and competitive properties, the emergence of new applications, such as transmission and distribution network power compensation systems, flexible AC transmission systems (FACTS) and the increasing amount of underground cabling in MV and HV power lines alike, has created a demand for better dielectrics. This thesis focuses on capacitor insulation systems, in which the ongoing research is looking for ways to improve the power densities. Improvement has been sought by tuning the manufacturing processes, but also in the form of entirely new dielectric materials with superior properties. Various approaches, such as polymer nanocomposites, have shown promising results [1]–[3].

The reliability requirement for many of the applications in which polymer insulations are utilized is high and the insulation should not fail during the expected service life. Failure in the dielectric is seen as the dielectric losses increasing over a threshold, or more often as a breakdown. In most applications, with the exception of metallized film capacitors, a single breakdown results in a total loss of insulating properties, requiring costly maintenance, causing financial losses and in worst case triggers power outages.

Due to the high reliability requirements, the aging behaviour of the novel dielectrics needs to be verified. Recent research suggests that the aging behaviour and mechanisms in i.e. nanocomposites may be entirely different than those observed in pure polymer materials. [4]–[6] There is also a scarcity of research and literature regarding the aging of novel dielectrics. Even though the short-term properties of the novel materials are promising, their aging progression needs to be verified before they can be regarded suitable for practical applications.

The purpose of this thesis was to develop a measurement method to assess the thermal aging of insulating polymer thin films. Thermal stress was chosen since knowledge on the effects of individual stresses is needed for the development of a multi-stress model. The test system was designed to allow the characterization of combined thermoelectric stresses in future research projects.

The research results will be utilized to evaluate the practical value of nanomaterials, and to develop a comprehensive view on the effects of progressing thermal aging on breakdown behaviour. Due to the biaxial orientation, processing additives and residues even traditional capacitor-grade thin films are relatively far from pure PP materials. Any of the aforementioned may influence the aging behavior, and this work intends to clarify whether or not models developed for pure PP can be readily applied to capacitor grade thin films.

Polymer materials may be relatively unknown to the majority of electrical engineers; therefore Chapter 2 focuses on the chemical and physical nature of polymers. The chapter gives a conception of the multiple structural layers recognizable in polymers, which is important as every layer from the atomic configuration to the morphology of crystallization affect the dielectric properties of the end products. The empirical part of this thesis focuses on the aging behaviour of Polypropylene (PP) and PP-based nanocomposites; therefore an overview of the manufacturing processes and general properties of PP thin films is given in latter part of Chapter 2.

Chapter 3 focuses on the electrical properties of polymers. The discussion begins by explaining the insulating nature of polymers with the band gap theory. The theoretical approach is continued, and concepts such as space charge and polarization are considered. Space charge is of importance especially for long-term DC stresses, often present in capacitor and DC cable applications. For these applications polarity changes and transients after lengthy static DC stresses may be problematic. Recent studies suggest towards differences in space charge behaviour between polymer nanocomposites and traditional polymers, and these effects may influence the long-term aging properties of polymer-nanocomposite insulation materials. In the latter part of Chapter 3 breakdown is reviewed both as physiochemical phenomena and as a stochastic process. Finally, the discussion is extended into the practical applications of polymer thin films. Film/foil and metallized film capacitor designs are evaluated as they represent the two main categories of film capacitors manufactured today.

The concepts of aging and degradation are approached in Chapter 4. Beginning from the definitions of aging and degradation, the discussion is continued towards the phenomenological and statistical viewpoints of aging. Aging mechanisms and the factors of influence are discussed separately, after which their relationship is evaluated. Various models have been used to predict the lifetime of insulations under varying environmental conditions and stress levels. These models, in addition to their limitations are discussed in the latter part of Chapter 4.

The empirical part of this thesis begins with Chapter 5, starting with the description of the materials selected to participate in the aging experiment. Two types of industrial capacitor-grade films, one SiO_2-PP nanocomposite and its reference film were subjected to a thermal step stress cycle spanning 1008 hours. Dielectric breakdown strength (DBS) of the films was evaluated, as previous research within the research group suggest it being a more sensitive indicator than alternative properties like the dielectric loss tangent. The DBS of the films was characterized using novel MultiBreak test

method, which by utilizing the self-healing capabilities of metallized film electrodes allowed a large number of breakdowns to be recorded from sample areas of 81cm^2. Finally, the purpose-tailored oven and the control systems used for the experiment are depicted.

The empirical part of this thesis concludes with result analysis in Chapter 6. The analysis begins with the depiction of the measurement results, after which the focus is shifted towards the possible reasons behind the observed changes. Finally, possible error sources together with their probabilities and possible repercussions are evaluated.

2. POLYMERS

Polymers are a diverse selection of materials which have been used as base ingredients for synthetic materials known as plastics and rubbers since the end of the 19th century. One of the reasons behind their widespread usage, ranging ranges from household appliances to undersea cable insulations is their ability to be designed and fabricated to meet different demands. This is based on the numerous amounts of possible chemical and structural configurations easily realized with polymers. Changes in either of the aforementioned are known to lead to vastly different properties. This diversity and how it is used to categorize various polymers will be discussed in the following sections.

Chapter 2 begins with the basic chemistry behind the transformation of monomer blocks into a polymer, extending into their spatial structure, formally known as morphology. The latter part of Chapter 2 focuses on the properties of polypropylene (PP), as polypropylene thin films were used in the experimental part of this thesis. Finally, the discussion is extended into the manufacturing methods used, and to the variations different choices will have on the end products.

2.1 Polymer chemistry

Polymers are defined as huge molecules composed of smaller molecules, usually out of one or few types. These small building blocks are called monomers, or sometimes simply mers. The chemical reaction of monomers assembling themselves into a polymer is called polymerization. The resulting polymer backbone can take many shapes, ranging from simple chains to exquisite spider-web-like structures. The amount of monomers in the backbone varies depending on great deal of factors, but as a general approximation it can be said that for most polymers used in practical applications the amount of monomers forming one molecule ranges from hundreds to thousands. This property is characterized with a quantity known as *degree of polymerization* (DP), defined as the average number of monomeric units in polymer molecules. Polymers with higher degrees of polymerization usually exhibit better physical and electrical properties and are therefore desired instead of their smaller-molecule counterparts. Larger DP is accompanied with relatively larger molecular weight, which justifies calling polymers macromolecules, a term used for any molecules of substantial size. [7], [8]

Polymerization processes usually alter the structure of basic monomers compared to their individual forms. This is caused by the rearrangement of electrons into

intermolecular covalent bonds. To demonstrate this, the polymerization process of formaldehyde into poly(vinyl chloride) (PVC) is illustrated in Figure 2.1.

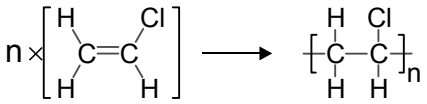

Figure 2.1. Polyvinyl chloride (PVC) is produced by polymerization of vinyl chloride monomers. [9].

Polymerization, as illustrated in Figure 2.1, is a process where particular intermolecular covalent bonds break and via the formation of covalent bonds single monomers rearrange themselves into chain-like structure. In the case of aforementioned poly(vinyl chloride), the double bond between two carbon atoms unravels, reforming into a single covalent bond. The electrons and vacancies left behind are used to form new covalent bonds between adjacent monomer units.

In the case of aforementioned poly(vinyl chloride) all atoms from the original monomer units are used in the polymer chain. This kind of additional polymerization is known as polyaddition. Alternative processes in which molecules joining together lose small molecules as by-products are referred to as polycondensation, and the resulting polymers are known as condensation polymers. Usually water or methanol is produced as by-products, with one example being the manufacturing process of Nylon 6-6 in which water is produced as a by-product. [10]

Apart from simple monomers in undefined but substantially larger spatial structure, polymer molecules can include so-called side or pendant groups, both of which representing different naming conventions for same thing. To promote disambiguation, later on in this thesis the term pendant group is unambiguously used. Pendant groups are molecules attached to the backbone, but which are not parts of it. Their presence, chemical structure and spatial configuration, including physical size, can lead to significant variations in different yet measurable physical properties, which broaden the diversity of polymer chemistry even further. To overcome this and to assess polymers more easily, various different approaches have been used to categorize polymers into different groups. Certain widely acknowledged methods will be discussed next.

For the categorization of polymers some kind of distinction is needed as a starting point. One of the more straightforward ways of categorizing polymers is to whether or not the polymer material can be found in nature. Naturally occurring polymers are identified as natural polymers. They include substances such as cellulose and lignin, which make up the mechanical structure in both plant and animal life. Another historically important natural polymer is latex, which is extracted from trees and even today considered as important raw material for rubber production. The first polymers used commercially were unrefined natural polymers, handy for waterproofing clothes but their sticky properties left room for improvement. [11]

When scientists started modifying these natural polymers to reduce their unwanted qualities, such as the aforementioned inherent stickiness, new kind of polymers called

modified natural polymers were invented. As their name implies, they were fashioned from naturally occurring polymers, such as natural rubber, using chemical treatments, one of the earliest being addition of sulfur. Of the large number of modified natural polymers created back in the day, some are still used nowadays. Notable examples of these modified natural polymers included extremely flammable nitrocellulose, used as a film base in photography and medical X-ray imaging from late 1880s to the end of 1950s, and vulcanized rubber, which still sees widespread usage. After the eve of modified natural polymers, it was not for long though, until polymer chemistry had advanced to a point where polymers could by completely synthetized. [11]

The third group of polymers consists of completely synthetic polymers, simply known as synthetic polymers. They are made from small molecules, such as ethylene gas, using specialized catalysts and in only rare cases naturally-occurring but heavily accelerated reactions to combine single monomers into a polymer structure of specific kind. For optimal results and polymer composition these reactions are almost always strictly controlled. Most of the polymers used today are purely synthetic polymers, notable examples being polyacetal (POM), polypropylene, (PP) and poly(vinyl chloride) (PVC).

Another approach is to classify polymers based on the atoms they consist of. The element considered for categorization purposes is usually carbon, and using this as a basis three distinct categories can be identified. Polymers including carbon atoms in their backbone are called organic polymers, whereas those with carbon atoms in the pendant groups but not in their backbone are called semi organic. If the polymer has no carbon in its structure, it is called inorganic. It should be noted, that outside the scope of polymer science, the distinction between organic and inorganic compounds is vague at its best, and not solely based on existence of carbon atoms.

Third method to categorize polymers in based on the number of different monomers they are made of. Polymers made up from single kind of monomer are defined as homopolymers, whereas polymers with multiple types of monomer units varying within the polymer backbone are defined as copolymers.

The backbone of a polymer chain can take different forms, as it can be either linear, branched or crosslinked. Besides, the amount of crosslinks can vary from only a few crosslinks to a point where the polymer resembles a web-like structure. As the name implies, linear polymers are simple linear chains where repetitive monomer units are bonded together. Linear polymers can be visually interpreted as shown in Figure 2.2, where A represents the monomer unit. Lines between them are covalent bonds keeping the structure together.

Figure 2.2. Single chains: linear homopolymer consisting of monomer units represented by "A".

Apart from being linear, some homopolymers are manufactured to include branches. An important difference between branching and the aforementioned pendant groups is that the branches are still considered to be parts of the polymeric backbone, whereas pendant groups, by definition, are not. Several naming conventions exist, and sometimes references the term side chain may be used for polymer branching, but with distinction from proper side groups. The branches can be very short, consisting only of few monomer units, or relatively long, up to lengths of hundreds of monomer units. The structure of branched homopolymer is illustrated in Figure 2.3.

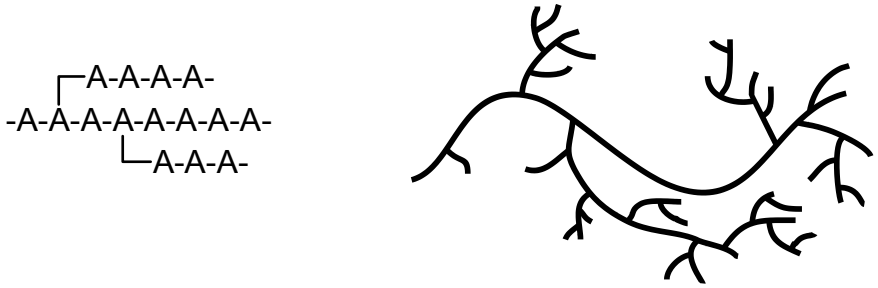

Figure 2.3. Branched homopolymer: numerous branches and backbones consisting of similar monomer molecules

For crosslinked polymers the monomer molecules are covalently bonded into chains, which are in turn hydrogen bonded [12] to other chains, forming a large web-like structure . Both the spatial configuration of the structure and the number of crosslinks can be varied. The superstructure can be either two- or three-dimensional, and the number of crosslinks between monomer chains can vary from relatively few to numerous. Heavily crosslinked polymers are not moldable after crosslinks have formed in a process known as curing. These so-called thermosets are more rigid than their less crosslinked counterparts, and are widely used in e.g. cable insulations where such rigidity is often needed, and forming is expected to take place only once during manufacturing. Simplistic two-dimensional interpretation of crosslinked polymer consisting of monomer A is illustrated in Figure 2.4.

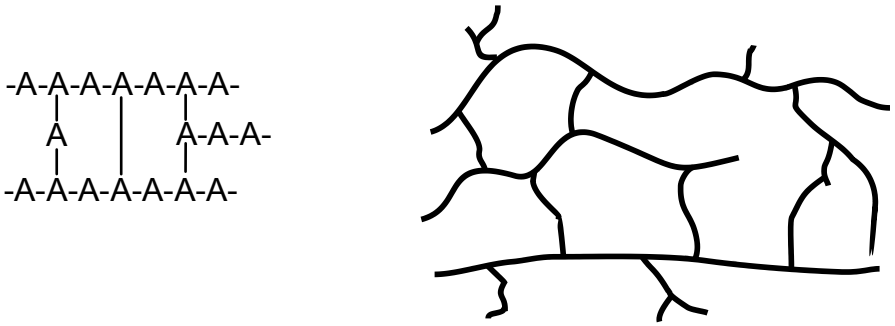

Figure 2.4. Crosslinked homopolymers are known for their rigidity, but they cannot be reformed.

As an alternative to homopolymers, which were defined as polymers consisting of only of one type of monomer unit, those with dissimilar monomers in their backbone are known as copolymers. Within the backbone the varying monomers can be either randomly distributed or they can alternate in different ways. In the latter case of

organized alternation the repeating units can be either single monomers, in which case the structure is called alternating copolymer; or blocks of similar monomers, in which case the structure is referred as block copolymer. The number of different monomers in a single copolymer molecule can vary, and is in no way limited to two. Notable examples of commercially important copolymers include acrylonitrile butadiene styrene, also known as ABS. [13]

In the same way as homopolymers could be either linear of branched, similar kind of distinction can be recognized in copolymers. Copolymers can be either linear, branched or crosslinked, but with copolymers there is one more special case to branched polymers, so-called grafted polymers, where branches and the linear portions of the backbone are made of different monomers. The process of attaching these usually smaller chains to otherwise homogenous backbone is known as grafting. As an example the results from grafting smaller chains consisting of repeating monomer unit B into linear polymer backbone consisting of repeating monomer unit A is illustrated in Figure 2.5 below.

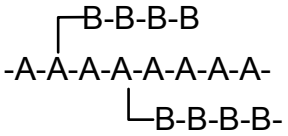

Figure 2.5. Side chains of monomer B are attached into linear homopolymer A to form grafted copolymers.

The concept of crosslinking is closely related to macroscopic concept of formability of plastics. Polymers consisting of long chains but with no crosslinks between them are held together by secondary or weak bonds, also known as van der Waals forces or hydrogen bonds. With increasing temperature the weak interactions diminish compared to thermal motion, and the polymer mellows. If the temperature is increased even further, the polymer eventually melts. When the temperature of melt is lowered, the weak interactions catch up again, and the plastic sets. Polymer materials or plastics exhibiting this kind of behavior are known as thermoplasts; well-known for their ability to be reformed repeatedly. On the other hand, plastics consisting of polymer chains heavily crosslinked with each other do not allow such reforming. Once the crosslinks have formed, they intrinsically break down rather than melt with sufficiently increased temperature. The latter kinds of plastics are known as thermosets, which in turn are generally more rigid than their non-crosslinked counterparts.

The aforementioned concept of melting is dependent on multiple factors, one of which is molecular mass. From the standpoint of polymer chemistry it is usually justified to assume that higher molecular mass leads to an increase in melting point. Molecular mass, as stated in the SI-system, is defined as the relative molecular mass compared to one twelfth of the mass of carbon isotope ^{12}C. Another important and closely related concept is the molar mass, which is defined as the mass of a one mole $(\approx 6,022 \times 10^{23})$ of atoms. It can be assumed that an increase in molecular mass results

in an increase in molar mass and vice versa. Phase transitions such as melting are covered in greater detail in section 2.2.

Phase transitions, in addition to physical properties are heavily dependent on the degree of polymerization (DP), with increasing degree of polymerization resulting in larger average molar masses, which in turn results in increasing melting and boiling points and increasing rigidity of the solid form. The increase is not linear, however. Below certain point known as critical DP, the resulting solid is brittle and weak, and after DP is increased beyond this critical value the physical properties improve rapidly. The improvements attained with increasing degrees of polymerization start saturating at certain point. As a downside when the DP is increased the polymer materials become increasing difficult to process, and the higher melting temperatures may demand specialized processing equipment. [14], [15]

Due to the nature of polymerization process, the length of the polymer chains is not constant even with the most precise manufacturing processes. On the other hand, if excessive curing takes place, the resulting molecules are so huge and intervening that their molar masses cannot be measured. For not-so-heavily crosslinked polymers the degree of polymerization is often measured as a part of the product development cycle, because, as previously described, it serves as a versatile quality indicator. Molecular masses measured from real polymers take forms of statistical distributions. The concept of DP measurements is complicated even further since distributions from same polymer can be made using different ideas as starting point, which results in completely different looking distributions. This in turn calls for exact definitions, which are discussed next.

Two elementary ways to estimate molar mass distributions are based on selecting different qualities to be measured. They can be examined by using either relative molar weight or the count of molecules as an averaging factor. It is usually expected that in typical polymers there is a substantial amount of small components with relatively small molecular masses, which can be seen in typical number-averaged distribution as shown in Figure 2.6. [15]

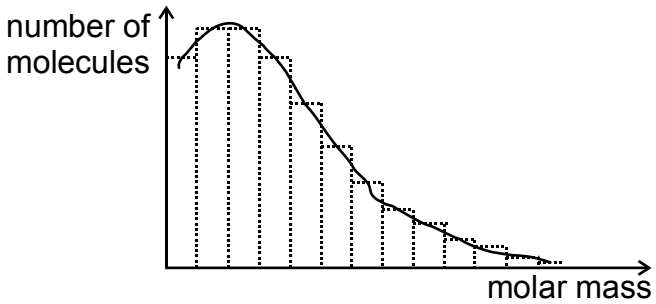

Figure 2.6. Numeric molar mass distributions are affected by the large number of small-molecular weight components. [15]

On the other hand, if the same sample is presented by using differential weight percentage as vertical axis, the resulting distribution is vastly different, as shown in Figure 2.7.

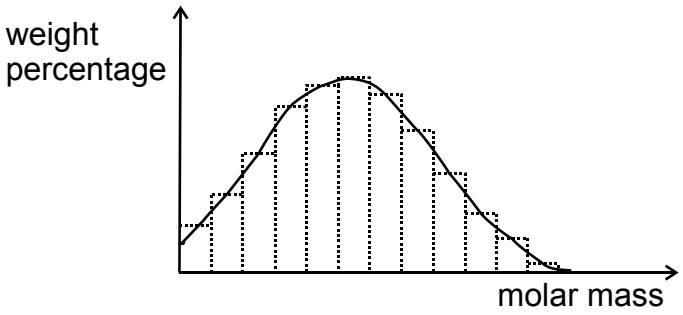

Figure 2.7. Differential molar mass distributions highlight the precense of the sparse yet heavy macromolecules. [15]

It should be emphasized that both Figure 2.6 and Figure 2.7 could represent the same material. The difference between the two figures comes of the large number of small-molecular-weight molecules left after the polymerization has finished, which affects the numeric distribution, whereas the differential distribution is more affected by the smaller number of heavy-weight macromolecules. The properties of resulting polymeric plastics are heavily influenced by their inherent variations in DP, with increasing number of small-molecular-weight components resulting in better formability, but rapidly diminishing mechanical properties.

As stated in the previous sections the molar mass of polymers tend to follow certain statistical distributions. To simplify and harmonize the results it is often reasonable to specify single numeric values with which to describe the said properties. Similar approaches which held true for the distributions can be used to calculate said factors. Two of the most widely used are number-average molecular weight $\bar{M}_n$ and weight-average molecular weight $\bar{M}_w$. The number-average molecular weight is calculated using Equation (2.1), where n_i is the number of molecules with molar mass M_i.[15]

$$\bar{M}_n = \frac{\sum_{i=1}^{\infty} n_i M_i}{\sum_{i=1}^{\infty} n_i} \tag{2.1}$$

In a very similar way the weight average molar mass can be calculated using Equation (2.2), where w_i is the total mass of molecules with molar mass of M_i. [15]

$$\bar{M}_w = \frac{\sum_{i=1}^{\infty} w_i M_i}{\sum_{i=1}^{\infty} w_i} = \frac{\sum_{i=1}^{\infty} n_i M_i^2}{\sum_{i=1}^{\infty} n_i M_i} \tag{2.2}$$

The difference between number- and weight-averaged molar masses becomes apparent when they are plotted for a sample distribution. Results from such plotting are best described with Figure 2.8.

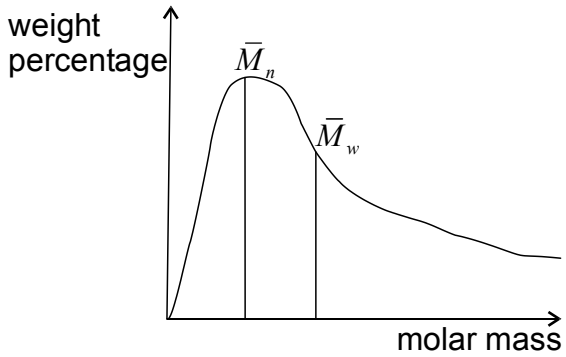

Figure 2.8. Differently calculated molar masses align themselves differently. Care should be taken to avoid misunderstandings. [15]

Apart from number- and weight-averaged molar masses various less frequently used molar masses such as viscosity- and z-average molar masses have been described in literature. Readers interested in further information are recommended to refer to references [15] and [16].

2.2 Morphology and the factors affecting it

Apart from heavily influencing phase transitions, both covalent and weak bonds play an important role when assessing the factors behind polymer morphology. In the scope of this thesis morphology is discussed from a viewpoint of analyzing the spatial three-dimensional structure of polymers in multiple different levels.

2.2.1 Isometry and tacticity

One of the crucial ideas behind the variations in morphology is based on the observation that molecules with similar chemical contents can be arranged in various ways, that is, they can take different configurations. These variations are known as isomers, being the starting point for morphological analysis.

Isomers can be divided into two main categories, structural and spatial isomers. In structural isomers the atoms are covalently bonded in different ways, resulting in vastly different materials with distinct properties. Structural isomers are not especially important in the scope of polymer chemistry. On the other hand spatial isometry, also known as stereoisometry or simply configuration, is one of the defining factors when polymer properties are considered. Stereoisometry refers to molecules with similar covalent bond structure, but in which the atoms are spatially arranged in different ways.

Stereoisometry is especially critical for polymers which have asymmetrical parts or functional groups attached to the linear part of their backbone. One notable example of such polymers is polypropylene, in which methyl ($-CH_3$) groups are attached to the linear CH-backbone. Owing to the asymmetrical structure, the said methyl groups can be arranged into two possible positions during polymerization process. The bonding is permanent, and after each monomer has joined to the expanding polymer structure no further displacement to other configurations is possible. The only way for polymer to

arrange itself into another configuration is through breaking and subsequent reforming of the covalent bonds, which usually leads to disintegration of the material rather than the forming of a new stereoisomer.

Depending on the nature of the polymerization process bonding monomers might have the freedom to bond in multiple ways, resulting in a random orientation of asymmetrical parts and therefore an overall arbitrary structure. In the case of more controlled processes, such as Ziegler-Natta or metallocene catalysis polymerization, the monomer bonding is controlled to a point where monomers with extruding parts take always the same orientation, or vary the orientation in an otherwise controlled way, resulting in overall regular structure. This organized orientation or the lack of it is known as stereoregularity. [11]

Proper stereoregularity is especially important for polymers which incorporate asymmetric or extruding parts in their monomer structure, since proper stereoregularity or the lack of it is heavily reflected on the properties of the resulting material. In the case of naturally occurring or otherwise uncontrolled polymerization such as free radical vinyl polymerization, the orientation of the said side groups is random. This kind of polymer is called atactic, and it doesn't normally pack in any way, which inhibits the formation of crystal structure or fibrils. In general it can be said that the properties of atactic materials are subpar when compared to their stereo regular variants, which also holds true for dielectric properties. This calls for more strict control of the polymerization processes. [11], [17]

One of the first methods to control the tacticity of polymers was to use specially manufactured catalysts to alter the way the polymerization happens in atomic level. One well-known method was named after its inventors, and bears the name of Ziegler-Natta polymerization [17]. This kind of polymerization processes use special catalysts and co-catalysts to carry out the polymerization and with the right choice of catalysts the polymeric structure can be made regular. Regularity itself can occur in two distinct ways. The asymmetrical parts can be oriented on the same side of the polymer backbone, resulting in isotactic material. Alternatively they can alternate consecutively, which kind of material is known as syndiotactic. The concept of tacticity, particularly from the viewpoint of insulating polymeric thin films, is expanded further in section 2.3. [11], [17]

2.2.2 Molecular conformation

While stereoregularity discussed before was not strictly speaking a part of morphology, but rather one of the factors behind it, the first true level of morphology is related to the rotational orientation of the polymer chain, known as molecular conformation. Possible variations in molecular conformation depend on the polymer structure. For simple linear polymers with small or nonexistent side chains, such as polyethylene, the backbones usually take equally simple planar forms. For polyethylene the resulting structure represents a zigzag. These planar conformations are results from atoms orienting themselves to the lowest possible energy. [16]

Unlike configuration, which was semi-permanently defined by covalent bonds, conformation is supported by weaker interatomic forces. These can be repeatedly broken without adverse effects, as a result from for example thermal movements during reforming. Nature tends to favor conformations with lowest possible energies, which lead to them being the most stable.

Molecules with large pendant groups or side chains cannot take simple planar forms due to the lack of space. Instead, they are arranged to more sophisticated three-dimensional shapes. Albeit the forms are highly dependent on the materials in question, as a generalization it can be said that shapes representing distinct spirals or helixes are the most common, both in natural compounds and artificially made polymers alike.

2.2.3 Phase transitions

Crystallization is defined as the packing of atoms and as the formation of a crystal lattice. Crystal lattice is in turn defined as well-ordered periodic organization of the polymer molecules. [16] Even though crystallization is not a proper phase transition, its influence on them entitles discussing them simultaneously.

On a macroscopic scale basically two types of polymeric materials can be recognized. Depending on their affinity to pack together and form crystal lattices they can be either crystalline or amorphous. Given the right conditions crystalline polymers form crystal lattices, whereas amorphous materials do not.

This characteristic trait is closely related to the tacticity of the polymeric matter and in general to the homogeneity of the bulk matter. Similar molecules, such as isotactic and syndiotactic polymers tend to pack together forming crystals or crystallites, while atactic or otherwise divergent molecules usually do not. [11] Moreover as stated by Dissado et al. in [16], only few polymers have a completely regular structure, and molecules may traverse through several crystallites as well. Due to this inherent irregularity amorphous areas exist between the crystallized portions. This gives a reason to call them semicrystalline, a term which is later on preferred.

Let us start examining the phase transitions from the liquid phase, during which no apparent distinction can be made between amorphous and semicrystalline polymers. When temperature is lowered the specific volume keeps dropping at a constant speed due to reducing thermal movement. When the melting point is reached the differences show up. For semicrystalline polymers the crystal lattice starts to form and an abrupt change of specific volume is noted due to the molecules packing together. On the other hand amorphous polymers do not pack together and the fluidness of the melt keeps decreasing, a phase which is referred as supercooled liquid. Polymers in this region are identified as rubber-like, a phase characterized by considerable elasticity.

It should be noted that for real polymers there is no such thing as specific melting point, but rather a wider temperature range at which the polymer melts. This is due to the heterogeneous composition of real polymer materials, which was discussed in Section 2.1. Melting starts with molecules with the smallest molecular weights, and is considered finished when the largest ones have melted. Alternatively, since on a

molecular scale melting refers to the severing of the intermolecular weak bonds, the polymer has melted when no permanent weak bonds exist between molecules. Nevertheless for clarification purpose the melting region is later on referred to simply as melting point, or T_M.

After the semicrystalline polymer or supercooled amorphous liquid is cooled further down to a point known as the glass transition temperature, or T_G, a vitrification process starts, and the material transforms into a rigid, glassy state. The relationship between the specific volume and temperature is illustrated in Figure 2.9. [8], [16]

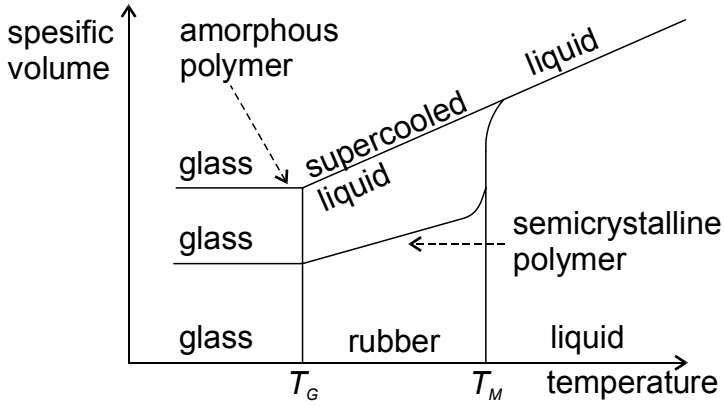

Figure 2.9. Phase transitions. Similar in liquid and glassy forms, the differences between crystallinity manifest themselves in the region between vitrification and melting points. Adapted from [16].

Temperatures T_M and T_G vary between different materials, and albeit dependent on the application, the possible range of operating temperatures do not overlap more than one state. For amorphous materials the operating temperatures are way below glass-transition point. They tend to be optically clear due to the lack of crystal lattice. In this glassy state they are hard, but fragile.

For semicrystalline polymers and elastomers operating temperatures are situated between melting and glass-transitions points. If temperature is reduced below T_G, vitrification turns them brittle and weak. For this reason T_G should be as low as possible, and in case of semicrystalline polymers where T_M if defined, it should be way above highest operating temperatures. The relationship between operating temperature range and transition temperatures is illustrated in Figure 2.10. [15]

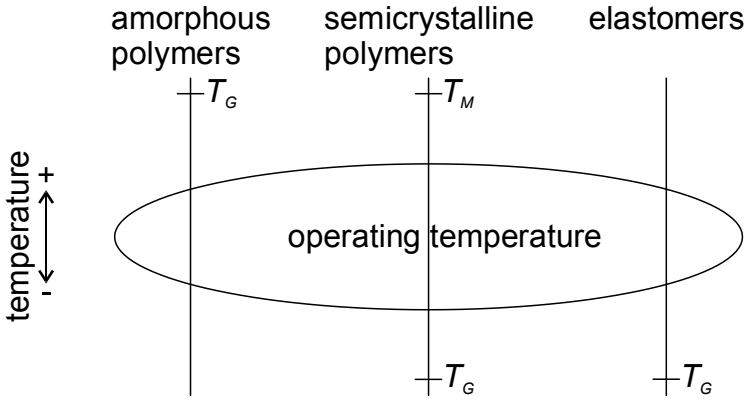

Figure 2.10. Operating temperature ranges differ for different types of plastics. Adapted from [15].

Out of the three types of polymers described earlier for the purpose of this thesis only semicrystalline polymers are considered relevant. Since at their operating temperature range the crystal lattice has formed, its properties and presence alone are reflected heavily in the macroscopic properties of the bulk materials. Due to this importance the properties of the crystal lattice are further examined in Section 2.2.4.

2.2.4 Crystallinity

Crystallization is a two-step process, where the first phase is the formation of nucleation centers. This is known as nucleation, which can occur by the formation of molecule clusters, where intermolecular weak attractive forces locally surpass the forces induced by thermal movements. Alternatively nucleation can occur around impurities in the melt. This makes it possible to have better control over the crystallization process, both in terms of crystallization density and rate. This is usually achieved by adding specific nucleation agents or other additives, such as antioxidants, which act as nucleation centers. [16], [18]

Even without any additives the process can be controlled by adjusting external conditions during crystallization. Control, at least to some extent, is achievable by controlling the temperature and pressure during the crystallization phase. Aggressive cooling, also known as *quenching*, results in materials with different properties compared to those allowed to cool down at a slower pace.

After the nucleus has been formed, the second phase called crystal growth starts. The crystals grow around the numerous newly formed nuclei. Polymers cannot crystallize completely, bringing the name semi-crystalline polymer, and amorphous non-crystalline areas are left between the crystals. The maximum attainable percent of crystallization for applicable materials is cited [15] to be around 95 percent, attainable with highly isotactic (>95 percent) materials. [15], [16]

The spatial structure of the crystals formed during these processes has been studied extensively in the past. The first model trying to describe them was called the *fringed micelle* model, which explained the crystals as long parallel chains running through multiple crystallized areas and traveling through amorphous areas in between. Later on,

this model has been proven to be adequate only for polymer with extremely low crystallinity. For semicrystalline polymers it is considered inadequate and not used anymore. [16]

The current knowledge of the shape of crystals is divided into distinct forms. First is more or less direct derivation from the fringed micelle model, known as lamella formation. These lamellae represent sheets. Single molecules can traverse through multiple lamellae, forming intercrystalline links. Longer molecules tend to traverse through several molecules, bringing about a more rigid structure and thereby connecting the degree of polymerization to the rigidness of crystallized form. [16]

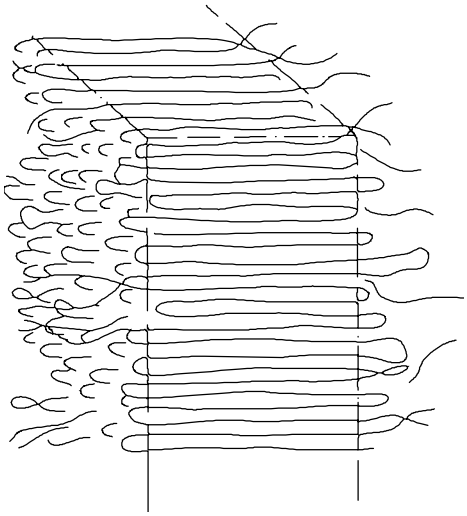

Figure 2.11. Lamella. The extending molecules continue throught adjacent lamellae, forming intercrystalline links. Adapted from [16].

For reasons not completely understood sometimes numerous lamellae start growing from a single nucleus, forming spheres known as spherulites. It is known that these spherulites are volume filling, i.e. they keep growing until they hit each other, leaving amorphous areas in between. The structures of lamellae and spherulites are illustrated in Figure 2.11 and Figure 2.12 respectively. [16]

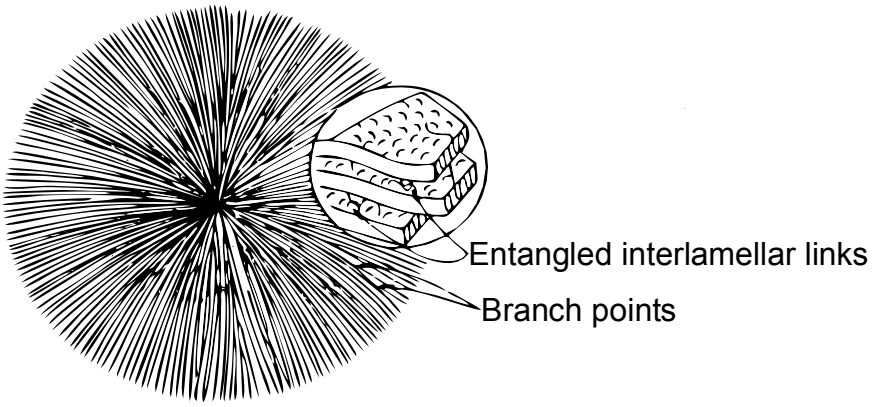

Figure 2.12. Spherulites are space-filling, they grow until they hit each other. Adapted from [16].

The formation of spherulites is proportional to the cooling rate during crystallization phase, with slower cooling closer to the melting point leading to spherulite formation.

On the other hand in case of highly accelerated crystallization, the spherulites have no time to develop. That kind of transition is usually achieved with additives acting as nucleation centers or quenching the polymer during crystallization. The properties of the crystallized material are dependent both on the existence of spherulites and their size. Highly sphrerulitic structure is known to lead to more rigid materials, in addition to smaller spherulites leading to increased dielectric breakdown strength. [15], [18], [19]

The spherulites are composed of pure polymeric matter, and as they grow they reject the impurities within the lattice. These impurities accumulate on the outer boundaries. This leads to a relatively heterogeneous structure, with spherulite globes composed of pure matter and both impurities and amorphous segments concentrated in between them. The existence and size of these spherulites and impurities are inversely proportional, acting as one influencing factor in certain degradation models, such as water treeing [20]. These degradation models and their importance will be discussed in chapter 4.

2.3 Polymer in detail: polypropylene

Polypropylene is one of the most widely used plastics. Manufactured in large quantities, its applications range from food containers to high performance, high frequency and low loss capacitors. Due to its non-toxicity, even when burned, it has been replacing poly(vinyl chloride) in both electrical and non-electrical applications. The non-toxicity makes it more environmentally friendly and provides additional level of fire safety due to its non-toxic combustion gases, especially when compared to the chlorine gas released when PVC is burned.

In addition to the non-toxicity, polypropylene exhibits many universally desired properties, such as inherent ruggedness and resistance to chemical corrosion, allowing it to be used outdoors or in otherwise harsh, for example industrial, environments. Like many polymer based materials, untreated polypropylene is susceptible to ultraviolet radiation (UV) induced degradation. As long as the application area and its susceptibility to UV exposure are known beforehand, this normally poses no problem, since these adverse effects can be mitigated by the use of purpose-tailored additives. [21]

Polypropylene itself is a synthetic polymer, additively polymerized from gaseous propene. Owing to its asymmetric structure, the resulting polymer can be either isotactic, syndiotactic, or atactic. One of the reasons behind the widespread usage of polypropylene is how the tacticity can be controlled. Purely isotactic form can be manufactured by either Ziegler-Natta or metallocene catalyst processes. Both the isotactic and syndiotactic forms have relatively high degrees of crystallinity, resulting in superior properties when compared to the amorphous atactic form. Out of these two forms capably of crystallization mainly isotactic form is used. [11]

Different design goals result in end-products with vastly different properties, and the comparison between polypropylene materials designed for different applications is futile. On the other hand, driven by the common design goals the properties of

capacitor-grade polypropylene are more uniform. The properties of one industrial quality isotactic and biaxially oriented polypropylene thin film designed for capacitor applications, Tervakoski RER, are summarized in Table 1.

Table 1: Properties of capacitor grade PP film. [23]

Chemical formula	$(C_3H_6)_n$
Tensile strength	≥180 MN/m^2
Young modulus	≥1900 MN/m^2
Glass transition temperature	-10°C
Softening point	140°C, vicat [15]
Melting point	165-170 °C
Density	0.905-0.910 g/cm^3
Volume resistivity	>1x10^{15} Ωm
Dielectric constant [22]	≈2.2
Dielectric breakdown strength, thin films[1]	700 V/µm

Residues of the polymerization catalysts tend to remain enclosed within the polymer bulk after initial manufacturing. Additionally, a variety of additives is compounded with the bulk polymer before the actual film manufacturing takes place. These additives include, but are not always limited to a primary and secondary antioxidants, and according to the requirements of the application in question stabilizers, for example those required for adequate ultraviolet resistance. These additives are examples of the physiochemical factors influencing the properties of resulting polymer materials. Even from the same batch of bulk polymer vastly different outcomes can be realized by choices made during manufacturing.

The choice and loading of any additives affect the electrical properties of finished materials. Discussed later on in more detail, any inhomogeneity in the polymer matrix may act as a weak spot. These weak spots may act as degradation centers and lower the dielectric strength, which is in principle undesirable for electrical insulations. Possible sources of inhomogeneity include, but are in no way limited to residual catalysts and antioxidants. Albeit essential during the polymerization process, residual catalysts serve no purpose afterwards. Deashing processes have been used to remove the catalyst residues, but research has been done to find ways to omit these onerous cleansing processes. [24]

The presence of antioxidants is not that straightforward however, as they are essential during manufacturing, processing and storage. Without them the polymer is susceptible to structural damage occurring at molecular level. High temperatures are involved in polymer manufacturing, and the reaction rate of any deleterious reactions would be radically increased. Without further delving into the nature of these reactions,

[1] It should be emphasized that this value is based on small area samples, neglecting weak points. With large-area measurements values are substantially lower, and highly dependent on film thickness.

considering the fact antioxidants can be used to inhibit these reactions it can be presumed these reactions are related to oxidation. If antioxidants are not used or if the antioxidant loading is overly low, the polymer suffers damage. This damage manifests itself also as considerably lowered dielectric strength. After manufacturing and storage the role of antioxidants is reversed however, as the films are either immersed in oil or molded into epoxy, both of which prevent them from coming in contact with atmospheric oxygen. The presence of remaining antioxidants has been associated with lowered dielectric strength. To combat this, ultraviolet treatment has been proposed in [25], [26] to consume the remaining antioxidants. Moreover, the long term properties of any of the remaining antioxidants during the service life spanning through decades under electric and thermal stresses is not thoroughly known. Even if an optimal balance between the selection and loading of antioxidants and electrical properties would exist, it might not be easy to reach. [2], [21]

Thin films such as the aforementioned Tervakoski RER represent one application for polypropylene. Since the focus of this thesis lies on thin films, a short summary is given about the manufacturing methods behind said films. Since the amount of polypropylene produced is extraordinary large, this kind of industry benefits from large unit size. The manufacturing process itself starts from the polymerization process described earlier. As a result raw polypropylene is formed, with residues of the catalysts still within.

The raw polymer is fed into an extruder, together with a selection of additives and stabilizers. The extruder, consisting of multiple repeating mixing and melting sections, followed by a molding die and cooling systems, produces pellets. Macroscopically these pellets are rather homogenous, but on nanoscopic scale they include inhomogeneity induced by the additives described earlier. Nevertheless, as long as the bulk material does not include any not-wanted impurities, it is considered as pure. A large quantity of polypropylene is sold as these raw pellets, shipped elsewhere for further, often more application-specific processing.

In the next production phase the pellets are fed into another extruder, but this time the resulting molten bulk is either blown into a bubble and with subsequent pinch rolls pressed into a film, or extruded through a narrow slit to produce relatively thick film known as *cast*. Of special importance for insulating applications, the electrical properties of polymer thin films increase greatly if the film itself is stretched into two directions, to a state known as biaxial orientation. In the blown-film process described first this occurs during the blowing, but with the latter cast film processes the film is first stretched in machine direction, after which subsequent transverse directional orientation is required. If for some reason this transverse orientation is omitted, the film is known as uniaxially oriented. After this orientation the film is cooled, the uneven edges are cut off. Finally, the film is rolled around a frame and either used on-site or shipped elsewhere. Notable uses for insulating biaxially oriented thin films include power and low voltage (LV) capacitors, discussed later in section 3.3. The manufacturing processes are illustrated in Figure 2.13 and Figure 2.14. [15]

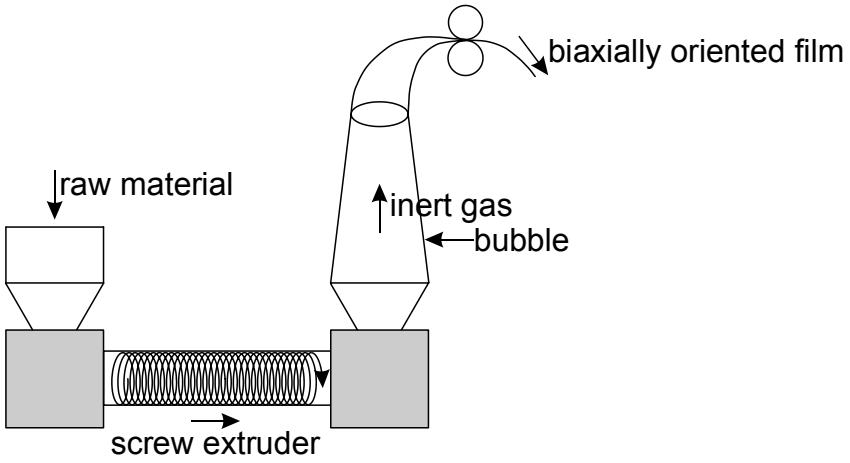

Figure 2.13. Blown-film process requires no additional orientational steps.

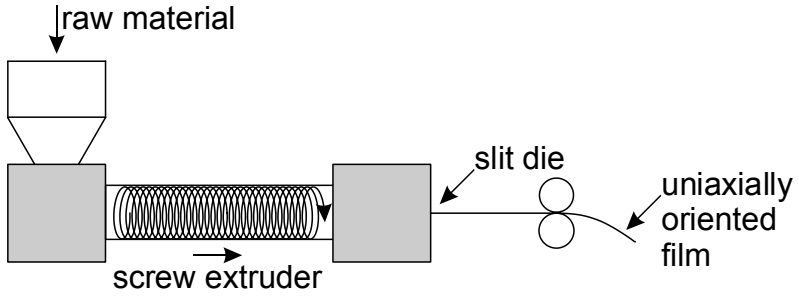

Figure 2.14. Separate transverse directional orientation is needed for cast film processes.

Despite all the possible variations which could be made during manufacturing, most thin films manufactured for capacitor applications are optimized for same insulating purposes, i.e. high dielectric strength and low losses. Consequently, when different polypropylene thin films are compared, the values shown in Table 1 are still in the correct region. This makes it possible to assess the limitation and benefits of polypropylene, and allowing comparison between possible material choices. Certain characteristics such as dielectric breakdown strength will be examined in greater detail during the latter chapters of this thesis.

3. POLYMERS IN ELECTRIC FIELD

Polymers are very able insulating materials, having found use in various applications ranging from multilayer electrical cables to power capacitors. The theoretical foundations behind the insulating properties are explored in the first part of this chapter.

Even though polymers good dielectrics, with sufficient electric field the insulating properties are abruptly lost and a breakdown occurs. In the middle part of this chapter the multitudes of factors behind breakdowns are accounted for, and two different viewpoints on them are highlighted. One is focused on describing the physics behind the various breakdown mechanisms, whereas the other is looking for statistical correlations between breakdown events.

In the latter part of this chapter focus is shifted towards the practical applications of polymer thin films, contemplating the design considerations imposed by the issues described earlier. Since the focus of this thesis lies on thin films which are manufactured and used for power and LV capacitors alike, the last section is focused on them and their future prospects.

3.1 Electrical properties of polymers

3.1.1 Band-gap theory and insulating nature

The insulating nature of polymers is explainable using the band-gap theory. Band gap theory is founded on modern physics, and readers interested in detailed explanations and theoretical foundations should refer to [12]. Band gap theory is based on the assumption that electrons orbiting the nucleus form a cloud, which is divided into orbitals with specific energy states. In this model electrons do not appear as traditional particles with defined location and energy, but rather as Schrödinger-derived probability functions.

Pauli exclusion principle states that no two particles, such as electrons, can have the exact same quantum mechanical state. For atoms this limits the maximum number of electrons in each energy level, and in consequence with increasing number of electrons higher orbitals corresponding to higher energies become manned. The outermost occupied electron shell is known as valence band, and the electrons there are known as valence electrons. Their interactions form the foundations for chemistry.

In polyatomic molecules the energy levels start overlapping as the electrons interact with each other. Pauli exclusion principle still holds, and the electron energies are shifted. This increases the number of possible energies to allow the accommodation of every electron.

In macromolecules, such as polymers with moderate-high degrees of polymerization, the number of electrons interacting with each other is so vast that the orbital structure begins to resemble bands rather than discrete energy levels. Initially these bands broaden with increasing number of atoms, but the development is regressive. With sufficient atoms the bands do not get noticeably wider, even if the number of interacting atoms keeps increasing. When the density of states within these bands gets large enough, the discrete states are so close to each other that electrons can move between these states with ease. At this point the band can be considered as a continuum. This development is illustrated in Figure 3.1 below.

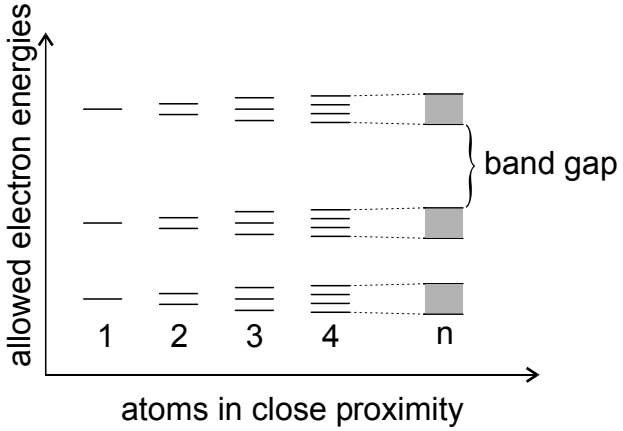

Figure 3.1. Orbital degeneration leads to the formation of distinct energy bands and band gaps between them.

Out of the multiple energy bands formed, only two are relevant for further discussion. The outermost electron band occupied at 0K is known as valence band, and the first unoccupied band is called conduction band. Depending on the atoms in question, between them a band gap might or might not exist. In this forbidden zone electrons cannot exist, and the density of states is zero.

Electrons in the valence band are bound to the atomic structure, and they cannot move freely around. To move freely around any structure, such as crystal lattice or molecular backbone, and to move in response to applied electric field, assisting in electrical conduction, the electron has to get to the conduction band. If an electron acquires enough energy, for example from thermal movement, it can hop across the band gap to the conduction band. Minimum energy required is equal to the width of the band gap. Larger energy gap makes it less probable for electrons to acquire the energies required; therefore resulting in radically less electrons in the conducting band, which in turn leads to low conductivity. For insulators the band gap is considerably higher than the average energies induced by thermal movement at normal temperatures, and for conducting materials such as metals the energy bands partially overlap. Overlapping allows electrons to traverse effortlessly to the conduction band, resulting in significant conductivity. For semiconductors the band gap is somewhere between the two extremes. [12], [16]

Applying the band gap theory to polymers is possible, albeit slightly more challenging. Besides the principal energy bands, the inevitable imperfections and

impurities, such as amorphous areas in the crystal lattice result in energy states between them [27]. These states are known as traps. Scattered in the band gap and relatively sparse, the density of these states remains low. This hinders electron movement, as electrons occupying these states cannot easily move between them, resulting in low mobility. Various mechanisms, such as electrons acquiring sufficient energy or quantum tunneling, can result in the movement of these trapped electrons, either between the traps or to either of the aforementioned energy bands. [16]

In addition to the electron-based conduction, the potential presence of ions will contribute to the total electrical conductivity. Polymer structures can contain ions, which are either contained during manufacturing processes, or created via dissociation of polymer chains. Under the effects of electric field these particles start moving, increasing the apparent conductivity. Unlike electrons their mobility is limited, and various obstacles and interfaces can result in the buildup of these charged particles. This is consistent with the observation that especially for static cases (DC) the effect of ionic conduction diminishes with time. This leads to the formation of local charge concentrations, known as space charge, which will be discussed next. [16]

3.1.2 Space charge

Space charge is defined as spatial charge fluctuations. Considering a polymer film sandwiched between two metal electrodes, the polymer-electrode surfaces act as a potential barrier, through which only electrons and holes can move. This requires sufficient electric field to surpass the height of the barrier, but the fields required are within the realistic operational conditions. Larger particles, such as ions, cannot cross the barrier. In insulations under AC excitation ionic conduction can continue to function, but for DC applications ion-based conductivity diminishes with time. As a result from ongoing DC excitation, these larger charged particles are concentrated near the electrode surface, forming a local charge build-up.

Formation and dissipation of space charge is balance reaction, where specific electric field results in the formation of a distinct space charge profile. In case of polymers the movement of charged particles is hindered, partly due to the trap states described earlier, and the equilibrium is reached after relatively long time delays, up to several years. This limits the effects of space charge mostly to DC applications, where these long-term processes should be evaluated to properly assess the electrical properties of dielectric materials.

Despite being a phenomena mostly associated with DC applications, at least according to Blythe et al small amounts of space charge can develop under AC excitation. This has been be explained by the inhomogeneity of resistance of the insulating material. It is reasonable to presume, however, that these space charge effects diminish in significance when compared to other possible degenerative mechanisms. [28]

Fundamental rules of electrical interactions state that charged particles are affected by electromagnetic force moving them towards any potential of the opposing sign. The

presence of opposite charge, or *heterocharge,* near the electrode contributes to the local electric field, lowering the total breakdown strength, and is therefore almost exclusively undesirable. On the other hand the presence of charged particles of the same sign, or *homocharge,* reduces the local electric field, increasing the apparent breakdown strength. With reversal of electrode polarities the heterocharge becomes homocharge and vice versa. [1]

Space charge formation can be seen as the combined result from charge-forming mechanisms, the movement of these charges, and the various mechanisms reducing the amount of charged particles. Most significant mechanisms behind the free charged particles are ionization and charge injection from electrodes, whereas electron-hole and anion-cation recombination inhibit space charge formation by actively reducing the amount of mobile charged particles. The formation of space charge is not limited to the movement of free particles, however, as the rearrangement of polar molecules can lead to distortion of otherwise uniform charge profile. These effects are known as polarization, and its extent will be discussed next, starting from various models used to explain the properties of insulating materials. [1]

3.1.3 Polarization

Polarization refers to charge separation in insulating material, as a result of applied electric field. It can be observed either on macroscopic level, looking at the properties of bulk material, most often as a function of frequency and electric field strength, or on microscopic level, trying to describe the interactions and movements of single atoms or molecules. The phenomena observed on macroscopic level are the sum of multiple mechanisms operating on molecular level. Let us discuss the macroscopic level first.

From a macroscopic viewpoint the insulation is considered as a layer of dielectric between two conductive surfaces. As such, an ideal capacitor model can be used to describe the effects of polarization and the quantities associated with it. Let us first consider a simple model based on an ideal capacitor consisting of two parallel plates with vacuum between them, illustrated in Figure 3.2a.

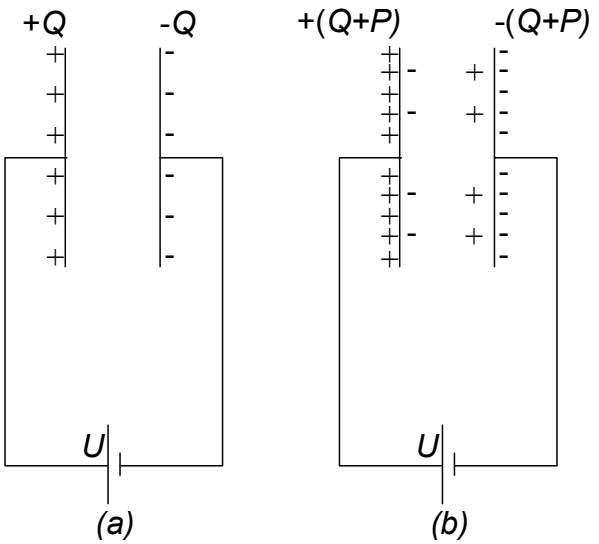

Figure 3.2. Two-plate capacitor models for (a) vacuum capacitor (b) capacitor with dielectric. Charge accumulates at electrode surfaces.

When the plates are connected to a voltage source, producing a potential of U, an electric field is generated between them. The resulting electric field, denoted as $\boldsymbol{E}$, is directly proportional to the applied voltage, and inversely proportional to the distance d between the plates. Despite being a vector field, for this perpendicular case the resulting electric field can be modelled with only one component, and by its magnitude alone, denoted as E:

$$E = \frac{U}{d} \tag{3.1}$$

The applied electric field leads to charge accumulation on the electrodes. According to Coulomb's law, the amount of charge stored on the electrode plates, denoted as Q, is directly proportional to the magnitude of this electric field:

$$Q = \varepsilon_0 E\,. \tag{3.2}$$

Constant ε_0 is called vacuum permittivity, having the value of $8.85 \times 10^{-12}\,\mathrm{Fm}^{-1}$. In case the vacuum is replaced with a dielectric, the dielectric reacts in the field by forming a local and opposing electric field, either by the formation of space charge described earlier or by the orientation electrically charged sections. This allows more charge to accumulate on the electrode surfaces, and leads to increased amount of charge stored, as illustrated in Figure 3.2b.

The effect the applied field has on the dielectric material is known as polarization, denoted by $\boldsymbol{P}$. Together with the aforementioned vacuum polarization their effects can be summed as electric displacement, denoted by $\boldsymbol{D}$:

$$\boldsymbol{D} = \varepsilon_0 \boldsymbol{E} + \boldsymbol{P} \tag{3.3}$$

The combined effects of vacuum and dielectric polarization can be accounted for by introducing a new variable, relative permittivity,

$$\varepsilon = \varepsilon_0 \varepsilon_r \tag{3.4}$$

where ε_r is a variable depending on the material, electric field strength, frequency and temperature [28], [29]:

$$\varepsilon_r = f(f, \boldsymbol{E}, T). \tag{3.5}$$

For simple line-frequency or direct voltage analysis under a limited and material dependent temperature range, polarization can be considered directly proportional to the electric field. Therefore feasible results can be obtained by regarding the relative permittivity as a material-specific constant. Using this, the equation for electric displacement can be rewritten as:

$$\boldsymbol{D} = \varepsilon_0 \boldsymbol{E} + \boldsymbol{P} = \varepsilon_0 \varepsilon_r \boldsymbol{E}. \tag{3.6}$$

Equation (3.6) is one of the fundamental principles used to describe dielectric phenomena. Electric displacement $\boldsymbol{D}$ is continuous between the capacitor plates, starting and ending at the charged electrodes, whereas local electric field $\boldsymbol{E}$ is not. This can be used to estimate the voltage distribution and local stresses in multi-layer insulators, which is especially useful when assessing the partial discharge probabilities in real dielectrics containing voids and other imperfections.

From a molecular viewpoint total polarization $\boldsymbol{P}$ is a sum of multiple relaxation mechanisms, each one representing a specific way the dielectric reacts in the applied electric field. For most mechanisms certain maximum frequency can be estimated, above which they stop working. Depending on the definition, three or four distinct polarization mechanisms can be recognized. The mechanisms themselves have individual frequency, electric field and temperature correlations. To successfully model the macroscopic properties of materials, it is often necessary to understand the underlying mechanisms, as the macroscopic properties are superposition from the various polarization mechanisms discussed next.

Electronic polarization results from the displacement of electron clouds in atoms under external applied electric field. Since the external field diminishes in strength compared to the interatomic forces, electronic polarization is relatively weak. On the other hand it can operate up to the highest frequencies, owing to the high mobility of electrons within the electron clouds. Electronic polarization is the only polarization mechanisms still working at visible light spectrum, being responsible for the refraction of light. [28]

Atomic polarization on the other hand results from the distortion of atomic nuclei in the dielectric material. As relatively large structures the nuclei have significantly lower mobility, and therefore atomic polarization stops working at a lower threshold frequency. The significance of atomic polarization is highly dependent on the material itself. Ionic materials generally exhibit notable atomic polarization, whereas other materials do not. [28]

The slowest of the traditional polarization mechanisms, orientation polarization, occurs only if the molecules in the dielectric contain permanent dipoles. Orientational polarization refers to the rotation and movement of these permanent dipoles. Depending on the size and mobility of the molecules these dipoles are bound to, it can take

significant time to develop. Orientational polarization is known to increase in effect with lower frequencies, which makes it possible to approximate the effective permittivity by using a Debye relaxation model, in which the relative permittivity is considered as a function of material-specific relaxation time τ and frequency ω. It should be emphasized, however, that albeit being mentioned often in literature, only in rare cases actual Debye-like relaxation is observed. For example polymer dielectrics are known not to follow the Debye model. In dielectrics where non-Debye behavior is observed advanced, often empirical or semi-empirical, models are called for, such as the Kohlraus/Williams/Watts (KWW) function and accompanied model. Even though these models ignore underlying phenomena, they are capable of representing the actual behavior. Due to their complexity these models are not discussed further in this thesis. [28], [29]

Fourth kind of polarization, known as Maxwell-Wagner-Sillars (MWS) polarization is only relevant at the lowest frequencies and for materials where inhomogeneous structure makes space charge accumulation feasible. For polymeric insulation systems at low frequencies and especially under DC excitation it is definitely relevant. MWS polarization represents the effects of space charge accumulation. Since the charged particles can travel relatively long distances, but at a low speeds due to their low mobility, it is not surprising space charge related phenomena can take considerably long time delays to develop. Even though this makes theoretical assessment difficult, a sophisticated model has been developed by the scientists it is named after. Owing to the complex nature of this model, it is not discussed further in this thesis, and readers looking for further information in either the Debye and non-Debye relaxation or MWS models should refer to e.g. [29].

Due to the long relaxation times, low-frequency MWS and dipolar polarizations tend to persist even after the external field is cut off. This is modelled as hysteresis in E-D plane. E-D hysteresis and nonlinearity, e.g. saturation at high fields, is highly analogous to the hysteresis loop observed in iron core transformers, and equally undesirable. [30] Inclusion of hysteresis into the already complicated relative permittivity model would require knowledge on the electrical stress history, making it time-dependent. This in turn would require it to be considered as a function of time. Since for commonly used insulating polymers the hysteresis loop is negligible, its effects can be ignored. It should be emphasized however that this may not be the case for modern high-energy-density materials, such as polymer nanocomposites, discussed later in subchapter 3.3.5, or multilayered films. Remnant polarization can have severe repercussions as it may result in significantly reduced energy densities and increased total losses.

Ignoring the hysteresis phenomenon for now, the threshold frequencies and the frequency dependency of total molar polarization are illustrated in Figure 3.3.

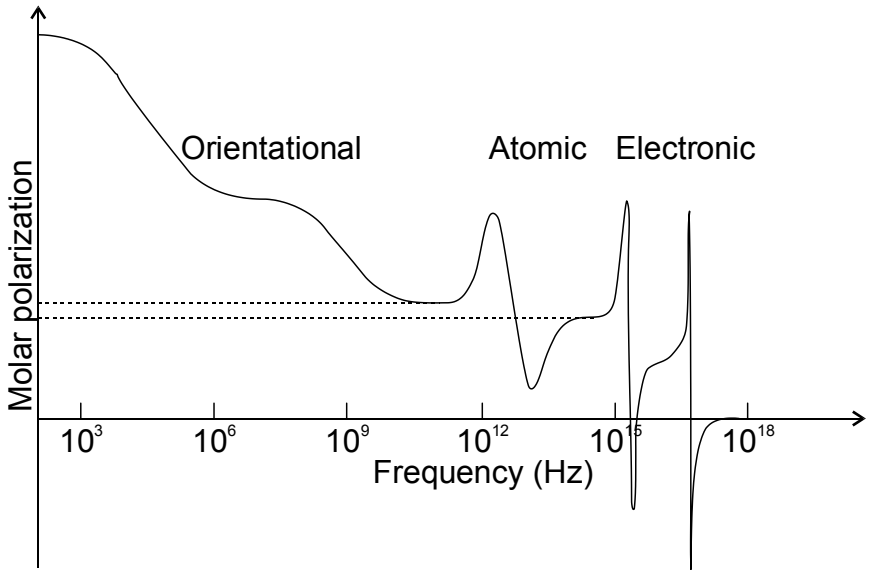

Figure 3.3. Polarization mechanisms and their step-like decrease at threshold frequencies. The distinct peaks correspond with increased losses near those frequencies [31]. *Adapted from* [28].

Since the effects of low-frequency MWS and orientational polarization is highly material and situation dependent, the chart is cut off from left, and more focused on the high-frequency mechanisms. The peaks seen at frequencies between 10^{12} and 10^{18} Hz are results from polarization mechanisms operating too slowly. They are known to correlate with increased dielectric losses in those frequency ranges. [31] On the other hand, the steady increase below 10^{9} Hz is related to material-specific orientational polarization mechanisms. Since the movements of the molecules contributing to these are usually hindered by i.e. their mutual interactions, this increasing orientational and MWS polarization is known to correlate with increased dielectric losses.

Another form of losses is introduced by the non-zero conductivity of real-world materials, which leads to leakage current flowing through the insulation. The various mechanisms behind this polymer conduction are not explained further, and readers interested in further information should refer to e.g. [16], [28]. To include these distinct types of losses in the aforementioned concept of permittivity, the capacitor model from Figure 3.2 needs to be expanded a bit further, which is done next.

Feasible results can be obtained by introducing a parallel resistance next to the ideal capacitance. This parallel RC circuit, as seen in Figure 3.4, represents the dielectric losses in the form of an ideal resistor and its ohmic losses:

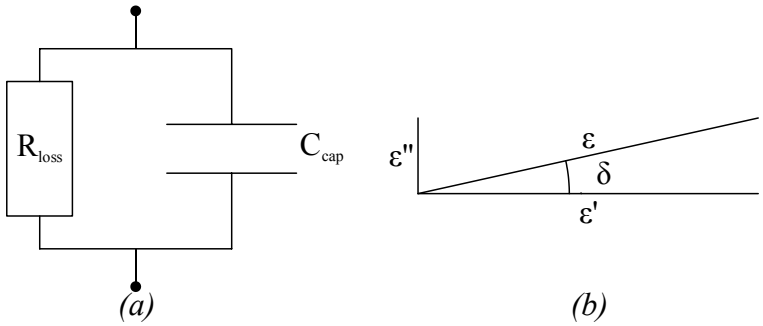

Figure 3.4. (a) RC circuit dielectric loss model and (b) resulting complex permittivity. Loss angle δ represents the angle between ideal and actual permittivities.

Whereas real permittivity *ε'* was used to represent the effects of polarization, imaginary permittivity *ε''* is introduced to account for the losses. Simple mathematical analysis shows that these can be plotted as a right angle. Using this, the total, resulting permittivity ε can be calculated. The tangent of the angle δ between the imaginary and real permittivities is known as loss tangent, tan δ. For ideal dielectrics the imaginary permittivity equals to zero, as does the loss tangent. For practical insulating materials the imaginary permittivity is miniscule compared to the real part, and the loss tangent can be approximated by using Equation (3.7): [31]

$$\tan\delta = \frac{\varepsilon''}{\varepsilon'} \approx \frac{\varepsilon''}{\varepsilon}. \tag{3.7}$$

The imaginary permittivity is directly proportional to the power dissipated in the dielectric, and the real part on the other hand directly proportional to the reactive power generated. By measuring these two quantities the condition of an insulation system can be measured. Possible degeneration can be seen as an increase in the loss tangent. These tan δ measurements are widely used when assessing the aging and condition of capacitor banks.

Due to the multitudes of mechanisms behind this simple approximation, it is no wonder the imaginary permittivity is highly frequency and electric field dependent. Frequency correlates with the polarization mechanisms, whereas the various conduction mechanisms discussed in [16] operate at separate electric field strengths, and some in a non-linear way. As a generalization the dielectric losses can be characterized with peaks at frequencies corresponding to the step-like increases in molar polarization. Even though the theoretical assessment of complex permittivity is difficult, good results can be derived from empirical dielectric spectroscopy measurements, as long as the measurements are done at field strengths comparable to real applications.

Finally, it is worth mentioning that the aforementioned capacitor model is not meant to portray actual capacitors. Instead, as was stated before, it is used to model the dielectric behavior and phenomena of insulating materials. To extend the model to represent whole insulation system used in actual capacitors, at least the electrical connections, resistances and structure-induced inductances should be included in the circuit model. This is done in subchapter 3.3. Readers interested in additional information should refer to e.g. [32], [33].

3.2 Electrical breakdown

3.2.1 Breakdown in general

As the voltage across an insulator is increased, the apparent current flowing through it increases. The measured current can be considered as superposition of both space charge movement and various conduction mechanisms. Excluding the space charge effects, the actual leakage current is small, and increases with increasing voltage. As the applied voltage is increased, various conduction mechanisms take effect, resulting in highly nonlinear and clearly non-ohmic U-I curve. [16]

As the voltage is increased, at some point the current rapidly increases, even if the voltage is held constant. A highly conductive channel has formed between the electrodes, and the current flowing through has become so notable the insulation is observed to lose its insulating properties. These breakdown events are characteristically both rapid and local, as most of the insulating area still remains intact. If the voltage across the insulator the moment before breakdown is noted as U_b, and the thickness of the sample at the breakdown area was *d*, the breakdown field E_b can be written as:

$$E_b = \frac{U_b}{d}. \tag{3.8}$$

Besides of being a material-specific property, the breakdown field is a function of the insulator thickness. To allow straightforward comparison between laboratory measurements and real-life insulators, often with varying thicknesses, an empirical formula known as power law has been determined. It states:

$$E_b(d) = kd^{-n}, \tag{3.9}$$

in which *k* and *n* are constants associated with the material in question. [34] According to Equation (3.9) the relative dielectric strength declines as the insulating layer gets thicker. This can be attributed to a higher percentage of voids and other imperfections, which may act as starting points for breakdowns at lower fields. Being a manufacturing issue, this can be partially overcome by stacking several thin sheets instead. [35]

For solid dielectrics the breakdown events are destructive, resulting in permanent loss of insulation; whereas for liquid and gaseous dielectrics the situation usually reverts if the voltage is sufficiently lowered. First breakdowns, associated with the lowest voltages, are usually results from imperfections in either the sample or the measurement setup. This justifies separating two concepts, the intrinsic or defect-free breakdown strength, and the actual breakdown strength observed in measurements.

The mechanisms behind breakdown events are based on the formation and movement of charge carriers. The mechanisms behind carrier formation are similar to the ones described in chapter 3.1, with most notable being ionization, collision ionization as a special case, charge injection, thermal movement, and when applicable the effects of electromagnetic radiation, such as light. The mobility and energy of these charge carriers is proportional to the applied electric field, but also dependent on

diffusion, electric charge, free space between collisions, inverse of mass and the inverse of the square root of temperature. At the same time various energy dissipating mechanisms act to either hinder the movement of these charges, or to remove them completely, with most notable being electron-hole recombination and charge carriers getting stuck in trap states. These trap states could represent for example attachment to molecules. Under normal conditions the charge-facilitating and charge-removing mechanisms are, or are progressing towards equilibrium. Breakdown occurs when this balance state cannot be reached. [28], [31]

3.2.1 Uncertainty in solids

There is considerably uncertainty in dielectric breakdowns observed in solids. This results from the multiple possible mechanisms behind the breakdown events, and the rapidly developing and destructive nature of these breakdowns, which makes retrospective analysis challenging. Various phenomena have been associated with breakdowns in solids. Based on their rate of progression one sensible way to assess these is to dissect them into two broader categories: rapid and degenerative. Rapidly progressing mechanisms are usually observed in breakdown tests with durations ranging from seconds to minutes. Slow, often degenerative mechanisms in turn are more often observed in real-world dielectrics after decades of constant use. Another aspect of uncertainty is induced by the interplay of these mechanisms, as they can progress either independently, together, or in a way that one mechanisms starts working where another stops. Despite the aforementioned difficulties, various breakdown mechanisms have been noted in literature, most notable of which will be briefly explained next. [16]

Intrinsic breakdown can either refer to so-called defect free breakdown strength, independent of the mechanisms, or to the ultimate breakdown strength proposed to act at electric fields in the range of excess 10kV/μm. Only a field of this magnitude can support electrons from the valence band to the conduction band, which according to the band gap theory discussed in Section 3.1.1 results in sudden loss of dielectric properties. Actual measureable breakdown fields are decades lower than the estimated intrinsic breakdown strength, which makes it justified to assume the intrinsic breakdown strength has little to none applications in real world. [12], [28], [31]

Electromechanical breakdown results from the compressive force and pressure caused by the electrode structure overpowering the resiliency of the dielectric. After the dielectric starts yielding, the decreasing distance results in even greater electric field and pressure, and the insulation collapses. It is not that relevant in terms of practical insulations. [31]

Electric breakdown starts from a local impurity or structural inhomogeneity causing disturbances in the local field. If the local field exceeds the maximum breakdown strength, the formation of a conductive breakdown channel starts. The actual process is the sum of multiple fast-developing physical and chemical degenerative mechanisms, which lead to the rapid destruction of the insulating material. The channel is not

necessarily straightforward, as it often branches, or forms so-called trees, before connecting electrodes, only after which it leads to the actual breakdown. [31]

Thermal breakdown occurs if the insulation cannot dissipate the heat induced to it, either by external heating or its own dielectric losses. Thermal stability is lost, and the internal temperature keeps increasing. In some materials increasing temperature leads to higher leakage current, which in turn increases the heat generated even further. This self-supported thermal runaway will eventually lead total to the loss of insulating properties, in the form of a breakdown. [31]

The aforementioned mechanisms are characteristically rapidly developing and relatively well-known, which makes them readily observable in short-term laboratory measurements. Real insulation systems are operated at electric fields substantially lower than what is needed to induce immediate breakdowns in laboratory setups. Therefore their breakdowns have to originate from different kinds of slow-developing degradation and aging mechanisms, which may lead to failures only after months up to several decades of use. These aging and degradation mechanisms are discussed later on in Chapter 4.

3.2.2 Testing considerations

To assess the dielectric strength of insulating materials various tests can be used. These tests can be coarsely divided into two broad categories, dynamic tests, where the applied voltage is a function of time, and static tests, where the voltage is held constant and times to breakdown are recorded [36], [37]. Dynamic tests are often preferred, since the variations in the acquired results are often smaller [36]. As a special case of static tests endurance tests, in which failures are not expected are used for quality control. [38].

The recommended testing procedures have been largely standardized by the International Electrotechnical Commission. Standards include but are not limited to standardization for tests at power frequencies in IEC 60243-1 [37] and direct voltages in IEC 60243-2 [39]. Besides these standards various technical specifications exist, such as CEI IEC TS 60871-2 [40], which describes endurance tests for power capacitors.

3.2.3 Statistical analysis

Methods for statistical analysis of breakdown data have been standardized in IEC standard 62539, *Guide for the statistical analysis of electrical insulation breakdown data* [41]. The standard covers the mathematical foundations used to calculate explicit distributions based on the breakdown data. These distributions are used afterwards when estimating breakdown probabilities at different voltage stresses, but only for similar samples as measured during testing. Despite this being the most commonly used approach to breakdown statistics; the concept of statistical analysis can be easily extended to include various scaling laws. These laws can be used to estimate the breakdown strength of practical insulations, often with vastly different characteristics, especially in terms of active area and exposure time. Even though this has been the basis

for design guidelines and limitations, these scaling processes are not standardized, and various studies, such as those covered in [42]–[45] implicate the scaling rules commonly used may lead to erroneous results. [41]

3.2.4 Failure probabilities

Breakdown phenomena are stochastic by nature. Therefore the events are seemingly random, and breakdown voltages measured for identical samples are known to show notable scatter. This can be attributed to breakdowns starting at local impurities and imperfections. The coincidental nature makes statistical analysis a feasible approach, especially since breakdown voltages are known to follow certain statistical distributions.

IEC standard 62539 explains the preferred methods for breakdown data processing, starting with the assessment of initial testing conditions. This is done to ensure the testing conditions have not been altered during testing. This is followed by the selection of the best matching distribution. After the seemingly appropriate distribution has been selected, its goodness-of-fit is evaluated. When the validity of the chosen distribution has been verified, corresponding confidence bounds are calculated, and the final results assessed. [41]

Various extreme value distributions are known to fit breakdown data. Extreme value distributions are used in a broad range of scientific disciplines to estimate events with extremely low probabilities, often with large deviations from the median. The reasoning behind their applicability to breakdown analysis lies in the weakest-link principle, as for many applications the dielectric strength of the weakest point or section defines the dielectric strength of the insulation system as a whole. As for another consideration supporting the choice of extreme-valued distributions, the breakdown areas are often miniscule when compared to the total insulating area. For the whole insulating system to withstand the electrical stresses imposed, the breakdown probability of each active area element needs to be extremely small.

3.2.5 Weibull distribution

The by far most commonly used distribution used for breakdown data analysis, and also recommended by IEC 62539 is the Weibull distribution. Weibull distribution can be represented either as two-parameter or three-parameter versions, where the two-parameter version is more often used for breakdown statistics. The more general three-parameter version is defined by three constants, α, β and γ.[2] Scale parameter or *characteristic life*[3] α is analogous to the median in Gaussian distributions, representing the failure probability of $1/e \approx 0.632$. Shape parameter β is analogous to the inverse of standard deviation in Gaussian distributions, and it is seen as steepness of the Weibull probability line. Small scatter of the data results in larger β values, whereas smaller

[2] It should be noted that multiple notations are used for the Weibull parameters, common variants including, but not limited to (α, β, τ) [19], (α, β, c) [20], (η, β, γ) [49].

[3] In the context of breakdown analysis term *characteristic breakdown field* is sometimes used.

values of β imply the events have a large deviation from the mean. Location parameter γ represents the voltage below which failure is physically impossible, and where the probability of failure is zero. Using the notation described above the cumulative density function (*cdf*) for a three-parameter Weibull distribution can be written as [46]:

$$\begin{Bmatrix} F(U) = 1 - e^{-\left(\frac{U-\gamma}{\alpha}\right)^{\beta}} & \text{for } U \geq \gamma \\ F(U) = 0 & \text{for } U < \gamma \end{Bmatrix}, \tag{3.10}$$

where $F(U)$ represents the probability of failure at voltages less or equal than U. Similar process can be applied for times-to-breakdown data. For most purposes, including breakdown mechanics in polymers, there is no obvious reason to use the location parameter γ [47]. Omitting the location parameter leads to a two-parameter Weibull distribution:

$$F(U) = 1 - e^{-\left(\frac{U}{\alpha}\right)^{\beta}}, \tag{3.11}$$

which is the most commonly used form. The effects of the parameters are illustrated in Figure 3.5. The computer-generated data is a result from multiple Monte Carlo simulations with 1000 points for each distribution. [41], [46]

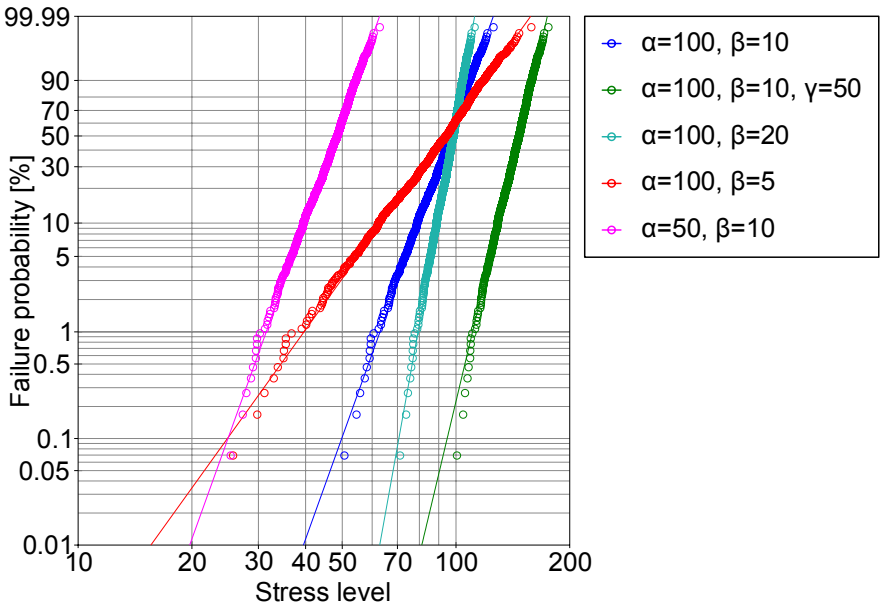

Figure 3.5. Weibull distribution can be characterized with two or three parameters. Parameter choices are reflected in the steepness and position of the probability line.

Despite statistical analysis is often conducted using specialized software, Weibull plotting is simple enough to be done using pen and logarithm paper. The process is as follows, starting from a group of N samples. If all samples broke down during testing, the data set is viewed as complete. In case some samples didn't break, the set is censored, and different operations apply. Since most of the time the test is continued until all samples break down, censored sets are less relevant. Readers interested in those should refer to e.g. [46]. Plotting of the corresponding Weibull distribution can be done by ranking the breakdown voltages, starting from the lowest one, by giving them ranks

from $i=1$ to $i=n$. These points are then associated with corresponding percentages. The cumulative failure probabilities can be approximated with equation (3.12) [48]:

$$F(i,n) \approx \frac{i-0.44}{n+0.25} \times 100\% . \tag{3.12}$$

Various techniques can be used to estimate the model parameters from these points. These parameter estimation methods are universal, and they are usable for a wide range of distributions. Albeit multiple methods may be viable, they can result in dissimilar results. This makes it advisable to refrain from altering the estimating methods between different sample groups.

The simplest form of parameter estimation is to plot the ranked values calculated using for example Equation (3.12) on a probability paper. With a suitable choice of probability paper the distribution can be linearized, and the model parameters can be estimated visually. Albeit simple to conduct, due to its reliance on hand-drawn lines using often scattered probability points as a reference, different people may come up with different results. Due to these issues the use of this *probability plotting method* is fairly limited to demonstration purposes only. [49]

Advanced methods to estimate model parameters include rank regression and maximum likelihood estimation. Rank regression is in essence the mathematical version of the aforementioned probability plotting. By utilizing so-called least squares principle, it will try to minimize the distance between the probability line and the rank values. This can be realized in either X or Y directions, both of which resulting in different outcomes. [49]

Maximum likelihood estimation or MLE tries to determine the most likely values for the parameters of the underlying distribution. Omitting the mathematics behind it, MLE is considered to be especially suitable for larger sample pools. With sufficient number of samples the estimated values converge with the right values. As a drawback a large amount of samples is needed, with the exact amount cited to be from thirty to over a hundred. Without a large enough sample pool MLE estimates can be biased. Furthermore, under certain conditions MLE results do not converge. Albeit these problems limit the applicability of MLE, it is considered as one of the more robust parameter estimation techniques. [49]

Specialized software can be used to calculate the parameters. Besides of allowing the user to choose between various parameter estimation methods, they may allow user to choose between various ranking methods and offer multiple methods for confidence bounds estimation. Due to the complexity of the mathematics behind these methods further discussion is omitted. Readers interested in additional information about any of these methods and the mathematics behind them should refer to e.g. [46], [49].

It is worth noting that the model parameters might, or might not correlate with the actual breakdown mechanisms. For some cases the correlation can be validated easily. One example being the Weibull-γ in the three-parameter Weibull distributions, since in some cases certain minimum voltage exists, under which breakdown is physically impossible. Nevertheless due to the complexity of breakdown mechanisms, especially in

solids, care should be taken before associating any estimated parameters with physical phenomena.

3.2.6 Other distributions

Gumbell distribution represents another extreme value distribution. Albeit being mentioned in IEC 62539, it is seldom used. Gumbell distribution is closely related to Weibull, as if k has a Weibull distribution, then $t = \ln(k)$ is Gumbell distributed. Taking advantage of this the cumulative density function for a Gumbell distributed variable t can be written as [41]:

$$F(t) = 1 - e^{-e^{\left(\frac{t-u}{b}\right)}}; -\infty \le t + \infty, \tag{3.13}$$

where u and b are the location and scale parameters respectively.

Albeit applying normal distribution for breakdown data results in erroneous results, its logarithmic variant known as lognormal distribution, has been used to represent breakdown data. Despite being mentioned in IEC 62539, it is very rarely used. [41]

If a single matching distribution cannot be found, multiple distributions each with their own weighting coefficients can be mixed together. Multiple ways to mix these distributions exists, and for example additively, multiplicatively and exponentially mixed distributions are presented in literature. [50] The use of mixed distributions, such as combining two or three two-parameter Weibull distributions, each with varying α and β, into one, arises from the multiple breakdown mechanisms described in 3.2.1. The breakdowns caused by single dominating mechanism can be plotted with one distribution, but if the breakdown voltages span over relatively large region, the different characteristics of breakdown mechanisms at low, medium and high electric fields, and their interplay at the corresponding transition points result in a so-called S-curve. The demand for these mixed distributions is notable especially when a large number of samples or a large number of breakdowns are measured. Breakdowns at very low and very high fields are uncommon, with most breakdowns concentrating in certain characteristic medium field strengths.

The goodness of the distributions can be evaluated either visually or mathematically by performing certain goodness-of-fit tests, such as the Chi-Squared-, (modified) Kolmogorov-Smirnov-, or a simpler Weibull-specific tests explained in [41]. Due to the complexity of these tests, their mathematical foundations are out of the scope of this thesis, and they are used as-is functions in reliability analysis software. These are used as indices, to ease the comparison between various models. Readers interested in additional information should refer to [41], [46].

3.2.7 Scaling laws

Another viewpoint to statistical analysis is to consider a material-specific absolute distribution, or absolute curve. For thin films this distribution can be seen to represent the breakdown probability curve of an undefined very large area, or when the tested

area approaches infinity. Since practical insulation systems are generally large in size, the absolute curve could be used as-is to approximate the breakdown probabilities of realistic insulation systems, such as power cables or HV capacitors. As the measurement area is increased, the measured curves start approaching this absolute curve asymptotically.

The estimation of this underlying curve is problematic in two ways. First one is related to the measurement area needed to get close enough to the absolute curve. Large areas are needed to record enough breakdowns to successfully approximate the very low and very high breakdown probabilities. Low field and low probability breakdowns are related to the inherent weak spots. Since manufacturing processes are stringently supervised, the density of these weak spots remains low. Regardless of their relatively low density, they exist, but large measurement areas are often needed to capture them. Consequently the probabilities in the low field region are extremely low and at the same time often the most interesting. In a similar way the high-field breakdowns are relatively scarce, but for the opposite reasons, as most samples fail before these high electric fields can be reached. In traditional breakdown measurements small areas are needed to record these high field breakdowns. In general, due to the inherent scatter associated with the stochastic nature of breakdown phenomena, large testing areas need to be tested and a large number of breakdowns should be to be recorded for accurate approximations. Even more data points are needed to estimate the confidence bounds adequately.

Large-area testing is often cumbersome and in many cases unfeasible, and determining the relationship between measurement area and the dielectric strength would allow straightforward extrapolation of the results acquired via small sample testing to real insulations. Certain method for doing this area extrapolation will be discussed next.

Let us first consider a traditional breakdown test in which a small number of small samples area measured. The total measured area is marked as A_1. One breakdown is measured for each sample, and applying Weibull distribution to these results has resulted in a Weibull probability line with parameters α_1 and β_1. The probability of defects being included in the sample pool was low, and a majority of the breakdowns occurred in samples without defects. Therefore these breakdowns represent the intrinsic breakdown behavior, as there was only one breakdown mechanism behind the breakdowns. A few or more probably none of the data points were in the extreme low or extreme high probability regions. Regardless, we can extrapolate the line from the medium probability regions to include these regions.

Next a larger number of samples with a larger total test area of A_2 is measured. Sufficiently large measurement area makes it more probable that some weak spots were present in the samples, and some data points with low breakdown fields located in the low probability regions of the probability plot are recorded. If very small samples were used it is probable a number of them broke down only after higher than average fields. If so, some data points in the high probability region are recorded.

If the low- and high field points align well with the medium probability points it may be assumed only one breakdown mechanism is dominating in all regions. If they do not, it can be presumed different mechanisms operate at these field regions and the area scaling discussed next does not apply. We will return to the latter case later on in this chapter.

The Weibull parameters for a larger measured area A_2 can be estimated from the parameters calculated using a smaller active area A_1. Due to the characteristics of the Weibull distribution the shape parameter β is not area-dependent and remains unchanged, whereas the scale parameter α_2 is shifted towards lower voltages. This shift can be approximated by using the area scaling law, which states [51]:

$$\alpha_2 = \alpha_1 \left(\frac{A_2}{A_1} \right)^{-1/\beta} . \tag{3.14}$$

The accuracy of this approximation is highly dependent on the material. Despite the approximation from Equation (3.14) has been shown to produce good results in some studies [52], in many studies such straightforward extrapolation is shown to fail [36], [45], [53]–[55]. These failures can be accounted for to the introduction of separate low and high field breakdown mechanisms, which divert the curve from the approximated line in these regions.

For these reasons the validity of the area scaling law should be assessed separately for each and every measurement and material. For some cases it can be readily used to approximate the underlying distribution, whereas for other cases the results produced by area scaling are erroneous. For the latter case the approximated lines do not converge with the aforementioned absolute curve, and more comprehensive measurements are needed to assess the realistic dielectric strength observable in large-scale insulations.

3.2.8 Survival chances

From a practical viewpoint it is not the failure but rather the survivability[4] of the insulation that is the most interesting. To assess this, a new reliability function known as dielectric survival $S(\boldsymbol{k})$ is defined, where $\boldsymbol{k}$ determines the operating point. Since only two states are allowed, the relationship between the unreliability function and failure probability $F(\boldsymbol{k})$ and survival function can be written as [42]:

$$S(\boldsymbol{k}) = 1 - F(\boldsymbol{k}) . \tag{3.15}$$

Let us consider a simple case where survivability is a function of time t, electric field strength E and insulation area A. Using this the operating point $\boldsymbol{k}$ can be written as $\boldsymbol{k} = \langle t, E, A \rangle$. The survival function is assumed to follow Weibull distribution, and it can be written as

$$S = e^{\left(-\left(\frac{t}{t_0} \right)^a \left(\frac{E}{E_0} \right)^b \left(\frac{A}{A_0} \right) \right)} , \tag{3.16}$$

[4] Survivability is a synonym to reliability, a term often used in literature.

where t_0, E_0 A_0 sets a reference point, and a and b are experimentally defined constants [16], [42]. As can be seen from Equation (3.16), increase in one parameter, for example in area, needs to be compensated to by either lowering the applied voltage or reducing the exposure time. Normally both the active area and the exposure time are substantially higher than at the reference point measured at laboratory conditions. This needs to be compensated by lowering the maximum tolerable voltage, which, as will be shown later, leads to quadratic loss in energy density. The concept of energy density and various other repercussions Equation (3.16) has on capacitor design principles are discussed next, starting from the capacitor fundamentals.

3.3 Practical applications

3.3.1 Capacitor fundamentals

Since the advent of electricity capacitors have been integral parts of more or less every electronic appliance devised. Owing to their usage in vastly different electronic subdisciplines and to the different requirements imposed thereof, it is no wonder capacitors come in every shape and size, and with exceedingly different characteristics.

Even though no strict framing exist, most capacitors have been designed for specific applications. Judging by the application they excel in capacitors can be divided into three broad categories: direct voltage, alternating voltage and pulsed power capacitors. Under these three categories various subcategories do exist, and for example AC capacitors can be divided further into line-frequency and high frequency (RF) applications.

A capacitor consists of conductive electrodes, separated by a layer of dielectric material, as illustrated in Figure 3.6:

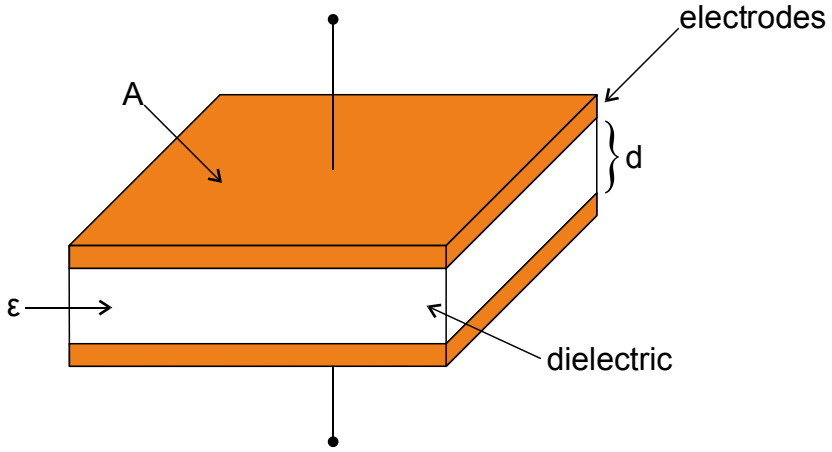

Figure 3.6. Albeit simple, parallel plate capacitor model can be used to explain basic capacitor concepts.

This parallel plate model is similar to the one discussed in subchapter 3.1 but for simplification the relative permittivity ε_r of the dielectric can is regarded as a constant. Whether or not this approximation will pull off depends heavily on the materials and

electric fields involved, and its validity should be considered individually for every case.

As discussed earlier, applying potential U across the capacitors leads to accumulation of charge Q. The relationship between the Q and U is evaluated as the apparent capacitance C, or:

$$C = \frac{Q}{U}. \tag{3.17}$$

For the idealized parallel plate model illustrated in Figure 3.6 the capacitance can be written as:

$$C = \varepsilon \frac{A}{d}. \tag{3.18}$$

The unit for capacitance is farad, F, which is defined as the capacitance required to store a charge of one coulomb at a potential of one volt. Even though farad was previously considered as an excessively large reference unit, nowadays supercapacitors with capacitances of several farads are produced. [56]

The accumulation of charges Q and -Q comes with equivalent increase in potential energy. If we consider Q=0 as the starting point and the capacitor lossless, the work either done or received during charging or discharging can be written as [12]:

$$W = \int_0^Q U(q)dq = \int_0^Q \frac{q}{C}dq = \frac{Q^2}{2C} = \frac{1}{2}CU^2. \tag{3.19}$$

As seen from Equation (3.19), the energy stored is proportional to the capacitance and to the square of the potential difference. Omitting the steps required, but applying the principles of Equation (3.18) to (3.19) results in an equation for energy density, or U_D which can be written as[5] [42], [57].

$$U_D = \frac{1}{2}\varepsilon_0 \varepsilon_r E^2. \tag{3.20}$$

Since energy density is independent of the capacitor geometry and dimensions, it allows straightforward comparison between various choices for dielectric materials. This sets some of the guidelines for capacitor development, as it demonstrates the two possible means to increase energy storage capacity. This can be done either by increasing the maximum tolerable voltage or by increasing the relative permittivity. On the other hand even a slight decrease in electric field strength leads to radical losses in energy density, unless compensated by considerable increase in relative permittivity. [1], [57]

For practical applications the energy density is often considerably lower than the in the ideal case in Equation (3.20), since a significant volume of the device is not storing energy. This space is not wasted, but used for interconnections, fuses, insulations and for the structural frame. Packing factor, or *PF*, is introduced to account for the packing

[5] In older literature such as [42] the relative permittivity ε_r is often denoted as K.

efficiency. This drastically reduces the energy density, down to between 30% and 70% from the idealized values. [42]

For better understanding of capacitor mechanics various equivalent circuits are used. These models are built around the idealized capacitance C. To account for the resistance and inductance caused by the electrical connections in or between the dielectrics and capacitor terminals both series resistance R_S and inductance L_S are added. As discussed earlier in Subchapter 3.1 the leakage current due to the nonzero conductivity of real dielectrics and the dielectric losses will be taken into account by introducing parallel resistance R_P. A capacitor model consisting of these components is illustrated in Figure 3.7.

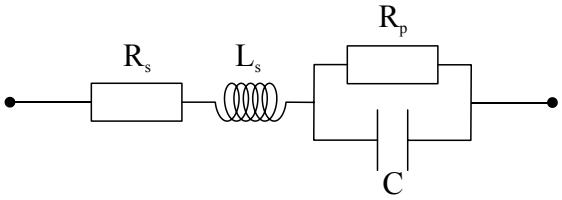

Figure 3.7. Capacitor equivalent circuit with series and parallel components can be used to explain the more complicated phenomena at higher frequencies.

In many applications the operating frequency is either constant or varies over a limited ranged, and the equivalent circuit from Figure 3.7 can be simplified by calculating the combined resistance of R_S and R_P at the operating frequency. This resistance is marked as equivalent series resistance, or ESR. In addition to being frequency and voltage dependent, ESR is current dependent, but only when the peak currents rise in to the region of multiple kilo amperes. The current dependency arises from ohmic heating caused by oxide layers between compression contacts. Unlike ESR, the series inductance, often cited as ESL, is mostly dependent on the capacitor geometry and structure. This justifies regarding it as a constant over the usable frequency and voltage ranges. [35] This circuit is illustrated in Figure 3.8 below.

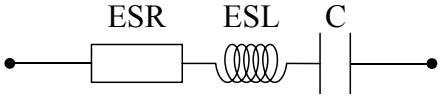

Figure 3.8. Capacitor equivalent circuit with series components is an approximation, adequate for all but the most detailed calculations.

Various practical qualities can be defined with the help of the concepts defined earlier. The capacitive reactance, or X_C, can be written as

$$X_C = -\frac{j}{\omega C}. \tag{3.21}$$

From power engineering viewpoint often the most interesting value is the reactive power generated, or *Q:*

$$Q = I_{RMS}^2 X_C = \frac{U_{RMS}^2}{X_C}. \tag{3.22}$$

The unit for reactive power is volt-ampere reactive, or VAr.

In a similar way the energy dissipated or lost in the ESR can be written as:

$$P_{LOSS} = I_{RMS}^2 R_{ESR}. \tag{3.23}$$

Since the capacitances and losses vary over a wide range depending on capacitor size and application, easily comparable indicator can be acquired by introducing a new variable, dissipation factor DF, which is defined as:

$$\tan\delta = DF = \frac{R_{ESR}}{X_C}. \tag{3.24}$$

It should be noted that this dissipation factor differs from the loss tangent defined earlier in Subchapter 3.1.3., as the loss tangent defined earlier was defined only using the parallel resistance. Nevertheless for most applications the series resistance is miniscule compared to the parallel resistance, and from a practical viewpoint the two concepts are effectively same.

In addition to the dissipation factor, the goodness of a capacitor can be evaluated by using Q (Q for Quality) values. The equation for Q value can be derived from Equation (3.24) [35]:

$$Q = \frac{1}{DF} = \frac{1}{\omega RC}. \tag{3.25}$$

In times gone by these Q values were used in RF engineering to evaluate various capacitor choices.

As was stated in Equation (3.21) the capacitive reactance of a capacitor decreases with increasing frequency, whereas the inductive reactance of ESL increases with increasing frequency, or

$$X_L = \omega L. \tag{3.26}$$

At certain frequency the reactances cancel out each other. At this operating point the equivalent circuit reduces to ESR alone. This self-resonant frequency, or SRF, can be written as [58]:

$$\omega_{res} = \frac{1}{\sqrt{LC}} \tag{3.27}$$

Since large currents can flow through the capacitor when operating near or at the SRF, design guidelines recommend staying far below it. Above the SRF the capacitor operates as an inductor, which complicates things further. As a rule of thumb larger capacitances result in lower SRF values, but for low-frequency applications such as 50/60Hz AC the SRF frequencies are magnitudes too high to be relevant.

Even far below SRF frequencies the presence of inductance may turn out problematic. Since inductance acts as a current limiter, or

$$\frac{di}{dt} = -\frac{E}{L}, \tag{3.28}$$

the rise time before peak current is reached is increased with increasing inductance. This proves to be an issue for pulsed power applications, where sharp pulses are needed. For such cases special designs are implemented to minimize both internal and external

inductances. On the other hand for line frequency and DC applications typical inductances pose no problem. [35]

Besides the aforementioned and well-known electrical qualities capacitors are designed to meet various design criteria. These include, but are in no means limited to capacitance tolerances, voltage reversal, and peak discharge current.

Apart from these purely electrical properties, capacitors are designed to meet design criteria imposed by various environmental conditions. Certain examples of these include operating temperature, humidity, vibration, and in special cases such as aeronautical usage altitude and ambient pressure.

One of the most eminent environmental restrictions is the expected ambient temperature and its variations. Variations in temperature are known to correlate with sometimes drastic changes in capacitance, losses and especially in case of high temperatures reduced lifetime and reliability. To some extent these effects can be mitigated with material choices, but this will often lead to compromises in other aspects, such as energy density. Another solution for low temperatures is to implement external heating, but the price for it is rather steep. [35]

Regardless of their properties and intended usage, capacitors can be divided into four categories based on their mechanisms of operation; thin film, electrolytic, ceramic and supercapacitors. Since the focus of this thesis lies in thin films and their applications, the other three are omitted from discussion. Readers interested in comprehensive review of capacitor techniques should refer to e.g. the literature works by Sarjeant [35] and Nishino [59].

3.3.2 Film/foil capacitors

Thin film capacitors can be divided into two categories, film/foil capacitors being the first. They consist of alternating layers of conductive aluminum thin films connected to either of the electrodes. The weak point in such design is the foil edge, where deleterious partial discharging tends to occur at high fields. The edges of these aluminum layers can be folded twice over or less frequently precision cut using lasers to produce a smoother edge, both of which increase the inception voltage of partial discharges. The electrode foils are insulated from each other by dielectric sheets with margins sufficiently wider to prevent flashovers. [35]

Depending on the requisite properties, various materials have been used as dielectrics. Traditionally power capacitors, such as those used for power conditioning and reactive power compensation, have used oil-impregnated Kraft paper as the insulating medium, but nowadays biaxially oriented polypropylene (BOPP) and polyethylene terephthalate (PET) dominate, among other polymer films. It used to be that of polymer films only PET was suitable for low voltage designs, as it could be made thinner than 0.5µm. The situation is changing, however, as although the minimum attainable thickness of polypropylene film has been around 3µm, even thinner films are being introduced into the marked recently. [60], [61]

The relative permittivity of polymer films is considerably low, around 2.2 for PP and 3.4 for PET; especially when compared to high permittivity ceramics such as barium titanate with ε_r of 1000. However, for basic polymers the low relative permittivity comes hand in hand with low dielectric losses. As a downside, looking back to Equation (3.20) this results in film/foil capacitors having considerably lower energy densities on low voltages, where other designs are often therefore preferred. [57]

The advantage of film/foil polymer design lies in their remarkable dielectric strength, in excess of 700V/µm, partly due to their uniform composition. This is considerably higher than for porous ceramics and electrolytic designs, which makes film capacitors the only feasible approach when high voltage applications are considered. [60]

Despite comparatively rare, weak spots exist in even the most diligently fabricated films. This is problematic since the first breakdown will render the insulation useless, resulting in a broken capacitor. To resolve this, multiple layers of thin dielectric are stacked on top of each other. This way the probability of multiple weak spots ending up on top of each other is kept infinitesimally low, and overall reliability is greatly improved.

Despite these precautions weak spots might exist or the insulation might fail due to local, often unknown circumstances. The resulting short circuited capacitor could render the whole system unusable, or in worst case of series capacitor arrangement, impose greater electric field strength in the remaining units, leading to a catastrophic domino effect. Since larger capacitor units consist of multiple individual capacitor elements, stacked both in series and parallel, fault-tolerance is realized with the use of fuses. These fuses are installed between the discrete elements. In case a breakdown occurs the current surge from adjacent elements burns them, leaving rest of the capacitor intact. This isolates the faulted portion, but at the cost of a significant capacitance reduction. Therefore breakdowns are extremely undesirable. To prevent them, considerable safety margins are used when setting the limits for maximum tolerable voltages, as imposed by Equation (3.16). For example, as a general guideline applied by Nokian Capacitors, the maximum nominal electric field is no more than 78V/µm, close to 1/10 of the often-cited 700V/µm for the film alone [62]. An example of the element arrangement is illustrated in Figure 3.9. Fuses are located between discrete elements.

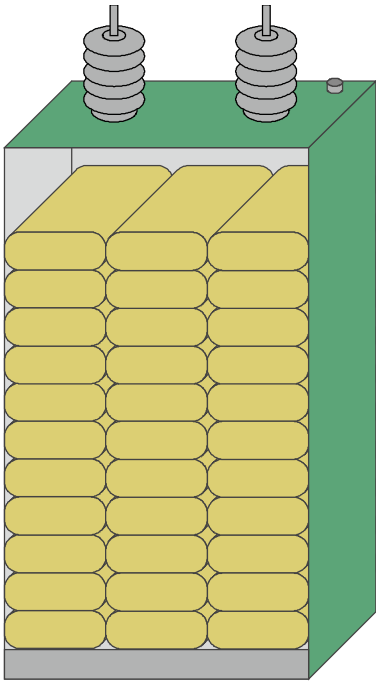

Figure 3.9. Larger film/foil capacitor units are made of smaller capacitors elements both in series and parallel. Fuses and bleeding resistors between them offer some protection against short-circuits and residual charge respectively.

Two distinct ways to interface the conductive layers to the end terminals exist, first one being tabbed windings. In this arrangement safety margins are left on both sides of the electrode, and connection is made through tab ribbons. The inductance of this tabbed arrangement is generally low, which makes it suitable for extremely fast pulsed power applications. [61]

More common way is to extend one edge of the electrode foils over the dielectric layer, leaving sufficient margin on the other side. This offset arrangement allows end connection slabs to be soldered over a large area, resulting in highest peak current withstand, only limited by the additional inductance compared to the tabbed windings discussed before. The peak current withstand is further increased by the metallic bonding between the conductors and electrode sheets, as it results in minute resistance and therefore negligible ohmic heating. [61]

After sufficient numbers of layers have been stacked, the structure is rolled up and fastened into a cylindrical case, or rolled up and then flattened to allow rectangular housings to be used. These processes often impose considerable physical stresses on the dielectrics, lowering the film integrity, aging compensated by lowered operating fields as discussed earlier.

Capacitor elements are traditionally immersed in insulating liquid. To promote the liquid impregnation, the dielectric surface is often textured, also known as HAZY®. This liquid impregnation process consists of vacuum treatment and simultaneous drying, followed by the inclusion of the impregnating liquid. After the capacitor unit has been hermetically sealed, it is heat treated or *formed* to promote stabilization. Modern

impregnating liquids are generally synthetic and highly aromatic liquids, which work by reacting with atomic hydrogen, suppressing partial discharges. [63]

In addition to suppressing partial discharges, the temperature dependency of the capacitance can be reduced by proper selection of impregnant. This is based on the opposing temperature-capacitance relationship between the solid and liquid dielectrics. [35]

The adverse effects of the impregnation include minor additional power losses and swelling of the dielectric film. Amorphous areas of polypropylene tend to dissolve, and the film can lose as much as 6 to 7% of its dry weight over time [64]. Besides these, given sufficient initial heat the impregnating liquids themselves are flammable. Since heat is often produced in the event of dielectric breakdown and sequential failure, possibility of electric fire exists. [35] Additionally the congealment of the liquid limits the lowest permissible operating temperatures. In the temperature range of -40…-50°C the reduced fluidity of the impregnant has been linked with lowered the partial discharge inception voltage at the electrode film edges. [62]

Even though all film/foil capacitors need to be shielded against moisture and atmospheric oxygen, it is not always done by liquid impregnation. In dry capacitors this is done by filling the structure with epoxy resin, which sets after a period time. Despite traditionally used only for low voltage applications, some high voltage units based on dry designs have emerged to the market. [65]

3.3.3 Metallized film capacitors

Contrary to the aforementioned traditional film/foil capacitors in metallized film capacitors the electrodes consists of thin, in order of 10nm [66] – 100nm [64], layers of metal deposited on the dielectric film surfaces. The metallization is facilitated by corona treating the film. In corona treatment the film is laid on an earthed surface and a planar electrode is moved above it, with an air gap between. The planar electrode is at potential in the range of several kV. The local electric field in the purposefully non-uniform parts on the electrode surfaces is high enough to sustain a continuous corona discharge, which generates plasma consisting of charged particles e.g. ions and electrodes. The electric field accelerates the oppositely charged ions, and they are propelled away from the electrode towards the earthed plate. [67] The film surface acts as a barrier in which the ions remain. The accumulation of ions results in increased surface charge density, making proper adhesion of the metal coating possible. Corona treatment is especially important for films which are not polar by nature, polypropylene being one example [66], [68].

After the corona treatment the metal layer is deposited by using a process known as physical vapor deposition (PVD). The base metal in question is either pure aluminum or aluminum/zinc alloy, and sometimes small amounts of alloying metals are added to prevent corrosion [61], [64]. PVD is a parent term for various vacuum deposition processes, where metal is first vaporized, then transferred as gas, and finally condensed on target surfaces. It should be noted that neither corona treatment nor PVD processes

are exclusive to thin film metallization, as both processes find use in diverse trades, from photography to semiconductor fabrication. [69]

The metallization profile is almost never uniform. First of all a free margin without metallization is left on one edge to provide sufficient protection against flashovers. Secondly, the metallization is often profiled as a slope, increasing in thickness towards the edge where end connection is made. Alternatively, the metallization can be of uniform thickness in the middle, but with one reinforced edge towards the end connections. The reasoning behind this lies in the increasing current towards the connector end. Such reinforcing is needed to keep losses at reasonable levels and to prevent heat induced damage to the electrodes. [61]

The resistivity of metallized films is often expressed as sheet resistance, with ohms per square (Ω/sq) as the unit. The resistance of any three-dimensional uniform object can be written as:

$$R = \rho \frac{l}{wt}, \tag{3.29}$$

where ρ is the resistivity, l the length, w the width and t the thickness. For an object with uniform thickness, both thickness and conductivity can be combined as sheet resistance R_S, or

$$R = \frac{\rho l}{tw} = R_S \frac{l}{w}. \tag{3.30}$$

The resistivity of the metallization in metallized film capacitors is in the range of few to hundreds of ohms per square. Sheet resistance makes comparison between different materials easier, as the value is independent of sample area size. For any arbitrary square length divided by width equals to unity, and the resistance measured between the edges equals to R_S. [66], [70]

Regardless of this reinforcing, the metallization is very thin compared to film/foil capacitors. This limits the maximum power density, as expressed with the maximum allowed instantaneous power output. Besides, due to the higher resistance, total losses in metallized film capacitors are generally higher than in film/foil variants. [61]

Despite the aforementioned weaknesses, the fundamental weak point and limiting factor in metallized film designs is the end connections [66]. The end connections are manufactured or *schooped* by plasma spraying metal on the reinforced ends of the capacitor winding. The metallized portions of the films are interleaved to leave sufficient margin between electrodes. [61], [63] Such arrangement is illustrated in Figure 3.10.

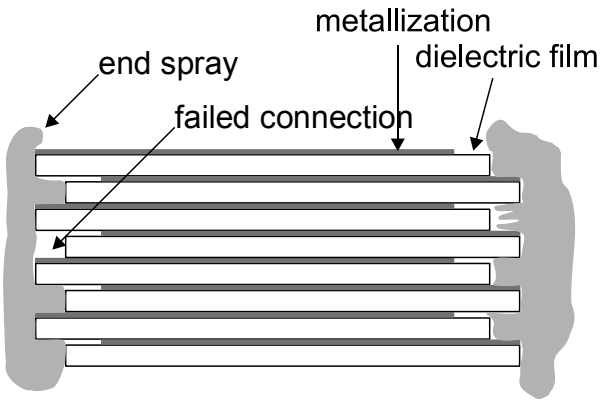

Figure 3.10. Offset arrangement used in metallized film capacitors provides adequate contact and protection against flashovers. [61]

Due to practical limitations, the metal particles in plasma spraying are significantly larger than the nominal free space between the dielectric films. The difference of magnitude is around 50µm versus 10µm. This thwarts the metal particles from penetrating the winding properly, and the contact between the end connection and metallization is not continuous, and far from perfect. [66]

According to the research done by Boggs et al., the end connection and metallization are not bonded metallically, but rather by the compression forces. This imperfect contact correlates with increased ohmic losses. Besides being the primary limiting factor at higher current densities, the end contacts also act as the primary center of degradation. The situation is made more difficult as the connection resistance has marginal effect on dissipation factor, making conclusive measurements at low current densities virtually impossible. Due to the presence of imperfect contact the aging mechanisms of metallized and film/foil capacitors are vastly different. These aging mechanisms are discussed further in Chapter 4. [61], [66]

Similarly to film/foil capacitors, traditional metallized film designs have used impregnating liquids to inhibit corona at film edges. Besides all-out impregnation, partial impregnation and especially dry designs are viable options. In partial impregnation only the film edges are immersed, while the middle part is left dry. In dry designs, which represent a majority of capacitors manufactured nowadays the capacitor element is filled with epoxy resins. [63], [71]

3.3.4 Clearing phenomenon

The major advantage of metallized film designs over traditional film/foil capacitors is their inherent ability to self-clear. Clearing allows metallized film capacitor units to survive multiple breakdowns without noticeable changes in capacitance or other electric properties, contrary to the large capacitance reduction or total failure observed in film/foil designs.

Clearing, or self-healing as it is often called, stands for the phenomena observed during and shortly after a breakdown occurs in the metallized dielectric. As a breakdown occurs, high current and high energy starts flowing through the newly

formed low-resistance short, forming an arc. The temperature of this arc rises to several thousand Kelvins, at which temperature both the faulted dielectric and nearby metallization combust, breaking down to atomic level. As the arc burns increasingly large area around the fault is left without metallization, and finally the arc extinguishes. Various contradicting theories have been presented in e.g. [72], [73] about the reasons behind this, and the subject is open to debate. Nevertheless, at this point the faulted spot has cleared, and with the weak spot gone, the remaining dielectric is able to withstand even higher electrical stresses. [63], [64], [73].

The areas destroyed during the clearing events are trivial, cited to be in between 2 and 8mm^2, when compared to total area of the dielectric often exceeding several square meters. Besides the clearing events are rapid, resulting in no interruptions in normal operation and negligible voltage drop at the terminals. For these reasons, capacitors can withstand numerous clearings during their lifetime. This brings about the often-cited term graceful failure, as metallized films capacitors tend to degrade predictably, without catastrophic failures. [63], [64]

Clearing events themselves can be categorized in two phases. Preclearing is done immediately after manufacturing. The capacitor is subjected to voltages above nominal, with intent to erase inherent weak spots. Secondary clearing happens during normal operation, as a result from various aging mechanisms starting to degrade the insulation performance. Metallized capacitors are considered to be at the end of their life cycle when the total capacitance loss is between two and five percent. The clearing process is illustrated in Figure 3.11 below. [61], [64]

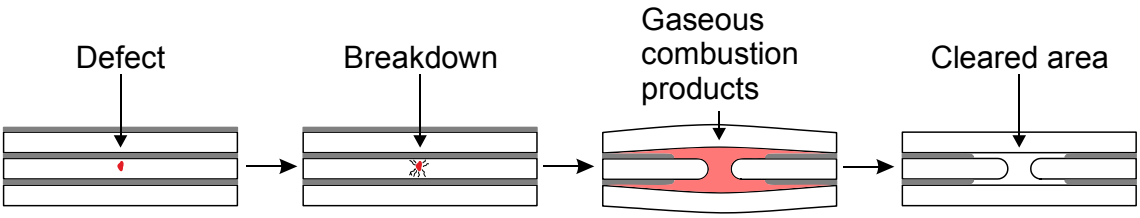

Figure 3.11. Clearing in metallized film capacitor. Energy discharged during breakdown isolates the faulted area, leaving surroundings intact.

Self-healing phenomena is heavily influenced by four factors: metallization thickness, applied voltage, capacitance and pressure. Metallization thickness is inversely proportional its resistance, which limits the short-circuit current during the breakdown. At the same time thicker metallization layer takes respectively longer time and higher energy to evaporate, delaying the clearing process. For these reasons, thinner metallization have been shown to facilitate self-clearing, and thick metallization either hinders, or as is the case with film/foil designs, downright inhibits it. Besides these factors, the minimum practical metallization thickness is limited by the aging mechanisms, namely corrosion, discussed further in chapter 4. [44], [55], [57], [63], [64], [72], [73].

Voltage has a straightforward effect on clearing phenomena, as it has been shown to be exponentially related to discharge energies, resulting in direct correlation between

the self-cleared areas and applied voltage. Higher voltages lead to larger destructed areas and higher capacitance losses for each clearing.

The effect of capacitance can be reviewed either as the external capacitance measured at terminals, or as the apparent capacitance at the clearing area. Increase in total capacitance leads to lower voltage drop at the terminals, and for practical applications capacitances are large enough for the voltage drop to be negligible. Alternatively looking at the local breakdown spot, the effect of increased capacitance is adverse, as higher capacitance can dispense more energy to the newly formed arc, leading to increased de-metallization before the arc is extinguished. To solve this contradiction segmented arrangements illustrated in Figure 3.12 are occasionally used. [57], [74]

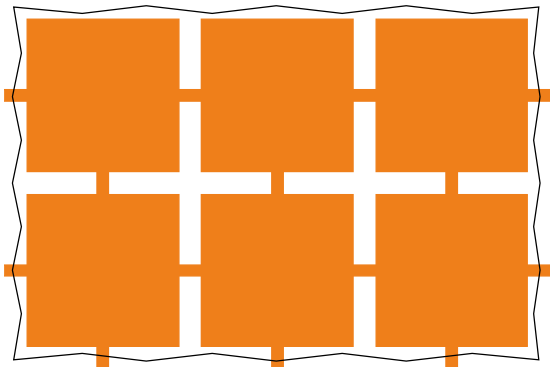

Figure 3.12. Segmentation in metallized film capacitors; as a breakdown occurs, the inrush current will burn out the adjacent thin portions, isolating the faulted segment.

Owing to their higher resistance, the connecting strips between segments act as fuses. As a breakdown occurs, the capacitance at the fault would be constricted to the one induced by that segment alone, as the segment is separated from its neighbors due to the ohmic heating caused by inrush current burning out the high resistance strips. As will be discussed later on, the decrease in apparent capacitance leads to decreased energy, which in turns leads facilitates clearing. This in turn decreases the risk of failed self-clearings, increasing reliability. [57], [74]

Albeit used by some manufacturers, this kind of segmentation has proven troublesome and unfeasible in many applications. First of all as whole segments are separated, the capacitance loss caused by single breakdowns is increased. Additionally segmentation leads to reduction in energy and power densities. Energy density is reduced as a portion of the electrode area is left without metallization, and further limited by the segments not overlapping entirely as the capacitor films are rolled up. Power density in turn is limited by the increased resistance, which can be troublesome especially for pulsed power applications. Additionally there has been controversy about the fuses acting properly. As the melting and subsequent disintegration of the metal layer happens only at high temperatures, thermal stresses are induced on the underlying polymer film. This has been proposed to cause structural damage, increasing the risk of cascading failure modes such as subsequent rapid clearings. [55], [75]–[77]

Out of the four factors, the effect of pressure is the most complicated one. On one hand high pressure has been expounded to facilitate clearing, with higher local pressure leading to smaller cleared areas. This is especially noticeable in rolled-up capacitors, as clearings in the inner turns tend to be noticeably smaller than those occurring in outer turns. The smaller clearings result from higher pressure, caused by the constricting forces imposed by the outer turns. [63], [64] Alternatively, studies exist that represent excessive pressure as a hindering factor [78]. Albeit higher pressure is observed to facilitate self-healing by decreasing the discharge energy and destructed area, high pressure is noted as well to decrease the overall dielectric breakdown strength. Additionally for some materials excessive pressure was shown to lead to clearing phenomena failing to isolate the faulted areas, leading to the total loss of insulation. Albeit it might be that these rapid self-healings were primarily caused by degrading material properties rather than the clearing phenomena itself, care should be exercised when pressure effects are considered. [78]

Clearing phenomena is often characterized with concept of discharge energy, E_{SH}, as expressed by Equation (3.31) [57], [68], [78]. U is the voltage, C the capacitance, R_S the metallization sheet resistance, $\alpha(P)$ is a function for inter-layer pressure, and b, c and k are experimentally defined material specific constants:

$$E_{SH} = \frac{kU^b C}{R_S^c \alpha(P)} \tag{3.31}$$

For test arrangements where metallization thickness and pressure are held constant Equation (3.31) can be simplified by introducing condition-specific constant a [78]:

$$E_{SH} = aU^b \tag{3.32}$$

For certain arrangement explained in [63], [64] the constants laid around 4.7 for b and 1.8 for c, indicating significant dependency on applied voltage.

In addition to these external factors, clearing phenomena and its success is critically dependent on the dielectric material. The core problem lies in the combustion products, as excessive formation of conductive graphite forms conductive paths, resulting in intolerable leakage currents even after the clearing has taken place. This brings about energy losses and thermal stresses leading to consequent breakdowns and eventually to total loss of insulation. The foundations of this lies deep in plasma physics and chemistry, and readers interested in them should refer to e.g. [64]. Nevertheless, the material dependency can be readily summarized as categorizing insulation materials in those in which clearing works, and in those where it does not. Polypropylene and PET, being the most commonly used dielectrics nowadays, as well as paper (mainly cellulose) clears well, whereas some materials, such as polystyrene, do not. [61]

Albeit aforementioned polymers are known to clear well, gas chromatographic analysis as explained in [64] has hinted towards the formation of conductive graphite. This might appear as a step-like increase in resistive current. Even though the increased power losses might be negligible, the graphite formation may have some effect on the long-term stability of cleared spots.

3.3.5 Future prospects

The ongoing research in the field of polymer dielectrics has several complementary ambitions, most notable of which being related to improvements in energy density and overall reliability. From the viewpoint of energy density, research goals are laid by Equation (3.20), since the energy density can be improved either by improving the relative permittivity or dielectric strength, or in ideal cases both. [79] Reliability is in turn contingent on the onset and progression of various degenerative mechanisms, discussed later in chapter 4. Besides these two, other properties such as high temperature resiliency are wished for and therefore being researched, but to a lesser extent [57].

Under these premises three distinct courses can be taken. First of all, as the properties of polymers are influenced by the joint effect of chemical structure and manufacturing processes, examining the properties of bulk materials has resulted in a number of publications, such as [44], [45], [79]. Variations are made either in molecular composition or in manufacturing processes.

Secondly, the properties of these altered materials need to be measured reliably to provide sufficient amount of correct feedback for further development. As for the electrical properties at least dielectric breakdown strength, permittivity and dielectric loss measurements are of importance. When conducted properly, permittivity measurements show little variations between samples. Dielectric breakdown strength measurements in turn exhibit large variations, requiring a large number of samples to produce adequate results. This has led to the development of automated measuring devices and entirely new testing methods, such as those explained in [52], [55]. With these, large amount of samples can be reliably measured, and the properties of development stage materials both easily and adequately assessed. In addition to these electrical properties both the aging behavior and adverse effects of use stresses need to be thoroughly evaluated before newly developed materials can be employed in practical applications.

In addition to these more or less practical viewpoints, drastic increase in available computing power has given rise to a new approach, computational solid state physics. In computation solid state physics theoretical models are used to calculate estimations for the properties of would-be materials. Depending on the system size, different techniques each with their own domains of applicability can be used. Density functional theory (DFT) in which electron density is modeled instead of single electrons is regarded suitable for modeling systems up to the size of a crystalline unit cell. As presented in [80], DFT can be used to provide reasonable estimates for phenomena relating to atomic interactions, such as the band gap, dielectric constants and intrinsic breakdown fields. Additionally the presence of impurities and the trap states they cause can be approximated. Larger band gaps, as discussed in Chapter 3.1.1 will generally lead to better insulating properties. To calculate larger systems and determine their properties,

such as those related to crystal structure, morphology and glass transition temperatures, molecular dynamics (MD) is considered as the only option. [80]–[85]

By harnessing the above mentioned techniques at least two distinct approaches can be taken. First of all the properties of existing polymers can be improved by chemical variations. For an example as demonstrated in [80], the inclusion of water molecules in pure polypropylene has been calculated to improve the dielectric constant. Alternatively, different monomer blocks can be combined arbitrarily, and the properties of resulting materials can be calculated. Due to the abundance of different monomers even with a small number of varying molecules the number of distinct would-be materials rises impractically high. To combat this and to keep the number of materials under more detailed calculations reasonable proper screening procedures are needed. These screening procedures can benefit from data-based approaches, in which machine learning is used to predict the DFT and MD results. [80]

The applicability of computational physics to insulating polymers is currently made challenging by two factors. The structure of polymer materials is complicated when compared to i.e. metal lattices. To model the properties of polymer thin film insulations the model needs to account for the effects caused by the multiple structural layers found in polymers. The model would need to cover the levels discussed in Chapter 2, i.e. the molecular structure, configuration and conformation, the morphology, but also the in case of semicrystalline polymers the amorphous areas between crystalline units. Therefore large units need to be modeled, and the calculations become demanding.

Second challenge of computational physics lies in the accuracy of the models used. At the current state of the art multiple models, each with their own domains of applicability are needed to model the properties of any materials as whole. As discussed earlier for polymers larger structures need to be modeled, for which no universal models exist. Albeit the accuracy of the models and techniques has improved, the results obtained may fall short of those acquired via measuring real materials. All things considered, despite its flaws and inherent weaknesses, computational physics represents a new possibility, providing insight and valuable estimates on development stage materials. [2]

3.3.6 Polymer composites

Traditionally polymer composites have been used to improve various non-electrical properties of plastics. Such composites have been manufactured by adding suitable micron sized filler particles during the manufacturing process. For example adding aluminum hydroxide will increase the fire resistance of polymer plastics, in addition to modifying the mechanical properties. [86] The downside from these improvements is degradation in electrical properties, often in terms of lowered dielectric breakdown strength and increased losses. The lowered breakdown strength can be at least partially attributed to the size difference between the host polymer and the filler particles, as the induced inhomogeneity leads to filler particles acting as weak spots.

However during recent decades the focus of polymer composite research has been on the effects of nanometric filler particles. These particles have one or more dimension in the nanometer range, in other words less than 100nm [3]. By reducing the size of the filler particles down to nanometric scale, a whole new particle-filler interaction can be attained. This makes it possible to avert the degradation of electrical properties. Even more, these nanostructured materials are seen as a prominent way to improve the electrical properties, namely the low relative permittivity and already high dielectric strength of traditional insulation polymers. Moreover, studies overviewed in [86] suggest that the degenerative mechanisms and electrical erosion could be hindered, prolonging the already high life estimates of polymer insulations. Together with improved non-electrical properties this brings about the term multifunctional materials, referring to plastics with overall improved properties. [3], [86]

For dielectric purposes the filler material choices can be divided into two categories. First category consists of permittivity-matching materials comparatively similar to the base polymers. Likewise the base polymers, such as PP, the resulting nanocomposites have rather low permittivity but high dielectric strength. According to studies evaluated in [87] and [88], in some cases the relative permittivity of the nanocomposite is measured to be even lower than for the base polymer alone, whereas for other compounds it is higher. Examples of these fillers include nanosilica, SiO_2 and calcium carbonate $CaCO_3$.

Another approach is to use high-permittivity fillers, such as barium titanate, $BaTiO_3$. The resulting composites exhibit higher relative permittivity, the drawback at least in some cases being lowered dielectric strength. This may be caused by agglomeration of the nanoparticles [89], or possibly by the uneven division of electric field stress. Inversely proportional to the relative permittivity, the electric field induced stresses would fall on the low permittivity base polymer alone.

The altered properties of nanodielectrics are proposed to result from the formation of an interface region between the base polymer lattice and the filler particles. It has been proposed by Lewis in [90] and further refined by Tanaka et al. in [91], that a layered interfacial region forms around each filler particle. Since the filler particles are considerably smaller than what was the case in micron sized dielectrics, the resulting total interaction area is markedly increased. As this interface region spans through the entire polymer matrix, the material properties are increasing defined not by the separate properties of the polymer and the filler, but rather by the interface volume. This way the material properties could be tailored by altering the properties of the interaction zone. [86], [88], [92], [93]

Proper compounding between the polymer and filler particles is vital for the formation of homogenous structure and proper interaction region. To measure the quality of compounding two distinct qualities are defined: distribution and dispersion. Distribution refers to the even spreading of filler particles in the polymer matrix, whereas dispersion refers to the degree of nanoparticle clustering. The cluster-forming processes are also known as agglomeration. These agglomerates are formed due to the

high surface energies, and for certain fillers such as silica, special surface treatments or compatibilizer agents are needed to keep the level of agglomeration at tolerable level. Agglomeration breaks the homogenous matrix, with agglomerates acting as weak spots, lowering the attainable dielectric strength. The difference between distribution and dispersion is illustrated in Figure 3.13 below. [86], [88]

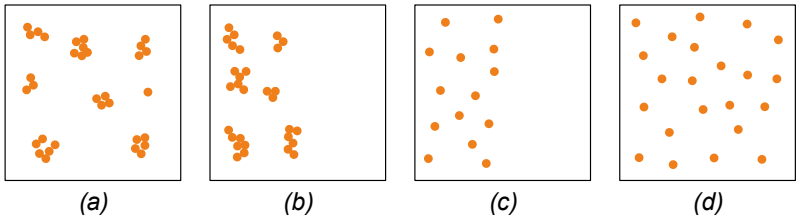

Figure 3.13. Proper dispersion and distribution are essential for smooth filler loading. (a) good distribution but poor dispersion (b) poor distribution and dispersion (c) poor distribution but good dispersion (d) good distribution and good dispersion. [88], [94]

The amount of filler particles is generally around 0.1 – 10 wt-%. The maximum percentage is limited by two factors. Albeit dependent on the manufacturing method, at least for some cases level of agglomerating increases with increased particle loading, and by the formation of percolation channels. In the scope of polymer science, percolation refers to the formation of channels consisting of the filler material alone. As the filler loading in increased past certain *percolation threshold,* these channels span through the insulation, leading to drastically lowered dielectric strength. [1], [93]

4. POLYMER AGING AND DEGRADATION

The service life of polymer insulation systems is outstandingly long, and insulating polymers are regarded as durable and passive materials. As such they should show little to none deleterious or observable changes between scheduled preventive replacements. Nevertheless they do age, and various theories have been presented about the mechanisms behind it. These theories and generic concepts are overviewed in the first part of this chapter.

From the viewpoint of reliability engineering it is often more important to know the practical aging behavior than the exact reasons behind it. For these purpose various more or less empirical aging models have been defined. These models and the mathematics of aging are discussed is the middle part of this chapter.

When novel polymer-based materials are developed, their aging properties must be thoroughly evaluated before newly developed materials can be regarded suitable for long-term use. Since the assumed service life, often measured in decades, is exceedingly longer than the time available for testing, accelerated aging tests are employed. These methods, in addition to the problems they involve are discussed in the final part of this chapter.

4.1 Engineer's perspective in aging

Aging, degradation and breakdown are the three core concepts when long-term reliability of polymer insulation systems is considered. In consequence three tasks are presented: to define these concepts, the corresponding mechanisms, and their interrelations. Starting from the concepts only the definition of breakdown is unambiguous. As discussed earlier, breakdown is defined as a sudden and local loss of insulating properties. Differentiating between degradation and aging effects is more open to interpretations however.

In the viewpoint of Fothergill, as explained in [93], the three core concepts are regarded as separate phenomena. Breakdown is defined as sudden phenomena, whereas degradation takes place over a period of time. They are mutually related, as degradation leads to decreased breakdown strength. In times less than the required service life, it is highly probable that degradation will lead to breakdown. Therefore "well-designed insulation systems, operated within the scope of design parameters, should neither breakdown nor degrade" [93]. Therefore any mechanisms which do not likely cause premature equipment failures should be regarded as aging.

Albeit simple in theory, applying the aforementioned classification between degradation and aging to practical insulation systems requires extensive knowledge on the system in question. Classification should be conducted based on the expected service life and the deleterious effects of the mechanisms on the insulation materials used. As for an example partial discharging and treeing up to certain levels may be considered normal, even though higher levels would lead to equipment failures. As such, unambiguous categorization of the mechanisms themselves may not be possible at all, even if the insulation system is well known.

Therefore a commonly used approach used by i.e. Montanari and Ranta in [95] and [96] respectively is to leave the distinction between aging and degradation vague, and in many cases the terms as synonyms. Later on in this thesis the mechanisms are discussed on a general level, and extensive categorization between degradation and aging is avoided.

One approach is to consider the aging and degradation mechanisms field- and time-dependently, as illustrated in Figure 4.1. In this approach aging what occur in time intervals spanning decades and which is eminent only when the electric fields too low to induce any rapidly-progressing mechanisms. Even though very difficult to observe directly, these effects can be indirectly observed. Both molecular and morphological changes are known to correlate with changes in breakdown behavior, and this pure aging is most often noticed as reduced breakdown strength or decreased times-to-breakdown, even in complete absence of visible degradation. Contrary to breakdown and degradation, these changes may occur throughout the insulation, not only in weaker spots. The time and electric field dependency of these mechanisms are illustrated in Figure 4.1 below: [93]

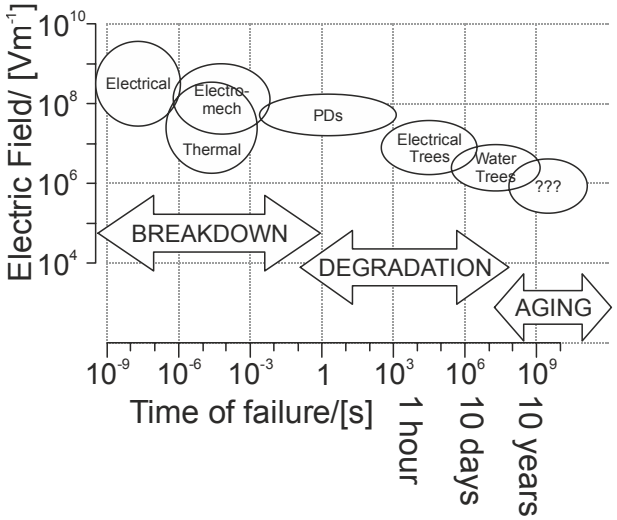

Figure 4.1. One possible way to categorize various electrical and non-electrical mechanisms taking place during component service life. Adapted from [93].

There is no consensus about the primary thermoelectric aging mechanism of polymers. At least four theories have been presented about the subject (see [93] for additional references). Despite the differences all models suggest that the formation of

nanocavities and charge traps is related to aging. Dissado, Montanari and Mazzanti have proposed in [97] that at least for crosslinked polyethylene (XLPE) aging is proportional to increased space charge concentration. Miniature cable measurements consistent with the proposed theory were brought forward. On the contrary Jones, Lewis and Llwellyn have proposed in [98] that at least for polyethylene electromechanical stresses act as an important aging factor. Crine, Dang and Parpal have proposed in [99] that at least for extruded cables increase of free volume, in the form of nano- and micro-sized cavities act as a major aging factor. It was proposed this theory could be applied to other insulating polymers as well.

Comparatively different approach regarding the aging mechanisms present in polymer composites was presented by Rowe in [4]. As summarized in [93], aging is proposed to occur at the interface regions. Together with linking of damaged areas and percolation type processes, the formation of continuous damaged interface regions is seen as the main aging factor in polymer nanocomposites.

Albeit the four aforementioned theories were backed by experimental results, a point should be made about the possible shortcomings regarding their application. First of all the existence of multiple theories suggest the subject is not thoroughly known. Secondly, since all theories and the related experiments were made for insulating polymers considerably different from biaxially oriented thin films used in capacitor applications, the applicability of the aforementioned theories and accompanied life models needs to be verified. Additional verification is needed regarding their applicability to different materials. The rising trend of nanocomposite materials is assumed to complicate things further, as it should be assumed the aging mechanisms can be exceedingly different than those observed to hold true for traditional polymers.

In addition to the “pure” aging mechanisms discussed earlier, various degradation mechanisms can be observed in case of faulted insulations. Unlike for the subtle mechanisms discussed earlier, more straightforward ways exist to either avoid them completely, or bring their deleterious effects down to a tolerable level. These mechanisms and the means used to inhibit them will be discussed next.

Chemical aging refers to the formation of free radicals and oxidation. Free radicals are formed via oxidation-reduction (redox) reactions, but also due to thermal, electrical, radiological and mechanical stresses. Regardless of the way they were formed the resulting free radicals are very reactive and capable of reacting with the base polymer. These reactions result in chemical and morphological changes such as depolymerization, chain scissions and crosslinking. Chain scission and crosslinking are complementary processes: first one leads to smaller molecular weight compounds, whereas the latter leads to connections polymer chains, increasing apparent molecular weight. Out of these two chain scission tends to dominate, and with it formation of free radicals leads to the formation of smaller molecular weight compounds. As discussed earlier in Chapter 2, smaller average molecular weight correlates with decreased dielectric properties, especially in terms of dielectric breakdown strength. [16], [96]

In practice capacitors are hermetically sealed either via liquid impregnation or by epoxy casting. This sealing provides an oxygen-free environment, but the polymer film needs to be protected against excessive oxidation during preceding manufacturing and storage phases. Commonly used method to prevent oxidative damage is to compound the polymer melt with antioxidant stabilizers. Antioxidants work by removing the free radicals, inhibiting any further reactions. This is accomplished by the antioxidant oxidizing itself. Since the thermal stresses during manufacturing are substantially higher than those during normal operation, considerable portion of the antioxidants is already depleted before the insulation is put into use. Depending on the viewpoint this can be seen beneficial, since the antioxidants residues have been linked with lowered dielectric breakdown strength. This dualistic nature of the antioxidants is examined in greater detail in Chapter 2.3. [100], [101]

Unlike chemical aging the various ways of electrical degradation are often visible or in extreme cases even audible. The question about whether or not they should be categorized as aging or degradation mechanisms is not continued further, and later on the term degradation is used exclusively. This is largely due to fact that materials have different susceptibilities towards these mechanisms, and proper categorization cannot be conducted by looking at the phenomena alone.

Means of electrical degradation include electrical treeing, indirectly water treeing, partial discharges and direct electron impact. Since the focus of this thesis lies on thin films, in which neither water nor electrical treeing are expected, these are not discussed further. It should be noted, however, that for thicker insulation structures, for example XLPE in power cables various treeing phenomena represent an important vector of degradation. Readers interested in additional information of the treeing phenomena should refer to e.g. [16]. Partial discharging and direct electron impact themselves should not be considered as independent phenomena, but rather as mechanisms acting together with the aforementioned chemical and aging processes. [16], [64]

Partial discharges (PD) refer to local breakdowns which do not short the insulating structure itself. Partial discharging tends to occur when the electric field changes in magnitude. The behavior and inception of partial discharges depend on the type of voltage stresses, and they appear where the local electric field strength surpasses the breakdown strength of the insulating material, usually gas or void inside cavities. Structural inhomogeneity such as defects, gas bubbles, film edges and uneven electrode surfaces distort the electric field, with local concentrations lowering the apparent inception voltage. Partial discharging is more of a problem in AC insulation systems, where the alternating electric field can cause repetitive discharges to occur multiple times during the 50Hz cycle. Under DC excitation partial discharging is characteristically more random, and the amount of discharges is decades lower than in AC systems. Discharging tend to occur mostly when the field changes in magnitude. [31]

The magnitude of partial discharges is deducted by measuring the variations in external current. The intensity of the partial discharges is defined as the amount of

charge discharged during the discharge events. As for all charge measurements, the SI unit is coulomb, with partial discharging measured in the picocoulomb (pC) range. Whether or not certain levels of partial discharge activity should be regarded as rapidly progressing degradation or harmless depends heavily on the insulation materials used. Some materials are more resistant to partial discharge induced stresses, but for polymer plastics extensive partial discharges are considered deleterious. For polymer cables often insulated using cross-linked polyethylene (XLPE) the partial discharge intensity should be in the range of few pC, with 5 pC being the allowable limit in most international standard tests. Lastly, it should be noted that currently available measurement techniques and high levels of electromagnetic interference set practical limits for the minimum energy threshold. Even if they cannot be measured, miniscule partial discharges have been proposed to occur in e.g. nanovoids and microscopic gas bubbles in insulating liquids. [16], [96], [102]

None of these aging mechanisms should be considered as isolated phenomena, but rather as a part in a chain or interactions that will eventually lead to accumulation of damage. After accumulating enough damage the insulation is considered to be at its end of life. These mechanisms can operate both simultaneously and in a way where another continues where another ends, or at least stops being meaningful. This can be caused by considerable differences in speed.

As for an example it has been proposed that the unavoidable aging processes lead to increase in free volume. This manifests itself in the form of miniscule cavities. Compared to the surrounding material the permittivity of gases or void inside these cavities is low, and according to (3.6) local electric field is substantially increased. Therefore even when the insulation itself is operated within nominal operating voltages, these cavities are susceptible to partial discharging. At certain point the partial discharge inception voltage is exceeded and partial discharge activity starts. These partial discharges can promote chemical degradation by the formation of reactive molecules, which in turn lead to deleterious reactions in the surrounding polymer. Besides, the cavity represents a free space in which charged particles such as electrons and ions can gain considerable momentum from the electric field. These particles collide with the polymer surface which in turn leads to formation of craters. Crater formation represents one form of progressive erosion, and the uneven surface will distort the electric field even further. These sharp corners in turn have been proposed to act as initiators for the aforementioned electrical treeing phenomena. [16]

Instead of looking at the actual mechanisms of aging, another approach is to define the external factors influencing or accelerating aging processes. Even if the underlying theories are ignored, defining these aging factors and their effects yields valuable information which can be used to determine tolerable operating conditions. These factors should however be discussed separately from their consequences. For example electric field is a well-known factor of influence, whereas partial discharges and charge injection are consequences of applied stresses. Another well-known factor of influence is temperature. These two are cited to be the main factors behind the aging of electrical

devices operating under normal operating conditions, and their combined aging effect is known as thermoelectric aging. For applications areas where the insulation systems are susceptible to mechanical stresses (such as vibration) these effects should not be considered separately but together with possible thermoelectric stresses. [64], [93], [95], [96]

A threshold value can be determined for electric stresses. When the stress level is below it, electrical aging does not occur. [95] This has considerable practical significance, as designing the insulation systems to operate below these thresholds would be reflected in improved reliability, and possibly more straightforward aging behavior. Care should be taken however, as it is not known if the threshold value stays constant throughout the insulation lifetime. If the threshold value fluctuates due to other aging processes, such as thermal or mechanical, even if the insulation is designed to initially operate below the threshold, the threshold may drop below the use stress levels. In this case unforeseen electrical aging begins to progress. This in turn may accelerate the aging progression and lead to untimely failures. [95]

Similar thresholds do not allegedly exist for thermal and mechanical stresses; as reviewed in [95] no convergence towards any threshold has been measured. Albeit theoretical thresholds may not exist, practical ones can still be estimated for applications where certain stresses are not expected. Depending on the situation certain stresses such as radiation and vibration can be regarded irrelevant. After the number of factors has been reduced sufficiently the remaining ones and their combined effects are more easily modeled, and the models can still be used to estimate expected service lives and maintenance intervals. Certain care is needed however, as all operating conditions and stresses imposed are not always known beforehand. [95]

4.2 Life and aging modeling

Let us start aging modeling by defining a property, P. Depending on the application P can be of any quantity, which is of importance for proper operation. For practical purposes properties which can be readily measured are preferred, with one example being capacitance loss of metallized film capacitors. It is reasonable to consider only time-varying or *degrading* properties. As the insulation suffers damage, these deleterious changes are reflected in its properties. Usually many properties can be defined, and when one of them has reached its critical value P_L, the insulation has reached its end of life. This lifetime is denoted as L. [31], [95]

It is reasonable to assume lifetime L depends on the stresses imposed upon the insulation. If the mathematical relationship between the stress levels and lifetime is known, as long as operating conditions are known the reliable operating life can be estimated. Additionally accelerated tests can be conducted at varying stress levels, either to verify the validity of these relationships or specify material-specific constants used for the equations.

Additionally if changes in P can be measured, or its relationship with another property K is well-known, and K can be measured instead, the accumulated damage and state of aging can be determined. Using this, the remaining reliable lifetime can be more accurately estimated. This is especially useful for applications where not all stresses or stress levels are known beforehand, or for insulations nearing their end of lifetime, but for which either the stochastic variations in aging progression are high or the long-term aging behavior is not well known.

4.2.1 Arrhenius relation

The value of any life model depends on its cohesion with experimental data. Albeit simple, the Arrhenius relation has been shown to correlate well with thermal aging behavior in traditionally used insulations. Often cited as the most common life-stress relationship, it is still extensively used.

Arrhenius relationship, later on referred as the Arrhenius life-stress model, is based on the Arrhenius reaction rate equation proposed by the Swedish Nobel laureate and physical chemist Svante Arrhenius in 1887. The reaction rate equation states that at a given absolute temperature T, the reaction rate $R(T)$ for any arbitrary reaction can be written as a function of reaction specific activation energy E_A, Boltzmann constant k_B, , and constant A: [31], [46], [95], [103][6]

$$R(T) = Ae^{-\frac{E_A}{k_B T}} \tag{4.1}$$

As stated by Equation (4.1), the reaction rate increases with increasing temperature. To derive the Arrhenius life-stress model, certain assumptions are set up. First of all, it is assumed there is only one reaction behind the aging phenomena, and this reaction follows Equation (4.1). Alternatively in case of multiple reactions individual reactions may exhibit non-Arrhenius behavior as long as their combined effect still follows Equation (4.1). Based on these assumptions lifetime L is proposed to be inversely proportional to the reaction rate of these processes. Omitting the steps required, the Arrhenius life-stress relationship can be derived. Commonly written as: [31], [95], [103], [104][7]

$$L(T) = Ce^{\frac{B}{T}}, \tag{4.2}$$

Equation (4.2) states the lifetime $L(T)$ as a function of absolute temperature T. C and B are model parameters to be determined, the determination of which is reflected in the accuracy of given predictions. These model parameters are often defined empirically via aging tests. This life-stress model can be linearized by taking natural logarithms on both sides of Equation (4.2), or:

$$\ln(L(T)) = \ln(C) + \frac{B}{T}. \tag{4.3}$$

[6] It should be noted that there is very little cohesion between different sources about the notation used for Arrhenius equations (4.1), (4.2) and (4.3).
[7] Equation (4.2) written as expressed in [104].

For practical purposes it is considerably easier to plot L as a function of stress rather than the inverse of stress $(1/T)$, and a reciprocal scale is used. Using this with the notation from Equation (4.3) the linearized life-stress plot can be plotted on semi-logarithmic paper. [31]

Arrhenius life-stress model can be used to predict the reliable operating life at any temperature. Albeit the Arrhenius equation can be used to calculate lifetimes for any arbitrary temperature, reaction rate Equation (4.2) which it was based on, is valid only under a limited temperature range. Besides, the valid temperature range is limited by physical phenomena and transitions (catching fire, melting), and by the statistical variations, which become increasingly important as the operating temperature is lowered and total insulation life increases. [31]

Let us mark the lower boundary value of the range in which the model can be applied as T_0. Using this notation, the thermal stress S_T can be written as a function of operating temperature T: [95]

$$S_T = \frac{1}{T_0} - \frac{1}{T}. \tag{4.4}$$

If insulation lifetime at T_0 is written as be L_0, the Arrhenius life-stress model can be written as:

$$\frac{L_T}{L_0} = e^{(-DS_T)}, \tag{4.5}$$

where D is a model parameter to be defined.

Arrhenius relationship is known to provide adequate estimates especially for organic materials, where temperature dependent decomposition reactions tend to dominate. It has been proven accurate for insulations operated under elevated stress conditions, either in accelerated life tests or during overloading situations. Examples of its application areas include traditional oil-paper power capacitors and transformers. As an example an Arrhenius curve for traditional oil-paper transformer insulation is shown in Figure 4.2.

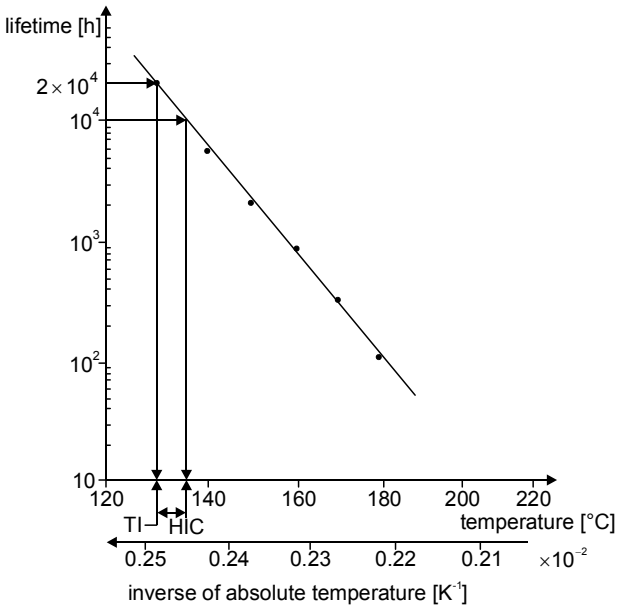

Figure 4.2. Arrhenius curve can be used to estimate transformer lifetime during overload situations. For long-term usage at lower temperatures its accuracy declines. Adapted from [31].

The effect of temperature on the aging progression can be seen as the steepness of the line in Figure 4.2. For comparison between different operating environments HIC (Halving Interval in Celsius) can be used. As seen from Figure 4.2, the HIC value for oil-paper insulation is only around 6 °C. That is, the lifetime halves if operating temperature is increased as little as 6 °C. [31]

4.2.2 Multiple process model

As prefaced in chapter 4.2.1, Arrhenius life-stress model for thermal aging is known to be valid only for certain materials. Any behavior which does not follow this model is known as non-Arrhenius behavior. In accelerated aging experiments Non-Arrhenius behavior is seen as curvature in the *log(L) – T* plane.

Polymers used in electrical insulations have been shown to exhibit non-Arrhenius behavior in regard to thermal stresses. To model their aging behavior a two-process model has been reviewed by Celina et al in [105]. This two-process model is based on two separate processes, one dominating in low (LT) and another in high (HT) temperatures. A crossover temperature of 83±2°C is proposed for PP. Both LT and HT processes are proposed to exhibit Arrhenius behavior, but the combined aging effect in the crossover region is a superposition of both of them. [105]

According to the review by Celina et al. [105], the two-process model has been shown to correlate well with experimental results presented by Richters and Gugumus in [106] and [107] respectively. However both of the aforementioned studies measured the polymer aging by measuring oxidation rates, this two-process model is naturally based on them. To which extent the oxidation rates correlate with electrical properties of polymer insulation systems normally operated under inert conditions is unknown.

4.2.3 Electrical stresses

Electrical stresses and their effects on insulation life time are normally modeled using either exponential or inverse-power models, both of which will be discussed next. Exponential life-stress model is based on the mathematical exponential distribution, which is used to represent systems with a constant failure rate. The probability density function of an exponentially distributed variable t can be written as: [49]

$$f(t) = \lambda e^{-\lambda(t-\gamma)}, \tag{4.6}$$

where γ and $1/\lambda$ are location and scale parameters respectively. Location parameter shifts the beginning of the distribution, representing a threshold before or under which failure is physically impossible. The physical meaning of the inverse of scale parameter λ is that of the failure rate. The distribution starts at [49]:

$$f(t = \gamma) = \lambda . \tag{4.7}$$

Converting the exponential distribution into exponential life-stress model is rather straightforward. To accomplish this variable t and the threshold value γ are replaced by E and E_0 respectively. As discussed earlier in Section 4.1 there is evidence suggesting the presence of a threshold under which electrical aging is negligible, justifying this threshold-based approach. Based on Equation (4.7) the scale parameter can be seen as the estimated life at the threshold level, or L_0. Finally, the failure rate is translated into a more ambiguous yet experimentally-definable voltage endurance coefficient h_{ex}. Using the aforementioned notation the exponential life-stress model can be written as [95]:

$$\frac{L_E}{L_0} = e^{(-h_{ex}(E-E_0))} . \tag{4.8}$$

Life-stress relationship following the exponential model can be identified as a line in E – log L coordinates, with failure rate or h_{ex} as the slope. [49]

Another approach to model non-thermal stresses is the inverse power model. It states that the life L at certain stress level E can be written as [103]:

$$L(E) = \frac{1}{KE^n}, \tag{4.9}$$

where K and n are model parameters. If the life at the threshold electrical stress is known, Equation (4.9) can be written in a more convenient way with only one model parameter. If L_0 is used to represents the life time at E_0, and again model parameter n is rewritten as experimentally definable endurance coefficient h, the inverse power life-stress model can be written as [95]:

$$\frac{L_E}{L_0} = \left[\frac{E}{E_0}\right]^h . \tag{4.10}$$

Applications exhibiting inverse power law life-stress relationships are identified by a straight life line in log E – log L coordinates.

4.2.4 Combined stress models

In practical applications multiple stresses are often present. It has been observed that the presence of multiple stresses leads to degradation which progresses considerable faster than what would be estimated from the sum of individual stresses alone, but slightly lower than what would be derived from their products. As discussed by Montanari et al in [95], a simultaneous stress model has been proposed, which can be written as:

$$\frac{L}{L_0} = \frac{L_1}{L_0}\frac{L_2}{L_0}...\frac{L_N}{L_0}G(S_1, S_2, ...S_n), \tag{4.11}$$

where individual stresses $S_1 ... S_N$ lead to a reduced lifetime L, compared to the reference lifetime L_0 in absence of any stress-originated aging at reference temperature. $G(S_1 ... S_N)$ in turn represents a correction function. The difficulty of the combined stress models lies in the definition of the correlation function. [95]

4.3 Time-varying stress models

Time-varying stress models can be seen as a special case of any of the aforementioned life-stress models. They have found use in accelerated aging tests, where failure must be assured happen within the testing period. This in turn can be used to shorten the product introduction time. One of the basic types of time-varying stresses is a step-stress, where multiple stages are used. After each stage has completed, the stress level is increased to a predetermined new value, and the testing is continued. [103]

The question presented by such time-varying testing is how the increasing stress levels should be accounted for, since all the aforementioned models deal with constant stress levels. For these purposes cumulative exposure models based on the concept of accumulated damage are used. These models assume the remaining life depends only on the cumulative exposure, and that the units do not have memory property, i.e. it is insignificant how the exposure was received[103]

4.4 Accelerated aging

Accelerated aging test refer to experiments conducted at elevated stress levels, with intention to cause measurable aging and stress induced damage during a limited time frame. Since both temperature and electric field strength are known as the primary factors affecting insulation lifetime, either one or both of them will be used to facilitate aging. A core issue associated with accelerated aging tests is related to the number of simultaneous aging factors.

One solution is to impose both thermal and electrical stresses simultaneously. This could yield results better suited for practical applications. The primary challenge associated with these multi-stress experiments is in classifying the observed degradation between temperature and electric field induced. To perform this comprehensive multi-

stress aging models are needed, which in turn require extensive knowledge about the underlying methods of aging.

To develop these models one approach is to determine the effect of separate stresses, after which their joint effect can be measured. This approach is consistent with the multiple stresses Equation (4.11) discussed earlier. Despite simple in theory, various challenges are presented by real-world aging tests trying to determine these underlying theories. These challenges are related with the above-normal stress levels and the valid stress ranges of the aging models. For example in case of thermal aging in polymers, as stated in Subchapter 4.2.2 there is indictment supporting the existence of separate low- and high temperature processes. If the presence of multiple processes or otherwise non-Arrhenius behavior is not recognized, applying simpler aging models, such as Arrhenius will yield erroneous results. With sufficient number of measurements these results can be used to deduce more accurate estimates about insulation lifetime at normal operating stresses.

Since the development of the aforementioned aging models is a demanding task, a widely used approach is to ignore lifetime predictions, and conduct aging tests to compare the general aging behavior of different materials under combined thermoelectric stresses. One possible application for these tests is to distinguish materials susceptible to rapid degradation. In case rapidly progressing degradation is observed under limited-time tests, it serves as strong indictment towards the materials unsuitability to applications where long life expectancy is a requirement.

5. RESEARCH METHODS

The empirical part of this thesis consists of the description of an experiment which aimed to measure the breakdown performance of insulating thin films during a progressive thermal aging cycle. In the first subchapter of this part the materials experimented on are presented. Additionally, the reasoning behind their inclusion into this experiment is discussed.

Due to its importance for proper operation dielectric breakdown strength was chosen for the defining factor when the influences of thermal stresses were assessed. The measurements were conducted using a novel measurement method, which will be discussed in the second part of this chapter. Besides of including a detailed description of the measurement setup, sufficient details are given about the procedures used to prepare the samples.

In the third part of this chapter focus is shifted on the methods used to facilitate thermal aging. The experimented revolved around a 1008 hour long aging cycle, in which the temperature was increased by 10°C every 144 hours. In addition to the reasoning behind the choice of a variable-stress experiment, the purpose-tailored hardware used to conduct the experiment will be depicted.

5.1 Selection of materials

One of the main objectives of this thesis was to examine whether or not different kinds of polymer thin films would exhibit similar aging behavior, and if the observed aging behavior could be seen to follow any of the well-known aging models discussed earlier. For these purposes it was deemed important that several distinct polymer thin films of various compositions would be tested. To provide additional informational value it was decided that a step stress would be used, and that six film samples per material would be characterized after each step. Together with the destructive nature of breakdown tests the experiment would consume a substantial amount of film during each test sequence. Therefore the film candidates were limited to those with adequate supply.

In compliance of the aforementioned requirements four polymer thin films were chosen for the experiment:

1. Tervakoski Films RER 14.4µm
2. NPO30
3. NPO49
4. Tervakoski Films RERS 9.0µm

Tervakoski RER 14.4µm is commercial biaxially oriented polypropylene thin film, manufactured by Tervakoski Films Group in the municipality of Janakkala, Finland. RER films are manufactured in both bubble and tenter processes, of which bubble processed film was used. Designed for electrical insulations, regardless of manufacturing method both types of RER film are advertised to exhibit controlled surface roughness on both sides to facilitate complete oil impregnation. With minimum thicknesses in the range of 9µm and 7.4µm for bubble and tenter processes respectively, the film is aimed towards high voltage capacitors. [23]

Tervakoski RER film was chosen for the experiment to serve as a reference. Being a traditional capacitor-grade BOPP film, it was presumed to represent the normal against which the other films could be compared to. Due to RER films being manufactured in industrial scale, it was available in large quantities. This allowed unaged samples to be used in fine tuning of the measurement setup, enabling actual aged samples to be measured without difficulty. RER film had been a subject in a multitude of previously conducted breakdown tests, and its unaged dielectric breakdown performance was well known beforehand. This would allow check-up tests to be conducted any time. These tests could be used to verify the breakdown measurement system was operating as intended.

Out of many test phase materials two were chosen for the experiment, NPO30 and its reference material NPO49. Both films were surplus from a previous NANOPOWER project, in which their properties were evaluated. It was planned these results could be used as a reference. NPO30 is a polypropylene based nanocomposite compounded with 4.5wt-% of Aerosil® R 812 S hydrophobic silica. Hydrophobicity, acquired by after-treatment with bis(trimethylsilyl)amine (HMDS) [108], is essential to prevent excessive agglomeration. A noticeable amount of silica was lost during manufacturing, and the real filler loading was measured to be around 3.78%. [2]

Apart from the added nanosilica, NPO49 and NPO30 are similar. Both use Borealis Borclean™ HC318BF powder as its base polymer. HC318BF is marketed as extra pure polypropylene designed for BOPP Dielectric films in capacitor applications. As such it is endorsed to contain neither any additives nor remains of nucleation agents. [109] NPO30 and -49 include 0.45wt-% of Irganox® 1010 as a main process stabilizer and 0.35wt-% of Irgafos® 168 as co-stabilizer. Irganox® 1010 is a phenolic primary antioxidant designed for processing and long-term thermal stabilization. Irganox® 1010 product guidelines recommend concentrations in the range from 0.05% to several percent. A high concentration was chosen during the NANOPOWER project based on test-trials in which lower antioxidant concentration was linked with noticeably degraded dielectric properties. [110] Irgafos® 168 is in turn a hydrolytically stable phosphite processing stabilizer, which prevents autoxidation and extends the performance of primary antioxidants [111]. Pre-mixing of raw materials was done automatically in a drum mixer, in a polyethylene bag. Compounding of pre-mixed materials was done at VTT, followed by film manufacturing at a Brückner pilot-line in Denmark.

NPO30 and its reference material NPO49 were chosen for the aging experiment to explore the differences in aging between nanocomposites and traditional polypropylene thin films. As discussed in Subchapter 4.1 there is evidence suggesting the presence of different kinds of aging mechanisms, and noticeable differences were expected. Additionally both NPO materials have been studied in previous projects, and there is evidence supporting their applicability to actual capacitor applications [2].

Tervakoski RERS 9.0µm is another biaxially oriented polypropylene thin film manufactured by Tervakoski Films Group. Its electrical specifications were advertised to be similar to the previously mentioned RER film. This was further backed up by Tervakoski Film representative Mr. Juha Laakko. As stated by Mr. Laakko, the differences between RER and RERS films were mostly related to their crystallinity. Therefore ignoring the variations related to the differences in thicknesses, in terms of breakdown behavior it was reckoned that both films would perform equally. [112]

Since after the three aforementioned films there was a little space left in the test oven, it was decided to include a limited amount of RERS films in the experiment. Contrary to well-researched RER film, only a few preliminary measurements had been conducted to characterize the breakdown behavior of the RERS film. These measurements indicated a slight but noticeable difference between RER and RERS films. These differences will be discussed later on in Chapter 6. Based on these differences in breakdown behavior it was decided to study whether or not these differences would extend into aging behavior as well.

5.2 Measurement methods

For practical applications dielectric breakdown strength represents a critical quantity which cannot be ignored. When dielectric breakdown strength has sufficiently degraded, the insulation has to be replaced. Since total breakdowns are extremely undesirable, condition monitoring is often implemented to replace insulations when further use would be at the cost of drastically compromised reliability. Since continuous condition monitoring is cost-effective only in special situations, knowledge of aging behavior is needed to schedule proper measurement intervals.

Albeit polymer aging has been studied before, certain issues may limit the applicability of the results for electrical properties. In a number of aging-related studies, e.g. in those reviewed in [105], aging progression is gauged using refined, yet chemistry based methods such as oxidation rate measurements. The correlation between such processes and electrical quantities of practical importance, such as dielectric breakdown behavior and dielectric losses are left vague at best. Since typical capacitor applications represent a rather stable environment for thin films, it may be justified to regard mechanical properties and those more related to material sciences as less significant, at least as long as those do not degrade sufficiently cause to breakdowns, i.e. to cause breakdowns of electromechanical origin. Otherwise as long as the dielectric survives the electric fields it is susceptible to it can be regarded as intact. For these reasons of

practical origin dielectric breakdown behavior was chosen as the variable to be measured during this accelerated aging experiment.

Changes in the dielectric breakdown behavior or in the dielectric losses (i.e. tanδ) can be used to evaluate the aging progression in dielectrics. Previous experiments within the research group suggest that out of these two the dielectric breakdown behavior is a more sensitive indicator. Therefore it was chosen as the measured variable.

The dielectric breakdown characterization of the aged samples was conducted using a novel method known as MultiBreak, an abbreviation for Multiple Breakdowns. Developed by M.Sc. Ilkka Rytöluoto and Dr. Tech. (El. Eng.) Kari Lahti, the method has been a subject of several articles published in peer-reviewed journals [44], [45], [55] and multiple conference papers [43], [78], [113]. By taking advantage of the self-healing properties of commonly used insulating polymers, the sample is sandwiched between two extremely thin electrodes. This structure allows self-healing processes to isolate the faulted areas, and similarly to metallized film capacitors the integrity of the remaining portion is not compromised. By combining this with large measured areas it becomes possible not only to capture the infrequent weak spots, but also continue the measurement and survey the intrinsic or defect-free breakdown strength.

MultiBreak measurement method was chosen after several discussions with Mr. Rytöluoto and Mr. Lahti. As its main attraction it requires a significantly smaller number of samples to provide adequate results, especially when compared to traditional small-area measurements. As detailed in [41], for traditional breakdown testing 10 samples and with them 10 breakdowns represent a bare minimum. Owing to their scarcity, capturing any of the expected weak spots with such small sample pool would be improbable. Besides given the possibility of separate low and high field breakdown mechanisms and to plausible calculate any probability distributions with realistically narrow confidence bounds, a far greater amount of samples would be required. A sophisticated estimate about the minimum number of distinct samples would be at least 30. Such a large amount of samples would require plenty of handiwork, and measurements would have taken time. This would have constricted the number of materials and temperature steps. By using the MultiBreak method the number of distinct samples could be reduced considerably. Together with already existing test equipment, it became possible to evaluate a broader selection of materials.

5.2.1 Film stack and preparation

Even though the carrying idea has remained the same, the details of the MultiBreak measurement method have been developed beyond what was described in [55]. The most recent iteration is based on even larger samples. The self-healing test capacitor or film stack is constructed using five film layers stacked on top of each other.

Upper- and lowermost films were approximately 105×120 mm sheets cut from 100µm thick Folex X-10.0 transparent polyester film, originally intended for use in monochrome copiers [114]. These sheets were cut using a Myers Precision Trimmer

Range paper cutter. The newly cut sheets were visually inspected, and items with noticeable tearing were discarded. The purpose of these polyester films was to protect the actual sample against physical damage. Additionally by making the samples more rigid they made overall sample handing easier. Besides, they were ought to form a barrier which would hinder the intrusion of oil into the active test area.

The electrodes comprised of two 130 mm long unilateral metallized films placed between the actual sample to be measured and the polyester sheets. The metallized sides were placed towards the sample. Due to its availability Tervakoski Films PSX 12.0 µm was used. Tervakoski PSX films are zinc/aluminum alloy metallized PP-films, with a heavy edge on one and free non-metallized margin on the other side. The metallized portion was 90 mm wide. Designed for low power capacitors, it is advertised to have a resistivity of 2-4 Ω/sq in the reinforced edge and 5-12 Ω/sq in the main body. [115] The relatively low resistivity implies a rather thick metallization.

Actual samples to be measured were positioned in the middle of this film stack. First of all three positioning squares and a unique identification number were drawn on the film surface. The unique identification number contained information about the material, the temperature at which it was removed from the testing oven, and about its relative position during testing. This identification scheme will be explored in more detail during chapter 5.4. The innermost positioning square was used to mark the active test area on top of which the electrode films would be placed. The positioning square in the middle was used to mark down markers representing a division into 25 square segments with the size of 20×20 mm. These markers would be used for thickness measurements later on. The outermost square would be used to cut the samples to a size of 110×110 mm. A margin of ten millimeters was left at the edges to prevent flashovers during testing. After preparation the samples were visually observed for any visible scratching or puncturing. In the few cases where any deformation was observed, the damaged portions were cut off. This reduced the active area by 4.5…9cm^2, which, considering the nominal area of 81cm^2 was considered insignificant.

After the samples were cut apart, their thicknesses were measured at the approximate centers of the squares formed by visually interpolating the markers drawn on the 100×100 mm square. The thickness measurements were conducted with a LE1000-1 bench top contact thickness gauge fitted with a ball point measurement tip and with a constant measurement force of 0.6...0.85 N. LE1000-1 has the accuracy of ± 0.1 µm and the resolution of 0.05 µm. The thicknesses were recorded and later on used for breakdown field calculations. [116]

The film stacks were fastened to a test bench illustrated in Figure 5.1. Its base consisted of a flat Bakelite plate, with two pairs of aluminum slabs positioned on two opposite sides. The extruding metallized foil edges were sandwiched between them. Electrical connection was made using safety binding posts, which also doubled as screws used to affix the plates. Albeit it was possible to fasten the plates on both edges, it was deemed unnecessary as using only one screw resulted in satisfactory electrical contact.

Special care was taken to ensure the slab-metallization junction remained functional. The binding posts were fastened using only minimal force necessary to prevent the electromagnetic forces from pulling the electrodes together. The metallization near the slab edges was visually observed after each test, and in case noticeable wear was observed, the slabs were cleaned and subsequently polished using grade 000 steel wool. This had to be done only once, near the end of the aging cycle.

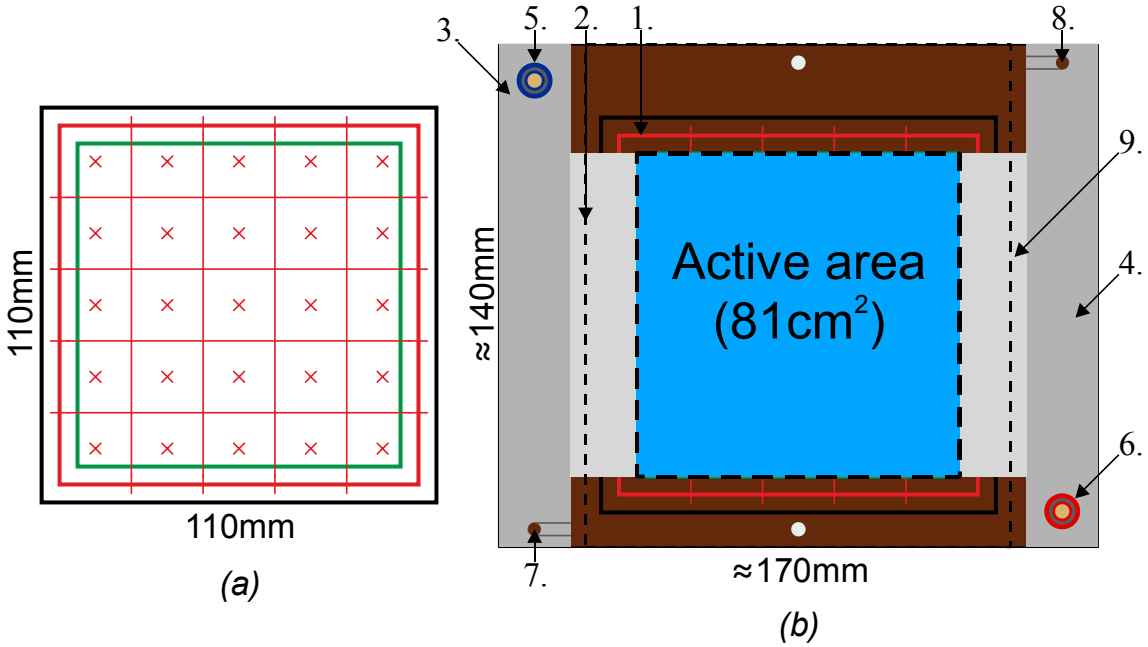

Figure 5.1. (a) Test film dimensions and red crosses marking the 25 thickness measurement points. (b) MultiBreak test bench: 1: Film stack, 2: Metallized electrode films, 3-4: Aluminum clamp electrodes, 5-6: Safety binding posts for ground and HV connections, 7-8: Holes for additional fastening screws (unused), 9: Transparent acrylic top plate.

Due to the thickness of the measured materials voltages up to 20kV were used, and it was deemed necessary to submerge the test bench in insulating dielectric oil. This was done to minimize the number of flashovers and to prevent partial discharges and other types of arcing near electrodes. Due to it being readily available Shell Oil Diala DX was used. The oil quality was visually observed before and after each test, and when not in the oil vat was covered to prevent excessive contamination by airborne particles and dust. Even though no significant contamination was observed during the test, it was decided to change at the oil when the aluminum slabs were polished. Since a small amount of oil was lost with each sample, the oil level was monitored and the vat was refilled regularly to keep the test bench fully submerged.

Special care was exercised during the handling and storage of the test materials. Materials were stored at room temperature, protected against UV radiation with metallic non-transparent bags. After samples had been prepared they were given protection against contamination by airborne particles by storing them in paper folders in zipper storage bags. Plastic gloves were worn without exception when handing the samples for additional cleanliness.

5.2.2 Measurement circuit

The measurement circuit consisted of a Spellman SL130P1200 DC high voltage power supply (HVPS) with a specified maximum output voltage of 130kV and with a voltage-independent maximum rated output current of 9.23mA. The device had a current limiter set to 9mA. Additionally the high voltage power supply incorporated an arc detect circuit, which was advertised to sense dynamic arcing at the output. If an arc was detected, the output would be inhibited for one second. After one second had passed, the output was ramped to the previous set level at a factory-specified fast rate. [117] The power supply was controlled via a National Instruments PCI-6221 DAQ card. Spellman resistive voltage divider HVD-100-1 with an input impedance of 1000MΩ and a division ratio of 1:10000 was installed parallel to the test bench to provide feedback of the DUT voltage. Both the power supply control and voltage reading were conducted using LabVIEW software.

Midway of the aging cycle, during the course of unrelated small-area breakdown measurements at voltages in the range of 40-50kV, the PCI-6221 DAQ controller card broke down. The failure manifested itself as constantly high output voltages at the DAC-controlled output lines. Various theories were presented about the origins of this failure, of which electromagnetic interference (EMI) was one of the more plausible options. It was known beforehand that the breakdown measurements generated local electromagnetic interference, as this had transpired itself as occasional failures in computer peripherals, keyboards being one example. Nevertheless since these failures had corrected themselves after a few seconds, the EMI levels were considered harmless. Metal plating had been installed throughout the test room inner surfaces to enable sensitive measurements in the future by attenuating external disturbances, and the plating was ought to prevent any discharge-generated disturbances from spreading.

Since the failure of the DAQ controller card was not noticed immediately, the constant high output caused a phenomenon of unknown nature to occur during the subsequent test. This resulted in the failure of the Spellman SL130P1200 power supply. As the aging cycle had already been started, it was decided to continue the measurements using a Spellman Model SL20P1200 power supply, with the output of 0-20kV at 60mA. The internal current limiter was set to 9mA to keep the measurement setup as similar as possible. The HVPS control was done using a similar DAQ card. The measurement circuit used is illustrated in Figure 5.2.

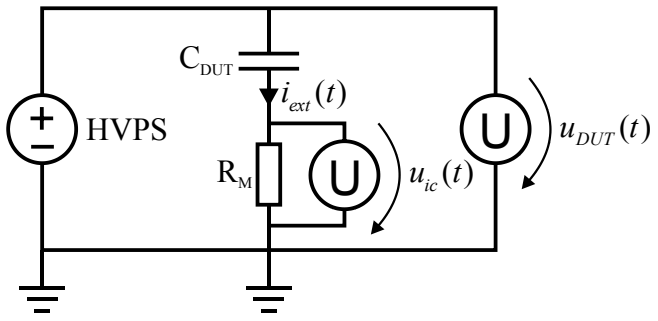

Figure 5.2. Measurement circuit used for MultiBreak measurements.

The DUT voltage $u_{DUT}(t)$ and external current $i_{ext}(t)$ were monitored by a 12-bit LeCroy HRO 66Zi oscilloscope. Whenever a discharge occurred in the test capacitor, the discharged energy would be replaced from the output capacitors in the HVPS. These current pulses were measured indirectly by measuring the voltage $u_{ic}(t)$ over a low inductance 1.0330Ω impulse current measurement resistor. A 10× attenuating probe was used to scale the current-induced voltages. Voltage measurements were conducted using a Tektronix P6015A high voltage probe with a frequency range from DC to 75 MHz. The oscilloscope was operated in sequence acquisition mode, and programmed to record a sequence after the voltage at the channel connected to the current measurement resistor had reached a positive value of 4.0V, which would roughly equal to a current of 4A. An offset timing was used to capture the first nanoseconds before device triggered. The scope parameters were largely set using a combination of trial-and-error and knowledge from previous measurements. It was possible to record 500 first trigger events. The recorded sequences allowed the determination of waveforms for breakdown voltage and external current. Using these it was possible to calculate the apparent discharge energy and various timing related variables. [44]

The measurement procedure can be summarized in twelve steps, which are as follows:

1. Construction of the film stack.
2. Data recorders started.
3. Pre-ramp to promote film adhesion.
4. Test bench moved to oil vat.
5. Video recording started.
6. HV ramp initiated.
7. First breakdown voltage gets written down.
8. After the sample has been depleted; HVPS powered down.
9. Data recorders stopped; captured sequences and trigger times saved.
10. Grounding the system via an earthing rod.
11. Video recording stopped.
12. Sample removed from test bench; used samples stored in a container for possible further inspection.

A pre-ramp was used before submerging the test bench to prevent excessive oil from entering between the layers of the film stack. For RER, NPO30 and NPO49 films the sample was subjected to a voltage ramp from 0 to 3kV DC at a ramp speed of 400V/s, and for thinner RERS film the pre-ramp voltage was limited to 1.5kV DC. The resulting electrostatic forces compressed the stack, and forced out the air pockets or oil residues that might have been inside. After the pre-ramp an acrylic plate was positioned on top of the stack, and the test bench was submerged in the oil vat while simultaneously pressing the top plate down to force excessive oil out.

After the sample had been placed in the oil vat, the voltage ramp was initiated without unnecessary delay. This was done to minimize any oil seepage to the film stack.

The voltage ramp consisted of two steps: a fast initial ramp-up at 400V/s, followed by a slow increase at 30V/s. The transition point was calculated to represent approximately the 40-60% of the literature-based breakdown voltage for small samples. Even though the weak spots were assumed cause a few breakdowns earlier, it was estimated that the intrinsic, or defect-free breakdown region would be reached between 120 and 240 seconds, in accordance with slow rate-of-rise tests described in IEC-60243-1 [37]. Since each subsequent breakdown would consume a small portion of the active area, the test capacitor would gradually fade away. The ramp-up was continued until either:

1. the intrinsic region had passed and no more breakdowns were recorded for 10…20 seconds, or
2. 500 events were recorded, or
3. the power supply shut down due to excessive arcing.

Out of these, the latter two were encountered only a few times. As situations 2 and 3 tended to occur only at the near end of the measurement, they were considered as insignificant. In case of the power supply shutting itself down the data recording was stopped, and the voltage was ramped beyond the last measured breakdown voltage at a fast ramp rate of 400V/s. This was done to ensure the shutdown was due to excessive arcing, and not by any short-circuit caused by the failure of the self-healing mechanism. During the course of testing no such failures were observed.

5.3 Aging cycle

Thermal aging was promoted using a progressive 1008 hour cycle. The cycle consisted of seven discrete steps with duration of 144 hours, equaling to six days. With an increment of 10°C, the temperatures ranged from 50 to 110 °C. Every 144 hours a number of sheet were removed from the oven, from which six samples for each material except RERS9 were cut off. Since the amount of RERS9 was limited, it was measured only near the end of the cycle, at 100°C and 110°C. The procedure to remove the samples took approximately 1…2 hours, during which the heaters were off and the samples were subjected to ambient air. An overview of the temperature profile is given Figure 5.3.

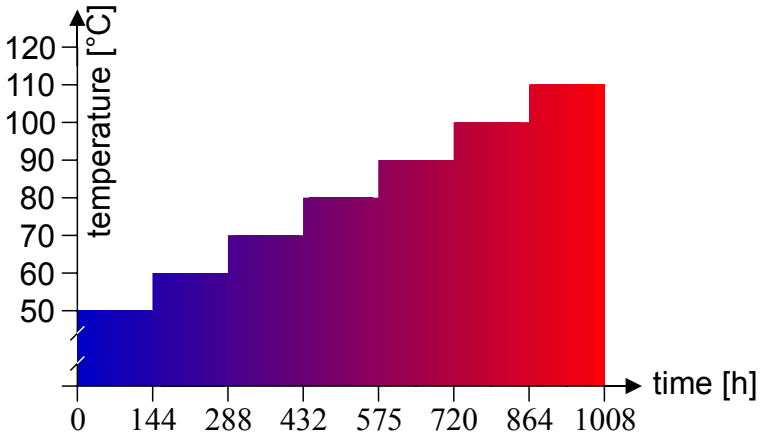

Figure 5.3. Oven temperature was ramped up in 10°C increments to cover a wide span around the proposed transition temperature of ~80°C.

The aging cycle was designed to cover a wide span around the maximum rated operating temperature of 78°C for Alstom power capacitors. Based on a discussion with Alstom Grid R&D and Engineering Director Jari Kotiniitty, it was decided to use a step size of 10°C [38]. It was anticipated that as reviewed in [105], multiple aging mechanisms might be present, with a transition point around 80°C. By choosing three measurement points both from the expected LT and HT-process governed regions, it was reckoned that if such processes had a correlation with dielectric breakdown behavior, the transition from LT and HT process would be discernible.

IEC standard 60871-2 regarding endurance testing for AC shunt capacitors having a rated voltage above 1000 V was used as a basis for the test duration of 1008 hours. As for standard aging tests conducted at 60°C two options are given, at a voltage of either 1.25 or 1.40 times the rated for durations of 3000 and 1000 hours respectively.[8] [40] Albeit the aging test to be conducted was different from the standardized aging tests, it was reckoned that even without electric field induced stresses, the duration of 1008 hours would be long enough to observe noticeable aging.

5.4 Aging setup

To provide controlled environment for the polymer aging a test oven was constructed. The films were clamped to sample holders supported by two rails. To keep the thin films apart it was deemed necessary to install additional clamps as weights on their lower edges. The clamps were noticed to leave dents in the samples, and the damaged portions were omitted from any further testing. The purpose-tailored oven with the removable sample holders is illustrated in Figure 5.4.

[8] The standard test can be conducted either with two or three units. The test is passed if either no breakdown occurs with the two units, or if two out of three units remain intact. [40]

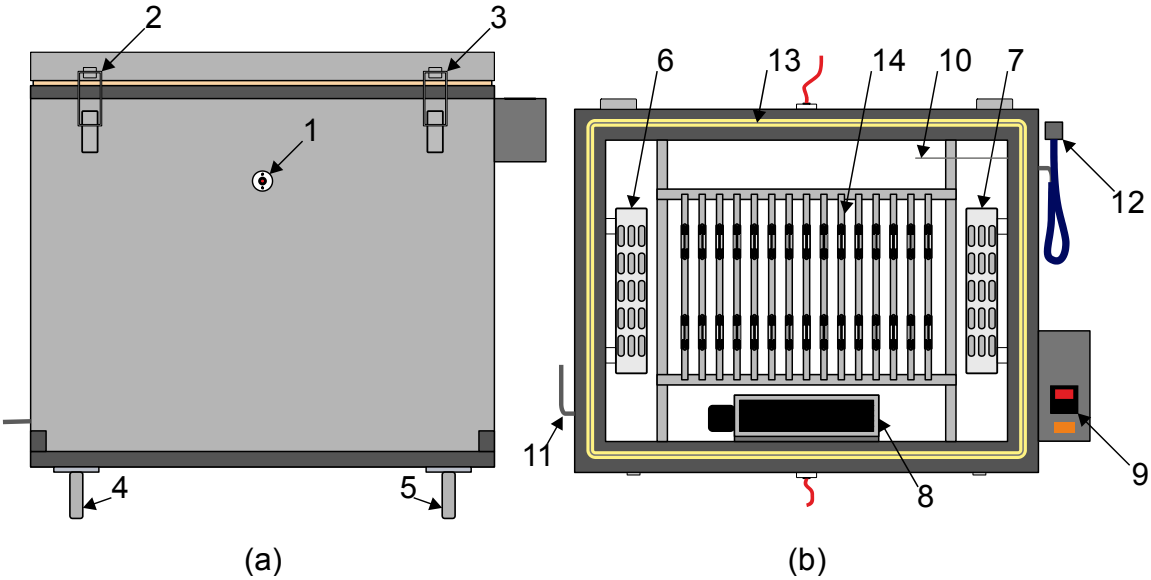

Figure 5.4. Test oven used for aging. Views from (a) front and (b) top, lid opened: 1: Sealed HV lead-troughs, 2-3: Clamps, 4-5: Wheels, 6-7: 4x150W heaters, 2 on each side, 8: Cross-flow fan, 9: Control unit, model TOHO TTM-4SP, 10: PT100 Temperature sensor wired to the controller, 11: Inert gas inlet, 12: Inert gas outlet with flow controller, 13: Two silicone gaskets for lid insulation, 14: Film holders (14 in row).

Heating was provided by two pairs of 150W heaters installed on opposite sides. Metal sheets were installed between the heater elements and the samples to serve as heat distributors and to promote natural convection. A high switching rate and precise control was possible with a choice of semiconductor relays. Temperatures were controlled with a TOHO Model TTM-4SP temperature controller with feedback from a PT100 temperature sensor. The controller was set to operate as a PID controller, with auto tuning enabled to automatically set the controller parameters. After enabling the auto tuning the controller worked as intended, with measured temperatures remaining equal to the set values.

As there were concerns about the sufficiency of natural convection alone, a temperature measurement system consisting of two Maxim Integrated model DS18B20 1-Wire sensors and a laptop was constructed. These 12-bit sensors were cited to have the accuracy of ±0.5°C from -10°C to +85°C, with an operating range from -55°C to +125°C [118]. To simulate actual measurement conditions A3 sized paper sheets were used, to which the sensors were attached with temperature resistant Kapton (polyimide) tape. The sensors locations are illustrated in Figure 5.5.

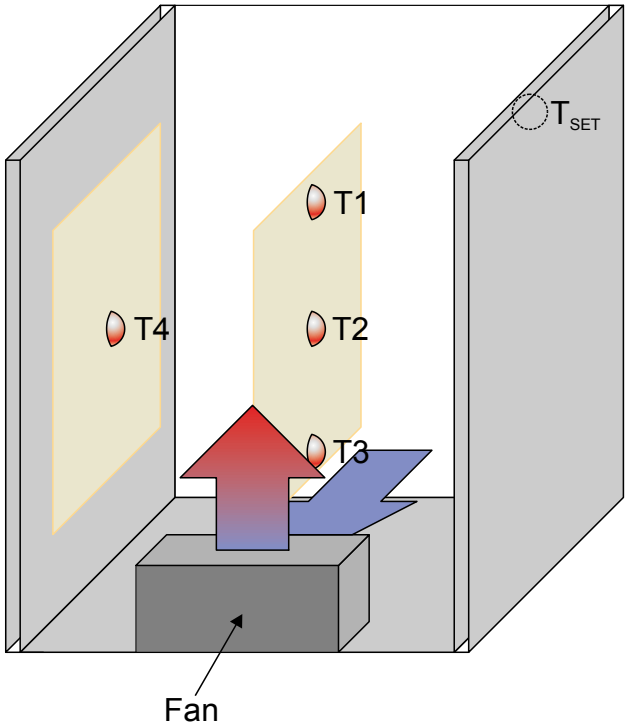

Figure 5.5. Temperature sensor locations. "Empty" paper sheets are omitted for clarity.

The oven performance was evaluated regarding its temperature distribution and accuracy. A number of tests runs were conducted, results of which are collected in Table 2. T_{SET} stands for to the target temperature for the controller.

Table 2. Results from oven evaluation runs. Both accuracy and distribution improved after a fan was installed.

Test number	Fan used	Test duration [h]	T_{SET} [°C]	T1 [°C]	T2 [°C]	T3 [°C]	T4 [°C]
1	No	2	50		44	43	
2	No	20	70		65	63	
3	No	1	70	68		63	
4	Yes	2	50	52		50	
5	Yes	2	70	72		70	
6	Yes	2	70		72		73

Test runs were continued until convergence towards steady-state temperatures was observed. Based on initial test runs it was observed that a better temperature distribution is reached by using a fan to stimulate air circulation. The fan speed was controlled via a variable transformer, operated at 60% of full mains output to achieve minimal flutter in the hanging sheets. With the fan installed and with a pre-warmed oven a 10°C increase was observed to take 1…2 hours, a satisfactory duration considering the total length of the cycle.

In capacitor applications the polymer films are protected from gaseous oxygen either by liquid impregnation or epoxy casting. To simulate these conditions the oven

was sealed and filled with inert nitrogen. As nitrogen is a well-known inert gas [119], given the relatively low temperatures used it was not expected to react with the polymer films. The oven was manufactured to be air-tight, with temperature-proof silicon sealant in all seams and two adjacent silicone gaskets on the lid. The outer gasket was more rigid to provide mechanical support, whereas the inner one was springier to ensure proper sealing.

Despite these precautions some leaks were expected, and the oven was fitted with equipment to provide continuous inflow of the inert gas. The oven was slightly pressurized, and the outflow was constricted by a flow meter – needle valve combination set to almost closed. A Sho-Rate model 150 flow regulator, in combination with a coarse high-flow industrial pressure regulator was used to set the inflow. Rubber hoses and push-to-connect fittings were used to connect the equipment. The piping and connections were tested for leaks using soapy water, and no leaks were detected.

A 200bar/50 liters bottle of Aga HiQ scientific nitrogen was used for the experiment. Given the size of the bottle, a volumetric inflow rate of approximately six liters per hour was estimated to be adequate for the gas bottle to confidently last the duration of 1008 hours. The value was set lower than what calculations would imply since it was not known how the regulator would react to changes in supply pressure, and based on previous experiments there was a potential risk of a runaway effect in which decreasing bottle pressure would lead to increasing outflow. The estimation held true, and the nitrogen supply lasted for the test duration.

To restore the inert atmosphere every time after the oven was opened and reclosed the tank was flooded for 10 minutes with a high inflow rate of several liters per minute. Afterwards the proper flow of 6l/hour was set using a volumetric flow measurement system consisting of a graduated glass, a stopwatch and a bucket of water. The volumetric inflow during either 30 or 60 seconds was captured in an overturned glass held under the water level. From this it became possible to estimate the hourly inflow. The accuracy of this measurement was estimated to be in the range of ±2ml/30 seconds. During the first weeks the inflow was checked after two days, but since no changes were observed, any further checking was deemed unnecessary.

6. RESULTS AND EVALUATION

Multi-level data selection procedure was implemented to select proper and independent breakdowns from the all of the current-triggered events and discharges recorded during MultiBreak measurements. This procedure is discussed in the first part of this chapter.

Measured changes in the breakdown performance of test films are presented in the second part of this chapter. Visually and mathematically fitting distributions are implemented to model the data, whose parameters in addition to calculated 5%, 63.2% and 95% breakdown probability percentiles are used to evaluate and characterize the changes.

The third part of this Chapter focuses on the big picture compiled of the previously reviewed measurement results. A summary of the changes is given after which a speculative chain of reasoning of the factors behind is given. Finally possible sources of error and their effects are evaluated.

The fourth part of this Chapter is focused on the possibilities of future work. Although the experiment provided valuable information on the thermoelectric aging of polymers and polymer composites, a larger number of materials and combined thermoelectric stresses are needed for results applicable to practical capacitor insulation systems.

6.1 Data selection

Behavior of the test films during MultiBreak measurements is divided in three regions: the weak spots, the intrinsic region, and the after-intrinsic region. Since the transition from fast to slow ramp up was at 4kV equaling to electric field of approx. 250V/μm, no discharge activity was normally observed during the fast ramp up at 400V/s. Starting from the beginning of the slow 30V/s ramp up there was a possibility of isolated breakdowns at relatively low electric fields. These breakdowns are assumed to result from weak spots in the polymer matrix, as they occurred randomly in the test area. Only in rare cases the first breakdowns were adjacent to the film edges, suggesting they were not caused by any inhomogeneity in the test arrangement.

The intrinsic breakdown period followed the weak-spot region when then defect-free (intrinsic) breakdown strength of the dielectric was exceeded. The period was characterized by unremitting breakdowns, which continued until the electrodes were isolated from the HV supply or earth due to segmentation caused by excessive vaporization of the metallization. These discharges represented the large majority of the total discharge events recorded during measurements.

Following the intrinsic region, the after-intrinsic region was characterized by seemingly random discharging across the isolated electrode regions and by few self-healing breakdowns. Due to the excessive damage induced during the intrinsic period it was considered improbable these breakdowns would neither be independent nor represent actual material properties. Nevertheless the ramp-up was continued until no events were recorded for 10…20 seconds. A typical film behavior displaying these three regions is illustrated in Figure 6.1.

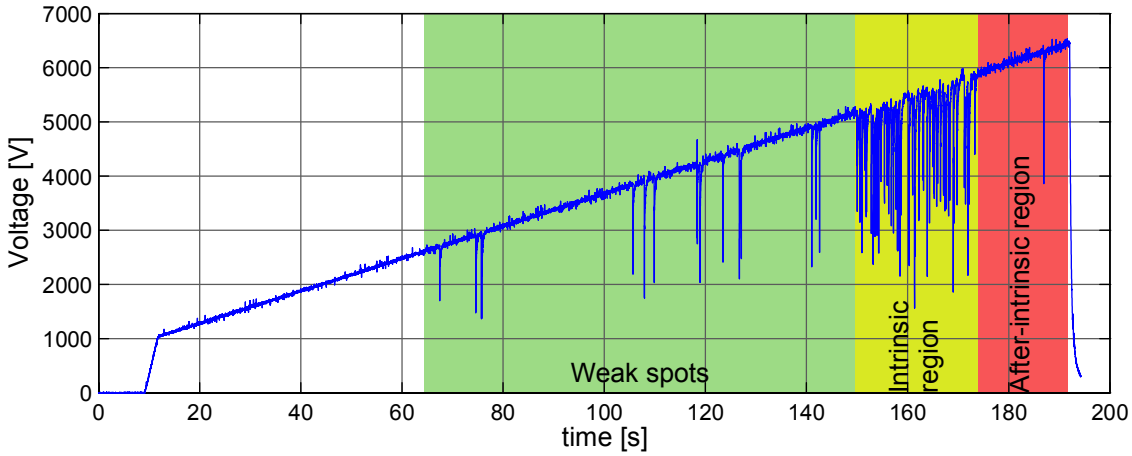

Figure 6.1. Voltage drops recorded during MultiBreak indicate discharge activity. Three characteristic regions can be seen from the LabView voltage record of one 9µm RERS film sample.

Often during the intrinsic period several consecutive self-healing breakdowns occurred in the immediate vicinity of each other. As the subsequent breakdowns occurred at significantly lower electric fields, only the first breakdown would represent the actual unaffected breakdown strength of the film, and any subsequent breakdowns were omitted from the analysis. The sequential breakdowns were likely caused by the thermal energy dissipated during the first breakdown causing subsequent thermal breakdowns. A voltage record displaying several consecutive breakdowns at lower voltages during one second is depicted in Figure 6.2.

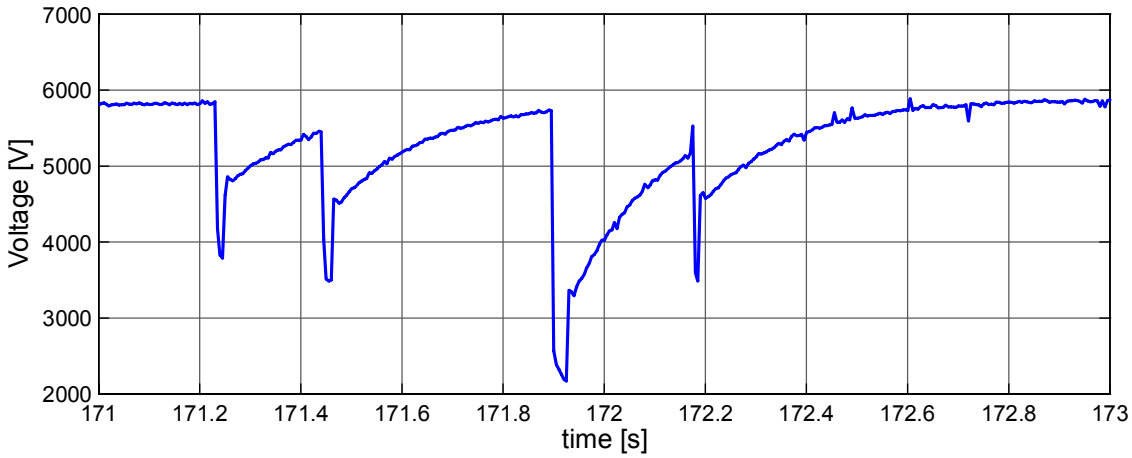

Figure 6.2. Voltage measurement during a MultiBreak measurement displaying subsequent heat-induced breakdowns at significantly lower fields, followed by a return to the 30V/s ramp.

At times during the weak spot region subsequent breakdowns occurred in the immediate vicinity of previously self-cleared areas. Contrary to the intrinsic region, a number of cases were recorded where the duration between subsequent breakdowns was several second. Given the thermal energy from the previous breakdown had had time to dissipate, its influence was considered improbable. It was concluded the subsequent breakdowns were likely caused by the local electric field exceeding the combined breakdown strength of the de-metallized area and of the previous breakdown hole. This was supported by the fact the de-metallized area is dependent on the breakdown voltage, and in the areas caused by early low-voltage breakdowns were miniscule compared to those seen at higher fields. Since it was likely these breakdowns did not represent the dielectric breakdown strength (DBS) of the polymer film but rather the DBS of the previously cleared de-metallized area, they had to be excluded from the analysis.

To evaluate material properties it was essential that only individual and uncorrelated self-healing breakdowns would be used for later analysis. Therefore it was necessary to identify and then exclude both aforementioned types of non-independent types of breakdowns and any non-breakdown discharge activity, such as surface discharges, discharges at the electrode edges, the high field discharges and possible partial discharging in gas bubbles.

To be qualified as an individual and isolated breakdown the discharge voltage and energy had to pass two-step selection criteria, which were implemented using custom MATLAB-based programs written by M.Sc. researcher Ilkka Rytöluoto. The used criteria were:

1. Voltage criterion: the breakdown voltage has to be higher than in the previous breakdown
2. Energy criterion: The discharge energy has to follow a trend set by the first two breakdowns

The voltage criterion was evaluated individually for each film sample[9], whereas the energy criterion was evaluated material-wise using all six film samples removed at the same temperature. Whereas the reasoning behind the voltage criteria is self-explanatory, the energy criteria is derived from Equation (3.32). Since the sheet resistance and external pressure remain constant during testing, the discharge energies E_B at arbitrary breakdown voltages E_B should follow a power fit in the form of Equation (6.1), where a and b are coefficients determined by the first independent breakdowns:

$$E_B = a(U_B)^b \tag{6.1}$$

A minimum threshold was calculated based on the first two pulses and the discharge passed the criterion if the discharge energy was above the threshold. Any discharges with calculated energies below the boundary were omitted as non-independent. A large number of discharges were omitted by the energy criterion, which implies these discharges were either not proper breakdowns, or they were influenced by variations in

[9] Disambiguation: *film sample* refers to a piece of material illustrated in Figure 5.1, whereas later on the term *sample* is used for the individual finite-time parts of which the recorded voltage and current waveforms consist of.

the surrounding conditions. Without taking a firm stand on the reasons behind these variations changes in the film structure, such as accumulation of partially conductive carbon residues or temperature-induced damage from previous clearings are seen as possible causes. The effects of the selection criteria are demonstrated in Figure 6.3.

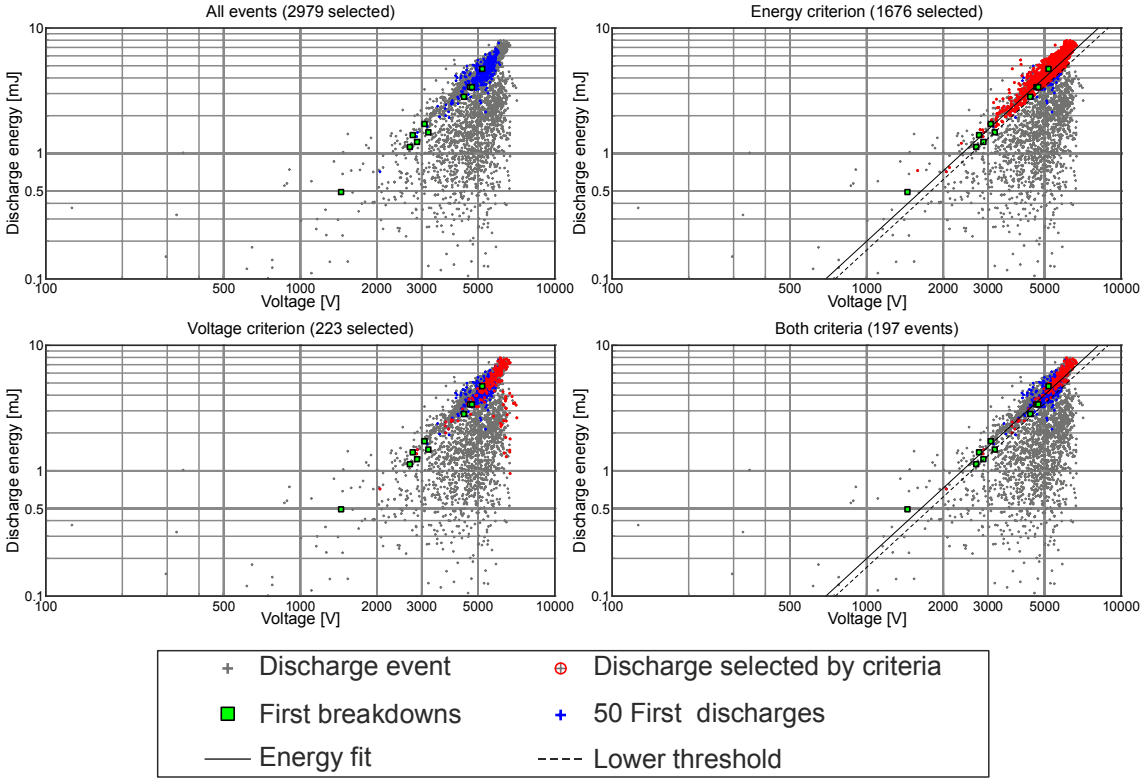

Figure 6.3. The effects of the selection criteria. First breakdowns followed the energy fit well. Approximately 94 % of the recorded discharge events are omitted as non-independent, most of which occurred near the end of the measurement.

Due to its importance for the energy criterion the outlines of the discharge energy calculation will be discussed next. As stated in Section 5.2 every time a discharge occurred in the test capacitor, the energy dissipated would be replaced from the external circuit, mostly from the output capacitors of the HVPS. The current pulses were recorded together with the DUT voltages, and discharge energies were calculated by numerically integrating them. As an example for typical waveforms recorded the current and voltage behavior, and the calculated momentary power during the first breakdown in one unaged RER14.4 film sample is depicted in Figure 6.4.

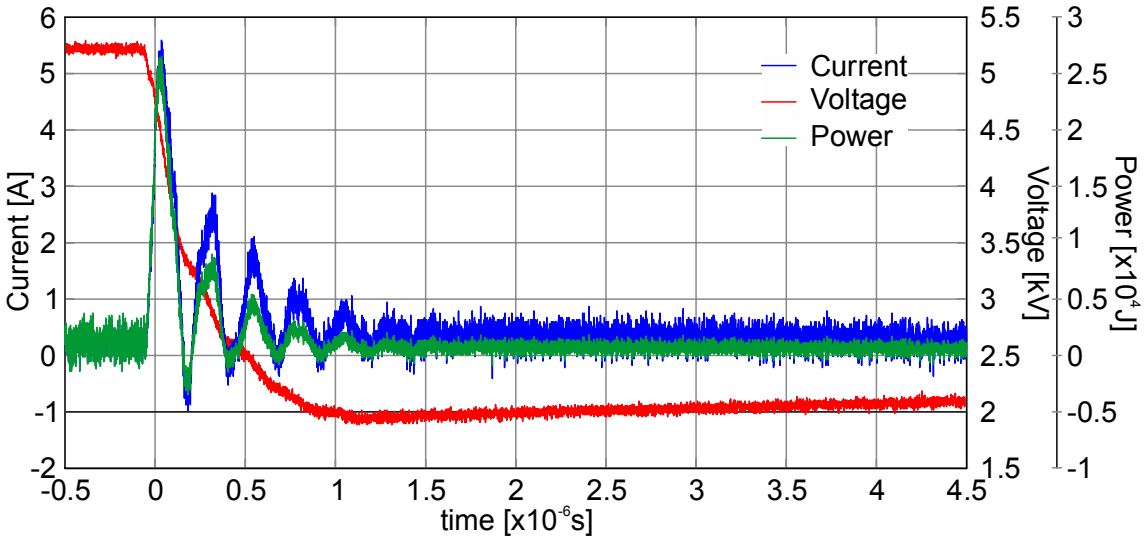

Figure 6.4. Voltage drop, external current and calculated momentary power during a self-healing breakdown at 5.3kV. The current oscillations are damped presumably due to the output capacitance in the HVPS. As the current drops to zero so does the power.

The current and voltage waveforms demonstrated in Figure 6.4 consist of 10000 sample points. For all of these sample points of the oscilloscope record, marked as s_N, the corresponding discharge powers P_D , visualized as a green line in Figure 6.4, were calculated by multiplying the measured voltage and current values, marked as $u(s_N)$ and $i(s_N)$:

$$P_D(s_N) = u(s_N) \times i(s_N) . \tag{6.2}$$

Since the sampling interval t_{sample} was constant and set beforehand, the corresponding discharge energies E_D were calculated:

$$E_D(s_N) = P_D(s_N) \times t_{sample} . \tag{6.3}$$

The total discharge energy E_{Dtot} for each pulse was calculated by summing up the factorials:

$$E_{Dtot} = \sum_{N=1}^{N=k} E_D(s_N) . \tag{6.4}$$

The measurements were recorded using a webcam and the first breakdowns were visually verified to exclude surface discharges from disturbing the energy criteria. In case the first recorded event was not a proper breakdown, the first actual breakdown was searched for, after which all events before it were deleted. Additionally in some cases the oscilloscope did not trigger at the first breakdowns due to the low magnitude of the current pulse. Even in these cases the breakdown was audible and discernable as a voltage drop in the LabView voltage record. The breakdown voltages were determined afterwards using the captured video and the LabView voltage record, and the first breakdowns were manually added to the list of verified proper breakdowns.

6.2 Statistical analysis

Traditionally the breakdown strength of materials is characterized using 2-parameter Weibull distributions, which yield comparable parameters indicating the electric field equaling to 62.2% failure chance (Weibull-α) and the dispersion of the measured breakdowns (Weibull-β). For the sanity of the comparisons the measured data must fit the distribution of choice relatively well, a quality which can be evaluated both visually and using mathematical goodness-of-fit tests.

The breakdown data was fitted with a representative distribution by comparing the goodness-of-fit results from modified Kolmogorov-Smirnov (K-S) tests and by visually observing how well the probability line would follow the data points. Single 2-parameter Weibull distributions were preferred, but in cases where evident deviation was observed, additively mixed 2-subpopulation 2-parameter Weibull distributions were used to reach a better fit. In all cases the number of subpopulations was kept at minimum needed to attain a visually matching fit.

A harmonized notation in which the populations were numbered in their conjectural and initial order of appearance was used. Separate defect population and its parameters are denoted as 1 and the intrinsic region with the majority of breakdowns as 2. Although in many cases individual points diverted from the probability line at high fields it was uncertain whether or not this was saturation caused by decreasing intact area of the test film. For this reason no third subpopulation was used.

Different parameter estimation methods were noticed to result in significantly different distribution parameters. Given the large number of data points maximum likelihood estimation (MLE) was tried first, but in cases where the estimated probability line diverted from the data points better results could often be acquired by switching to linear recursion on either X (RRX) or Y (RRY). In cases where neither resulted in a visually good fit with the majority of data points individual low-field outliers were excluded from the parameter estimation to attain a visually good fit. Fisher information matrix (FM) was used to calculate the confidence bounds, but in cases where the aforementioned failed to converge beta-binomial (BB) method was used.

6.3 Aging trends

6.3.1 Breakdown behavior of non-aged samples

The breakdown performance of NPO-materials had been evaluated during a previous NANOPOWER-project, whereas unaged reference samples of RER and RERS materials were measured by the author. All film samples were cut from the same roll (RER and RERS) or from the same batch (NPO materials) to exclude possible variations between batches from affecting the results. Since there was an abundance of RER film 30 samples were measured, equaling to a measured area of 2430cm^2. As for

RERS and NPO materials a reference of 10 samples equaling to a measured area of 810cm^2 was used.

Unaged RER and NPO films demonstrated homogenous breakdown behavior, and no outliers deviating from the main distribution were observed. A two-parameter Weibull fit was used to model the data. On the other hand the breakdown behavior of the RERS9 film was characterized by the presence of weak spots. The weak spots, as seen in Figure 6.5 deviated from the main distribution, and a two-subpopulation additively mixed 2-parameter Weibull distribution was used. The behavior of the unaged test films is portrayed in Figure 6.5.

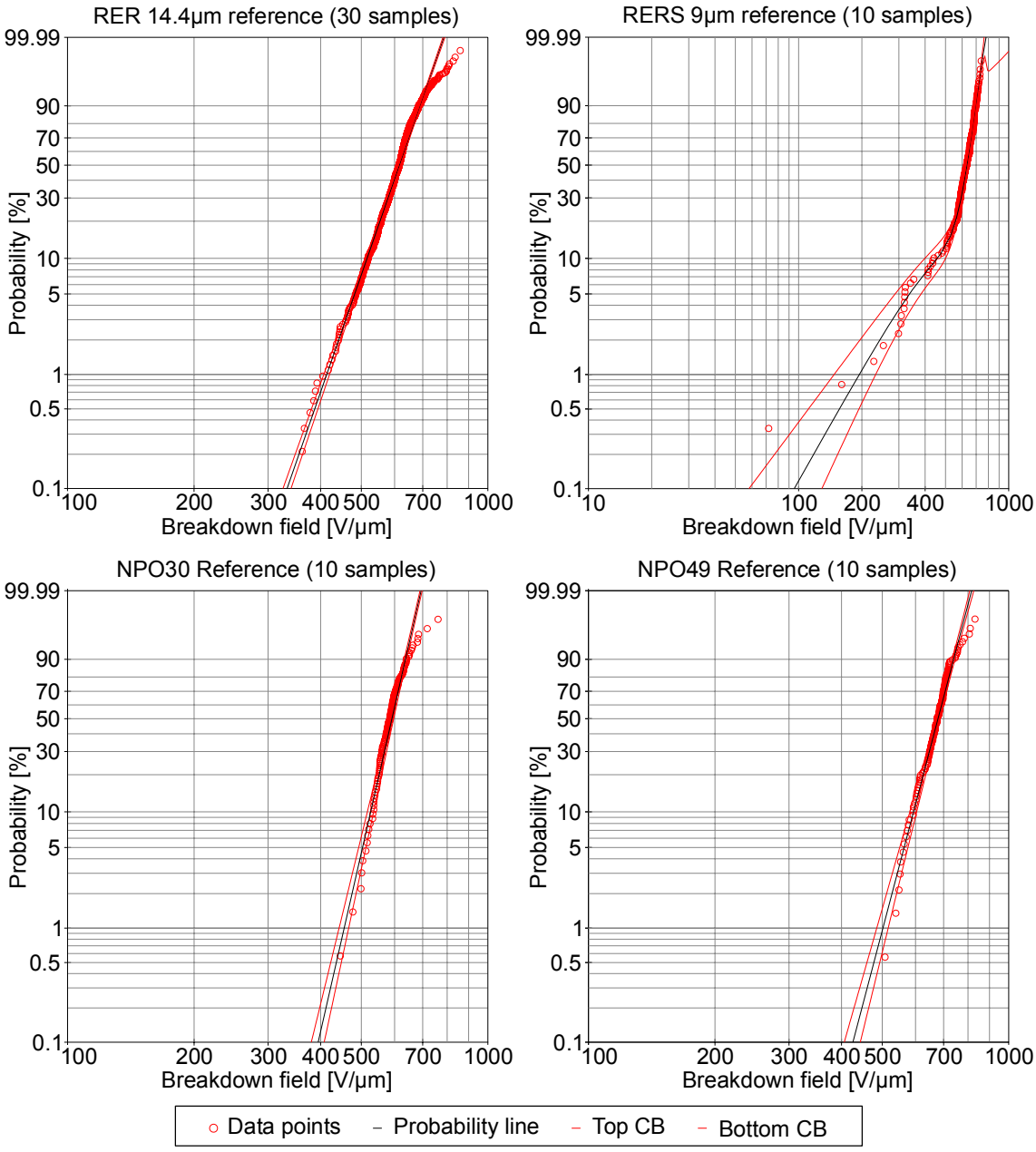

Figure 6.5. Breakdown behavior of unaged test films. RER and both NPO films displayed homogenous breakdown behavior and a single Weibull fit was adequate. RERS film was characterized by the presence of weak spots, and a two-subpopulation Weibull fit was used.

As seen from Figure 6.5 the breakdown data from the unaged materials fit well to the chosen distributions and a large majority of data points were located between the one-sided 90% confidence bounds. Out of the unaged films NPO49 had the highest 63.2% breakdown strength, whereas the NPO30 displayed the most homogenous breakdown behavior. If the intrinsic breakdown strength represented by the majority of breakdowns is considered RER and RERS films were comparatively similar, as seen from the Weibull scale parameters α_2 of 637 and 660 for RER and RERS respectively. The presence of defects in the RERS film is taken into account in the defect population characterized by large scatter (Weibull β_1 of 3.278) and low characteristic breakdown strength (Weibull α_1 of 419.3). The Weibull parameters are reflected as the steepness and vertical position of the curves in Figure 6.5. In addition to distribution parameters the breakdown behavior of the test films was evaluated by percentiles representing the 5%, 63.2% and 95% breakdown probabilities. In the three cases where a single Weibull distribution was used the 63.2% equaled to the α_2. The distribution parameters and percentiles with one-sided 90% confidence bounds from the unaged films are displayed in Figure 6.6.

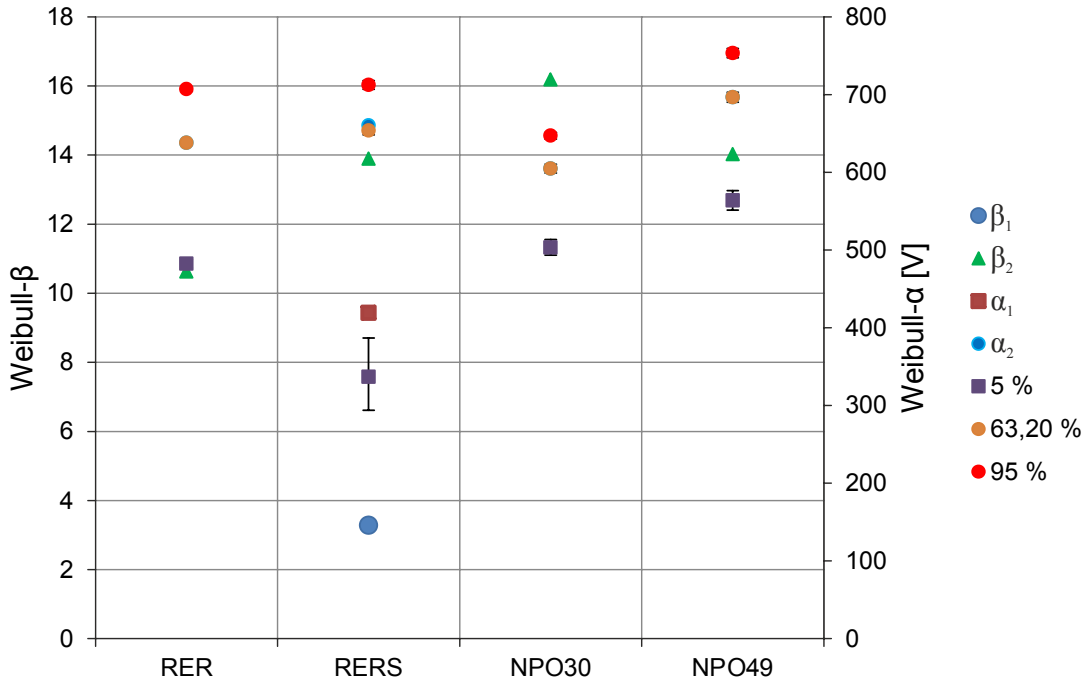

Figure 6.6. Distribution parameters and percentiles of unaged films. Smaller scatter of breakdown voltages is reflected as a higher β values. Out of the tested films NPO30 displayed most homogenous breakdown behavior, whereas NPO49 displayed highest breakdown strenght.

The numerical values corresponding to Figure 6.5 are given in Table 3.

Table 3: Weibull parameters and percentiles of unaged films.

	RER	RERS	NPO30	NPO49
No. of breakdowns	793	205	121	124
No. of subpopulations	1	2	1	1
Portion 1		0.13		
β_1		3.3		
α_1		419		
Portion 2		0.87		
β_2	10.6	13.9	16.2	14.0
α_2	638	660	605	697
5 %	482	337	503	564
63,20 %	638	654	605	697
95 %	707	712	647	753

As seen from Table 4 the absence of outliers in RER and NPO films results in narrow confidence bounds even in the low probability regions.

6.3.2 Changes in RER film

The changes in the breakdown behavior of RER film were characterized by the appearance of weak spots after 70°C and by the relatively constant intrinsic breakdown strength. The appearance of weak spots after being subjected to 70°C is displayed in Figure 6.7.

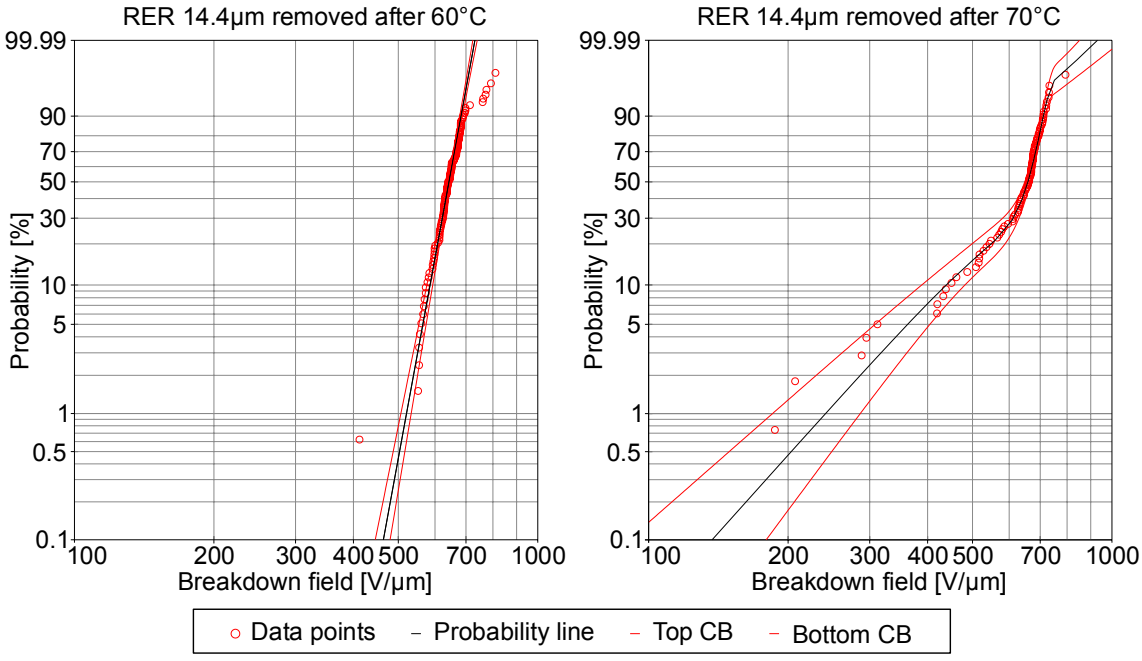

Figure 6.7. Comparison between RER film removed at 60°C and 70°C. The appearance of weak spots after 70 °C is evident, and a two-subpopulation Weibull fit was used to model the data.

After 70°C weak spots were observed in every subsequent measurement until their disappearance after 110°C. The appearance of weak spots is seen in the 35% decrease in

the 5% percentiles between 60°C to 70°C. The small amount of data points from lowest voltages resulted in broader confidence bounds towards lower probabilities. The relative portion of the weak spot subpopulation peaked at 0.49 after 80°C and 90°C, and the disappearance of the weak spots was seemingly foreshadowed by the decreasing relative portion from 90°C to 100°C. The disappearance of the weak spot subpopulation resulted in the 5% percentiles returning close (561V/µm) to those measured before their appearance (565V/µm). It was suspected the apparent disappearance of the weak spots after 100°C was either

1. a stochastic issue resulting from the uncertainty associated with breakdown phenomenon or
2. a result from unfamiliar physiochemical or morphological changes occurring at high temperatures.

The issue is further discussed in Section 6.4.1. The disappearance of the weak spots is illustrated in Figure 6.8.

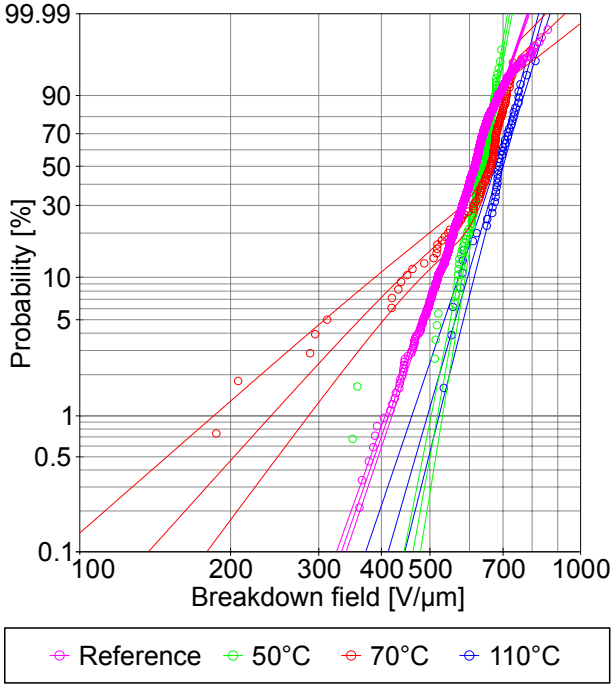

Figure 6.8. Breakdown behavior of RER film removed after selected temperatures. The disappearance of weak spots after 110°C is visible, as well as an overall shift towards higher breakdown fields.

Seemingly independent of the presence of the weak spots both Weibull β_2 and the 63.20% percentile increased slightly during the measurement, as evident from Figure 6.9.

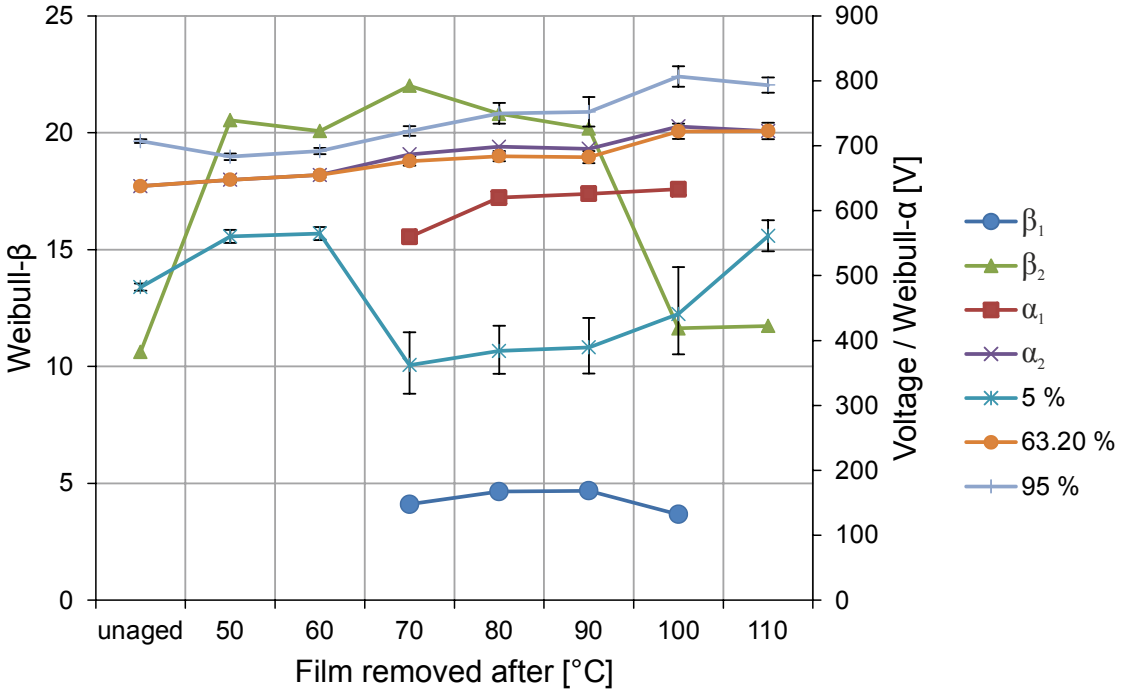

Figure 6.9. Breakdown behavior of 14.4µm RER film: distribution parameters and percentiles with one-sided 90% confidence bounds. The presence of weak spots after 70°C is apparent from the introduction of a second subpopulation with large scatter and low characteristic life.

Numeric values corresponding to Figure 6.9 are given in Table 4.

Table 4. Weibull parameters and percentiles for RER.

	ref.	50°C	60°C	70°C	80°C	90°C	100°C	110°C
No. of breakdowns	793	102	111	93	118	89	81	48
No. of sub populations	1	1	1	2	2	2	2	1
Portion 1				0.32	0.49	0.49	0.21	
β_1				4	5	5	4	
α_1				560	620	626	633	
Portion 2				0.68	0.51	0.51	0.79	
β_2	11	21	20	22	21	20	12	12
α_2	638	648	655	687	698	695	730	723
5 %	482	560	565	362	384	389	441	561
63,2%	638	648	655	676	684	682	722	723
95 %	707	683	692	723	750	752	807	793

RER film was noticed to curl at the free-hanging film edges. The curling was noticeable immediately after 50°C, and increased towards the higher temperatures. The curling hindered the sample preparation, but as the film was wider than what was required for the samples in most cases it was possible to leave out the curled edges.

For breakdown field calculations the thicknesses of the 30 reference film samples were measured. As expected from a capacitor grade film, the measured average of 14.25µm was close to the reported nominal of 14.4µm, with a standard deviation of 0.57µm. The nominal thickness of 14.4µm was used in breakdown field calculations,

but to rule out any temperature-induced systematic changes the thicknesses of randomly selected samples were measured immediately after the 80°C. The measured thicknesses in the range of 14.08…14.46µm showed no temperature correlation and remained well within one standard deviation from the unaged reference.

Based on the appearance of weak spots and the constant 63.2% breakdown strength it was deducted that thermal stresses did not affect the polymer matrix as a whole, but that aging had occurred locally. It was suspected the appearance of a distinct weak spot subpopulation indicated a different breakdown mechanism. Given that no weak spots were measured in the 30 reference measurements or in any of the samples removed after 50 and 60°C, and since the film samples were from the same roll, a pre-existing fault in the film was considered improbable.

6.3.3 Changes in NPO30 film

The changes in the breakdown behavior of nanosilica NPO30 were characterized by an increasing scatter towards higher temperatures. The first breakdowns occurred at lower voltages towards the end, but contrary to RER film no separate weak spot population was observed. A visually good fit was acquired with 2-parameter Weibull distributions, using which percentiles representing 5, 63.2 and 95% breakdown probabilities were calculated. The increasing scatter resulted in decreasing values of Weibull-β parameter, broader confidence bounds and simultaneously decreasing 5% and increasing 63.2% and 95% percentiles. The distribution parameters and percentiles are displayed in Figure 6.10.

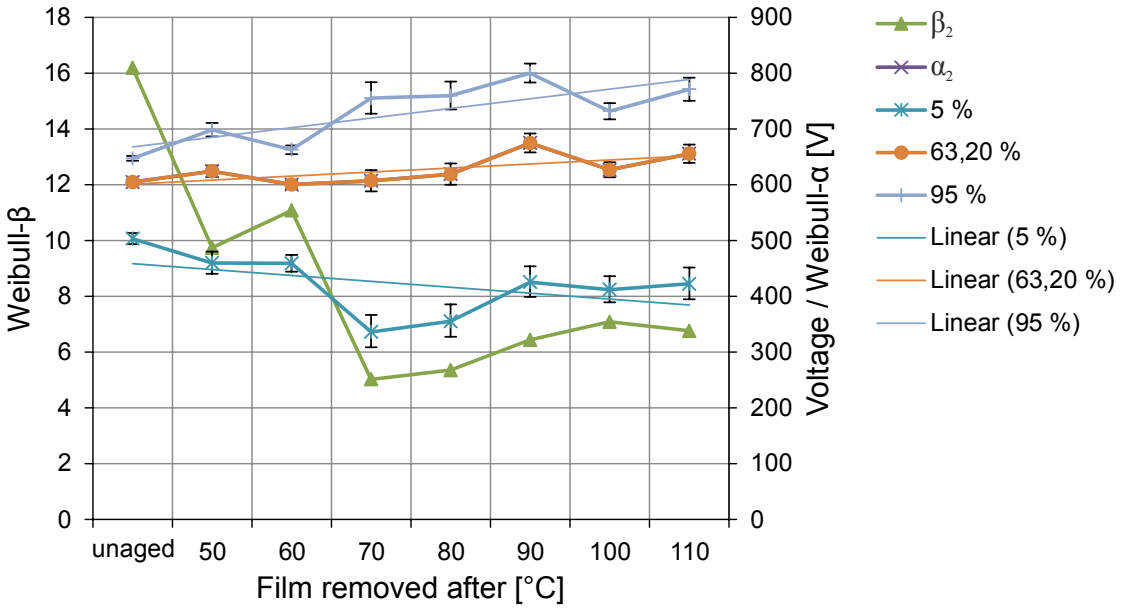

Figure 6.10. Percentiles and Weibull parameteres of NPO30 film. Increasing scatter in breakdown voltages is seen from lower β_2 parameters and from broad confidence bounds.

Weibull parameters and percentiles corresponding to Figure 6.10 are displayed in Table 5.

Table 5. Weibull parameters and percentiles for NPO30.

	ref.	50°C	60°C	70°C	80°C	90°C	100°C	110°C
No. of breakdowns	121	72	91	72	67	78	84	64
No. of sub populations	1	1	1	1	1	1	1	1
β	16.19	9.74	11.08	5.03	5.36	6.44	7.08	6.76
α	605	624	600	607	619	675	627	655
5 %	503	460	459	336	355	425	412	422
63.20 %	605	624	600	607	619	675	627	655
95 %	647	698	663	755	759	800	732	771

Although a single Weibull distribution modeled the large majority of data points well, especially towards low probabilities data points diverted from the probability line, with the first breakdowns remaining outside of the calculated 90% confidence bounds. The uncertainty regarding low probabilities at lower fields is increased, and the calculated 5% percentiles should be used with care. A multiple-subpopulation model was considered but ultimately rejected, as although it would have resulted in a visually better fit in the low probability region the deviation was seen as a result from the stochastic nature of breakdown phenomena, and not as a sign of a separate low-field breakdown mechanism. As for an example of typical deviation the results from film samples removed after 70 and 110°C are displayed in Figure 6.11.

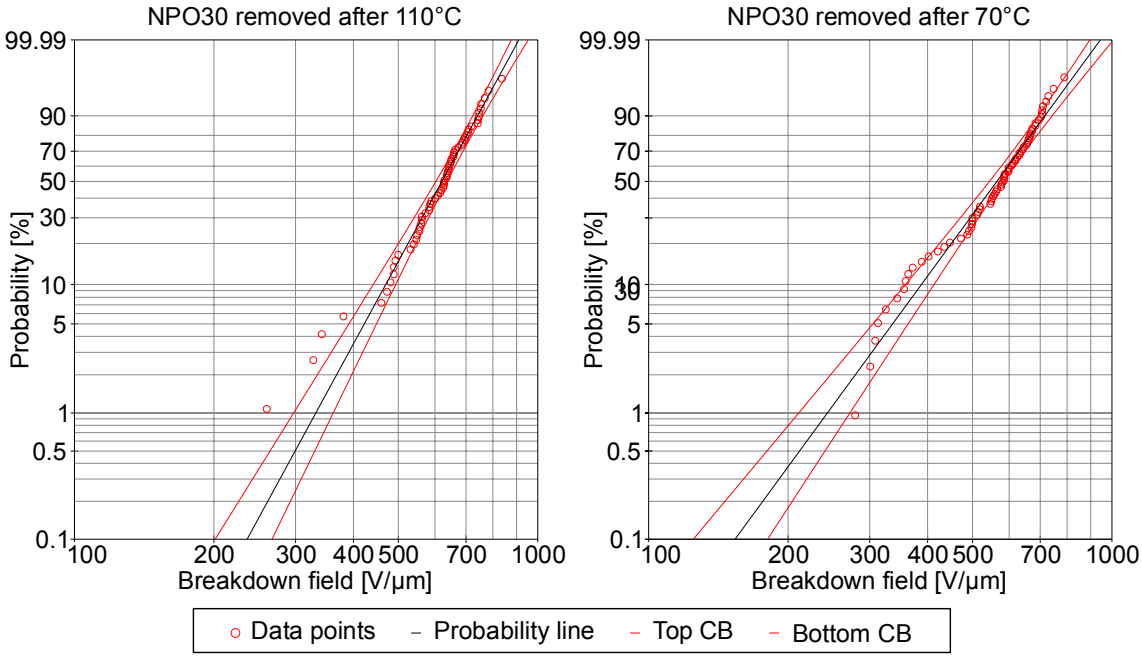

Figure 6.11. Breakdown data measured after 70 and 110°C. Stochastic nature of breakdown phenomena is seen as low probability data points diverting from the single Weibull probability line.

The total average thicknesses of the NPO30 film varied from 15.05 to 16.08 between measurements, with total standard deviation of the six film samples used for each measurement ranging from 0.89 to 1.52. As expected from pilot-scale films the thickness variations were greater than in RER film, both between film samples and the 25 measurement points in each sample. Contrary to the RER film, NPO30 had a characteristic thickness profile, for the film was thicker towards the edges. With edge thickness being in the range of 17…20µm, the middle parts were preferred for sample preparation. Given that no systematic changes in the average film thicknesses were measured and the measured averages were within 10% of each other, their effect on the results was deemed insignificant.

The data measured after 50 and 60 °C consist of 4 and 5 samples respectively, compared to the nominal of 6. Visible scratching was observed in two films samples removed after 50°C, and in the subsequent measurements the first breakdowns occurred near or at the damaged areas. It was suspected that the breakdown behavior of these samples was influenced by the combined effect of condensation of the electric field and lowered dielectric breakdown strength in the damaged areas. As a result the measurement data from these samples was excluded from further analysis.

Breakdown analysis on the samples measured after 60°C revealed the presence of a small (relative portion of 0.166) weak spot subpopulation. Further inspection revealed the weak spots originated from a single film sample, in which no visible damage had been observed before testing. Moreover the weak spots were concentrated in one quarter of the film sample. A material defect was suspected since the breakdown behavior of this individual film sample diverted not only from the rest measured at the same time, but also from film samples measured at different temperatures. Therefore it was decided to exclude the sample from further analysis. This removed the defect population entirely, as demonstrated in Figure 6.12.

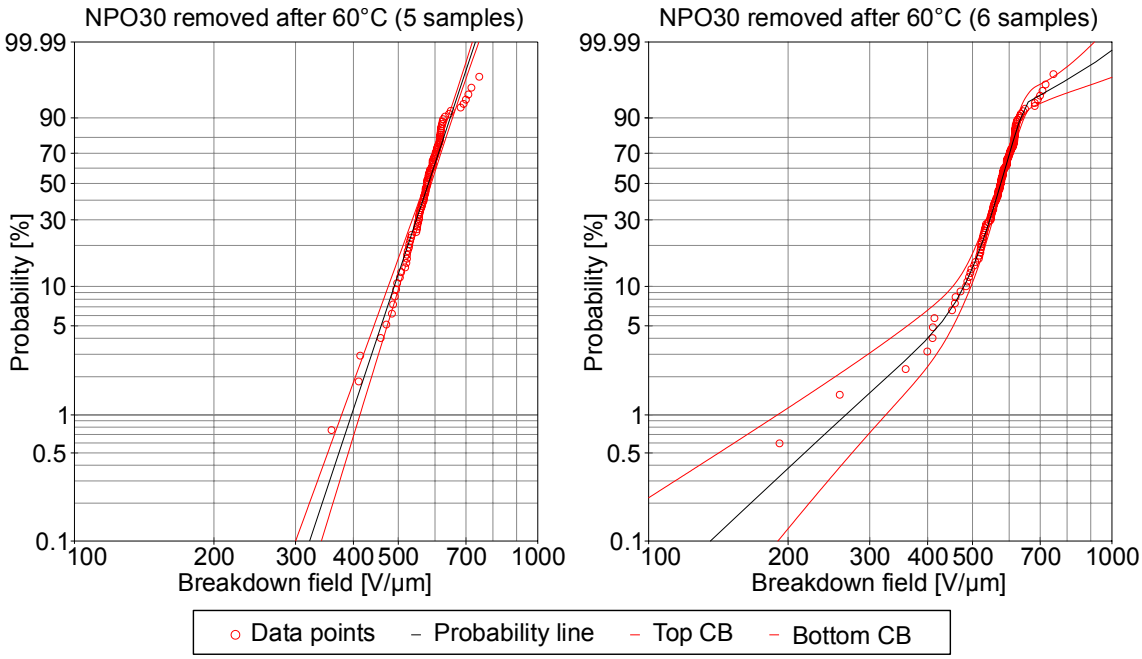

Figure 6.12. A distinct defect population was measured in one of the six film samples removed after 60°C. The exclusion of this presumably damaged sample removed the weak spot subpopulation entirely.

Given that the weak spots did not follow the main distribution, it was suspected a different breakdown mechanism had taken place in the presumably damaged portion of the film. Confirmation of the presumption through retrospective analysis was unfeasible as the samples were thoroughly destroyed during the measurement.

If the overall changes are considered, the breakdown behavior of NPO30 was homogenous throughout the aging. Further discussion on the underlying aging and breakdowns mechanisms is conducted in Section 6.4.1.

6.3.4 Changes in NPO49 film

Similarly to the other pure PP film RER, a distinct weak spot subpopulation was measured in NPO49 after 50°C. A two subpopulation 2-parameter Weibull distribution was used as it resulted in both visually and mathematically good fit. Contrary to RER film however the relative portion of the initial weak spot subpopulation, later on marked with subscript 1, increased constantly, until after 80°C the originally dominant population had disappeared completely. As its relative portion increased the characteristic breakdown strength (α_1) of the first subpopulation increased, and as a result the 63.2% breakdown strength of the material remained relatively constant between 50-80°C. The scatter of the first subpopulation (β_1 of 2.5…4.3) however remained noticeably higher than that of the unaged reference (β_2 of 14.0), and after 80°C the breakdowns displayed noticeably higher scatter when compared to the unaged reference.

After 90°C the dispersion of the breakdown voltages declined suddenly, and the breakdown behavior started to resemble that of the unaged reference, with the exception

of few outliers in the low field and low probability region. The outliers were omitted from Weibull parameter estimation after 100°C and 110°C to reach a visually good fit with the main population. The behavior of the NPO film is depicted in Figure 6.13.

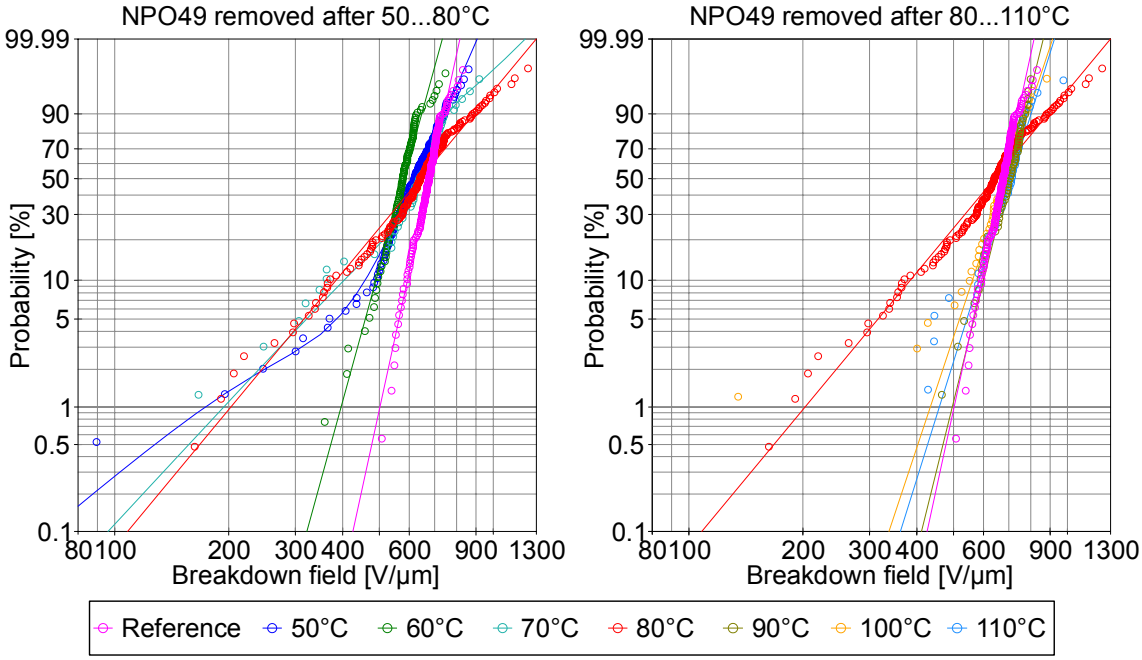

Figure 6.13. The changes in the breakdown behavior of NPO49 film. A weak spot population appeared after 50°C only to disappear after 90°C.

The disappearance of the weak spot subpopulation resulted in a 73% increase of the calculated 5% percentiles. However as seen in Figure 6.13 individual breakdowns diverting from the Weibull probability line were measured at low fields. The distributions fitted to the large majority of breakdowns do not model the low field behavior well, and individual breakdowns were recorded at low fields with a significantly higher probability than what could be extrapolated from the calculated probability line alone. Weibull parameters and percentiles calculated are displayed in Figure 6.14.

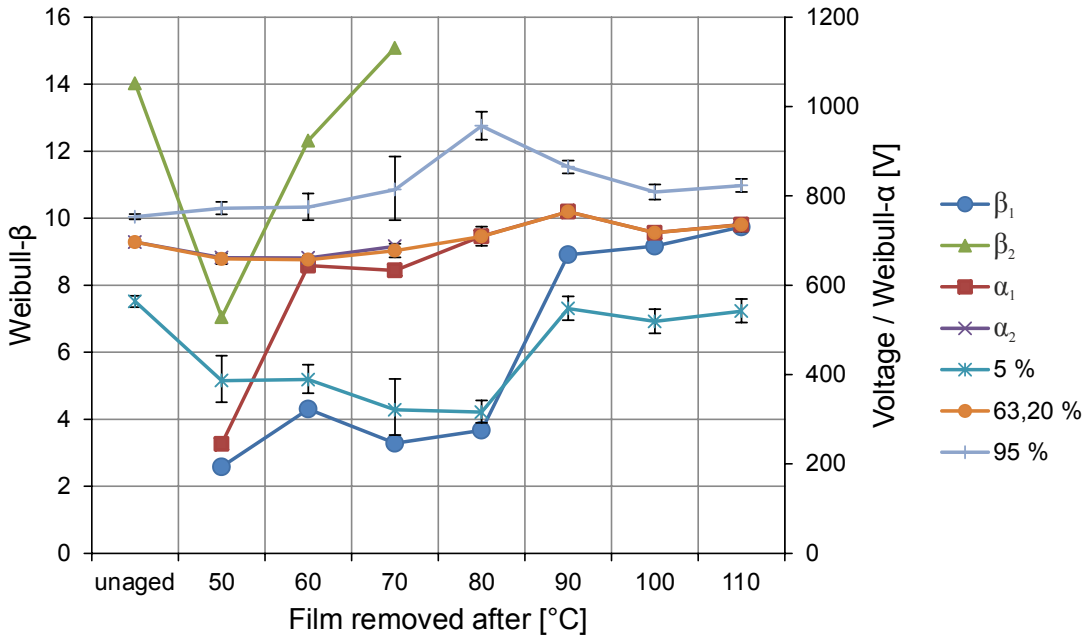

Figure 6.14. Percentiles and Weibull parameters for NPO49 film. The appearance and disappearance of a "weak spot" subpopulation is seen in fluctuating 5% percentiles while higher probability percentiles stay relatively constant.

The Weibull parameters, the relative portions of the subpopulations and percentiles corresponding to Figure 6.14 are displayed in Table 6.

Table 6. Weibull parameters and percentiles for NPO49.

	ref.	50°C	60°C	70°C	80°C	90°C	100°C	110°C
No. of breakdowns	124	132	175	55	144	69	57	50
No. of sub populations	1	2	2	2	1	1	1	1
Portion1		0.03	0.46	0.49				
β_1		2.58	4.3	3.28	3.67	8.91	9.17	9.74
α_1		245	644	633	709	764	717	735
Portion2		0.97	0.54	0.51				
β_2	14.03	7.05	12.32	15.08				
α_2	697	662	661	687				
5 %	564	386	389	321	316	548	519	542
63,20 %	697	659	657	677	709	764	717	735
95 %	753	772	775	814	957	865	809	823

Contrary to the RER film, neither of the NPO films curled noticeably during the experiment. The average thicknesses of the six NPO49 film samples for each measurement were in the range of 15.03…16.27µm, with standard deviation of the 25 measurement points ranging from 0.28 to 1.16µm. The thickness variations between samples were higher, with standard deviation calculated from the six samples ranging from 0.94 to 2.2µm. The thickness profile of NPO49 was similar to that of NPO30, with film thickness increasing towards the film edges. Since the NPO49 supply was limited individual samples were cut from relatively close to the film edges, and thicknesses up

to 20µm were measured. Given the breakdown fields were calculated using average thicknesses of the 25 measurement points this was seen as one source of possible error.

6.3.5 Changes in RERS film

RERS 9µm film was characterized by the disappearance of the distinct weak spots. A 2-parameter Weibull distribution was used to model the breakdown behavior of aged samples. 5 samples were measured after 100°C and 4 after 110°C, the results of which are depicted in Figure 6.15 below.

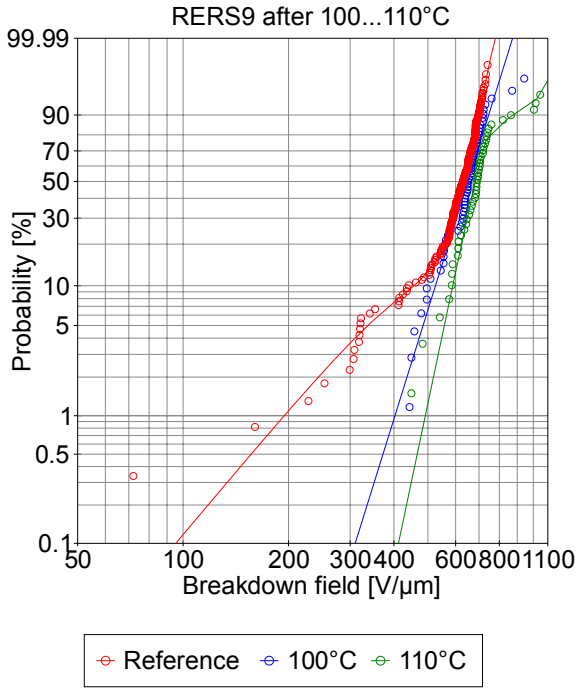

Figure 6.15. RERS breakdown behavior after 100 and 110°C. No distinct weak spots were measured in the aged samples.

The films were folded twice during the aging, which resulted in them being stuck together. The films were separated carefully, but due to tearing only 9 seemingly intact film samples could be produced. Unlike RER, RERS did not curl noticeably.

6.4 Aging mechanisms and factors of influence

6.4.1 Summary and speculations

Based on the measurement results described in Sections 6.3.1 – 6.3.5 the changes in the breakdown behavior of the thermally aged samples can be summarized as:

1. The appearance of a distinct weak spot subpopulation in pure PP materials (RER, NPO49) after a temperature step of 50…80°C.
2. The disappearance of the previously measured weak spot subpopulation in pure PP materials (RER, RERS, NPO49) after a temperature step of 90…110°C.
3. The absence of a distinct weak spot subpopulation in PP-based nanosilica NPO30.

4. Increased scatter of the breakdown voltages in NPO30.

The formation of the weak spot subpopulation in pure PP-based materials is presumed to result from locally occurring degradation. A number of studies reviewed in [93] have been discussed previously in Section 4.1, in which thermoelectric aging has been associated with defect formation in the insulation bulk. The measurement results indicated that thermal stresses alone were enough for defects to appear. Labeling the measured weak-spot formation either as degradation or aging is ambiguous, since as discussed in Section 4.1 even the very definition of polymer aging is ambiguous. The nature and characterization of the presumably physiochemical and/or morphological factors behind the defect formation are left indeterminate for the time being.

The application of theoretical aging models to the results is not straightforward, and is omitted, since:

1. the material used contained additives and residues, making application of models derived using pure PP samples dubious
2. the step stress used would require the models based on accumulated damage and
3. the broad range of temperatures used may have resulted in different processes and different aging mechanisms operating at different temperatures, in which case accumulated damage models are not necessarily valid and
4. in case of any of the processes relied on any of the additives, the process would grind to halt as the supply was depleted, requiring time-variant analysis and models

Out of the aforementioned 1. and 3. may be linked, as the long-term behavior of processing additives and antioxidants under thermal stresses is totally unknown. Therefore the possibility of unknown processes occurring, which may have had effect on the dielectric breakdown behavior, is high.

The measured differences in the breakdown behavior of between aged NPO30 and pure PP materials may be seen a sign of different aging mechanisms. This viewpoint is supported by studies reviewed in [93] which suggest than aging of polymer nanocomposites occur as damage in the interfacial region. Given that the overall properties of nanocomposites, breakdown behavior included, are determined by the interfacial region any aging-induced changes should be reflected in the breakdown behavior of the material as whole. Therefore changes in the polymer-nanoparticle interfacial region are seen as the most probable reason behind the absence of a defect population and the increased scatter of the breakdown voltages.

The application of traditional aging models to the breakdown behavior measured in pure PP materials is fruitless, as none of the single-process models would explain the apparent disappearance of the weak spots. Therefore a hypothetical reasoning chain behind the measured changes in pure polypropylene materials is given next. The discussion is based on the hypothesis that the appearance and apparent disappearance of the weak spots in pure PP-based materials was a sign of multiple processes dominating

the behavior in different temperature ranges, i.e. they were not results from the stochastic nature of breakdown phenomena.

To assess the situation two complementary temperature-dependent processes are hypothesized. Labeled as 1 and 2, LT process number 1 is behind the defect formation and HT process number 2 acts to mend the already formed defects. Initially at relatively low temperatures the defect forming process 1 dominates; the number of defects and with them the relative portion of the weak spot subpopulation increases. This would explain the appearance and the increasing relative portion of the defect population. As the temperature is stepped up, the reaction rate of process 2 increases, which would explain the decreasing portion of the defect population. The reaction rate of process 2 increases faster than the reaction rate of process 1 and at some point process 2 becomes dominant, having remedied the previously formed defects and suppressing any further defect formation. This would explain the disappearance of the majority of the weak spots.

As a side note the weak spot population measured in the reference film samples of RERS may be seen either a manufacturing issue or as a sign of an unknown defect-forming process operating at room temperatures. Given that RERS samples were measured only near the end there was no way to assess whether or not the relative portion of defect population increased at lower temperatures, which would have supported the two-process model discussed earlier. Given that during storage all films including RERS were subjected to ambient air and with it to gaseous oxygen, even if the defects in RERS were a result from an aging process, the process itself may not be the same as what was experienced during the aging, or what would occur in actual capacitors.

The driving forces behind the processes should be considered separately, as even if temperature-dependent reaction rates are assumed the processes themselves may depend on additives present in the polymer matrix. If it is assumed the defect-forming process 1 represents actual aging of the polymer matrix, it may be reasonable to assume the process itself does not depend on any additives. In this case it would progress continuously through the insulation life at a temperature-dependent rate. Alternatively the process may be related to changes in the antioxidants or residues of processing additives, in which case the process grinds to a halt or changes as its feedstock of reactants is depleted. In this case actual long-term thermal aging would be caused by other processes, whose effects may be negligible to those of the hypothetical processes 1 and 2. Alternatively if the reaction rate of process 1 at service temperatures is slow and the initial reactant loading is high enough, the reactants may last for the insulation lifetime, in which case the aging progression could be dominated by process 1, even if more subtle aging processes existed.

Similar reactant-based approach should be considered for the hypothetical defect-redeeming process 2. In case the defect-redeeming process 2 depends on a supply of reactants, at some point it would grind to a halt too. In case a high temperature level was

retained and if process 1 was not reactant-dependent, the defect formation would resume at a higher rate, leading to faster aging and possibly untimely insulation failures.

Changes in the antioxidant levels and their conversion are seen as one possible explanation for processes 1 and 2. In [25] UV treatment was used to attain an improvement of 7% and 13% in 63% and 5% breakdown probabilities. It was also suggested that the improvement was related to the almost complete conversion of antioxidant Irganox 1010. Therefore it may be possible hypothetical process 2 is be related to changes in antioxidants, as Irganox 1010 residues were measured in NPO49 films. As antioxidant are necessary to prevent degradation from occurring before the capacitor units are hermetically sealed, both RER and RERS film can be assumed to contain antioxidants. The types and concentrations used however were not known. If the antioxidant-based approach is continued one step further one hypothesis is that the defect-forming process 1 was related to intermediate products in the antioxidant conversion chain, and process 2 meant the antioxidant had been depleted. In this case prolonged exposure to high temperatures may result in aging and degradation caused by entirely new mechanisms. If the new mechanism was weak-spot forming by nature, it could account for the few weak spots measured in the latter measurements.

Morphological changes related to relaxation of stresses are seen as another possible explanation. Stresses may develop during the manufacturing and orientation phases, and as discussed in Chapter 2 a correlation between morphological changes and dielectric breakdown behavior exist. The problem of this approach is that it may not explain the absence of weak spots in the initial measurements. It should be noted however that the sample films displayed macroscopic physical changes, such as curling and wrinkling during the aging cycle, which implied towards physical changes taking place. Therefore the possibility of morphological changes as one factor behind the changes in dielectric breakdown behavior should not be ignored.

6.4.2 Error sources

The possible errors in the measurement can be summarized as:

1. uneven temperature in the oven
2. the MultiBreak selection criteria not filtering out all non-independent breakdowns
3. human error during handling damaging the film samples, resulting in weak spots
4. unforeseen variations in the inherent quality of the test films
5. possible loss of inert atmosphere due to unknown issues with the gas regulation.

Even after a fan was added a temperature gradient of 3°C was measured. The temperature measurement spots were determined intuitively, and higher gradients may have been present. However due to the positioning of the samples any horizontal gradient should have negligible effect on the stresses imposed on the film samples measured after each temperature step. Moreover given the constant gas flow the possibility of a gradient higher than 3…4°C was considered negligible. Even though the individual portions and films samples may have been subjected to slightly different

temperatures, the measurement results can still be used to see the big picture and the characteristic changes in breakdown behavior.

Although the MultiBreak selection criteria filtered out a large majority of the non-independent breakdowns and non-breakdown discharges, there was a finite possibility a few non-independent breakdowns passing the criteria and being included in the subsequent probability calculations. The issue was the most notable regarding the first breakdowns, as it was noted some breakdowns occurring adjacent to previously cleared areas passed the criteria. As discussed in Subchapter 6.1. these may have been cases with breakdowns via the previously cleared areas. Nevertheless without concrete evident any of these breakdowns were not removed manually, as although these may have resulted in few additional breakdowns in the weak spot region, their effect on the overall breakdown behavior was considered negligible, as the first breakdowns were definite breakdowns, and in cases were distinct weak spot subpopulations were measured a large majority of the weak spots were scattered around the test area, removing the possibility of a whole defect population being based on one defect and subsequent breakdowns adjacent to it.

Even though the films were handled carefully from sample production all the way to the breakdown measurement itself, possibility of mishandling of the films during storage and transport cannot be ruled out. The quality of the film samples was visually verified and the samples were cut from film sections where no excessive physical damage was evident. Unseen damage may have been the result behind the exclusion of one NPO30 films sample discussed in Subchapter 6.3.3, but given that for other materials and measurements no such divergence between individual samples was noticed, the chance of mishandling induced damage influencing the results is considered low.

Even though mishandling induced damage would be presumably local, inherent variations in the film quality could have resulted in different electrical properties of different portions of the film. To combat this, the film samples were cut from consecutive parts of the film rolls. Moreover as every pure PP materials displayed similar behavior, the possibility of quality-related issues being the sole reason behind the appearance and disappearance of the weak spots is considered very low. Yet despite of it being low, it cannot be ruled out.

A failure in the gas regulation may have resulted in a loss of the inert N_2 atmosphere. In this case the aging behavior observed in the test films could have been entirely different that was is occurring in practical capacitor applications. Redox reactions may have been present, and the antioxidants may have transformed to other compounds due to the presence of atmospheric oxygen. To combat this, after the removal of samples in the middle the oven was purged with high pressure nitrogen for several minutes. The purge was conducted by connecting the coarse pressure regulator to the inlet tube directly, after the regulator outlet was increased to 2…3 bar for several minutes. The drop of the gas bottle pressure during this purge indicated a substantial loss of nitrogen, backed up by the excessive outflow from the outlet valve. After the

purge the hose was detached from the inlet and quickly re-connected to the low-flow regulator. The outflow from the over pressurized oven should have prevented excessive amounts of oxygen from leaking in. Even though a minute number of oxygen may have leaked in, it should have been vented due to constant inflow of N_2 through the low-flow unit. Moreover a slight drop in the gas bottle pressure was noted after each six day period, supporting the presumption of an uninterrupted constant flow.

6.4.3 Implications

The breakdown behavior of the thermally aged pure PP samples did not show consistent behavior as the temperature was stepped up. As discussed in Subchapter 6.4.1 the weak-spot related inconsistency manifested after 70…90°C. Although the temperatures were above the maximum rated ambient temperatures of 50…60°C for most capacitors, they are below the maximum continuous service temperature of 90…100°C for general purpose PP [120] and well below the melting point of 165…170°C [23]. Therefore if this inconsistency is not recognized temperatures above the estimated transition at 60…70°C may be used for accelerated aging experiments. Aging behavior of pure PP films after being subjected to such temperatures may be dominated by different mechanisms than at service temperatures. Erroneous results can be drawn from such experiments. The disappearance of the weak spots results may lead overly optimistic results, which is by definition the worst case, leading to overestimations regarding the insulation lifetime.

On the other hand the breakdown behavior of the measured PP-based nanosilica displayed consistent behavior throughout the temperature range of 50…110°C. This can be seen a sign the primary aging mechanism did not change towards the higher temperatures. Temperatures at least up to 110°C may be used to accelerate aging, as the results from higher temperature stresses may be used to gauge the aging behavior at nominal service temperatures. It should be noted however that this conclusion may not apply for other nanomaterials or even to other types of nanosilicas. Without knowledge on the underlying phenomena the possibility of inconsistent aging behavior should be ruled out individually for each material before such experiments are conducted.

Based on the experimental results it is recommended that accelerated aging and endurance tests for pure PP materials should be conducted at a maximum temperature of 60…65°C. On the other hand aging experiments for PP-based nanosilica materials may be conducted at higher temperatures up to 110°C.

Moreover the factors behind the measured changes should be verified to identify any reactions depending on a limited supply of reactants, such as antioxidants. Such reactions may dominate the observed aging or breakdown behavior at first, but as their supply runs out the main aging and degradation mechanisms may change. It is recommended that the possibility of such reactions is either ruled out or verified before any definite conclusions are made. Possible methods to measure these changes include FTIR, or in case of very low concentrations high performance liquid chromatography (HPLC).

As a final consideration regarding accelerated aging tests the measured sample areas should be large enough to capture the possible weak spots diverting from the main distribution. The intrinsic breakdown strength of RER film showed little variations, and the conclusions based on the intrinsic behavior alone neglecting the separate defect population would have been entirely different. After all with a small measured area the possibility of a weak spot subpopulation going unnoticed is high. On the other hand for NPO30 even smaller active areas would have been enough, as the weak spots followed the main distribution.

6.5 Future work

The thermal aging experiment was successfully used to determine the material-specific characteristic progression of the dielectric breakdown strength. Based on the characteristic behavior a transition temperature of 70…90°C was determined, which sets limit for thermal stresses in any further aging experiments. The next step in providing a test environment mimicking the conditions found in practical capacitors is the addition of an electric field induced stress. This new test system could be based on the on the pre-existing oven.

This experiment utilized samples areas of 486cm^2, which although larger than those used in traditional small-sample measurements was not extensive enough to verify whether or not the disappearance of weak spots in RER film was a result from stochastic variations. Therefore the next generation measurement system should utilize even larger measured areas. To reduce the possibility of mishandling induced damage the future breakdown measurement should be conducted in situ after the aging cycle, utilizing the same electrodes used in facilitating the electric field stress. An artists' vision of the next generation measurement system is depicted in Figure 6.16. The system can be designed to fit in the pre-existing oven. Glass plates could be used to sandwich ever larger film stacks than those used in MultiBreak measurements. With the use of self-healing metallized film electrodes the measurement system could withstand multiple breakdowns. Also the final breakdown performance characterization could be conducted utilizing the same electrodes, and unnecessary handling-induced mechanical stresses would be avoided.

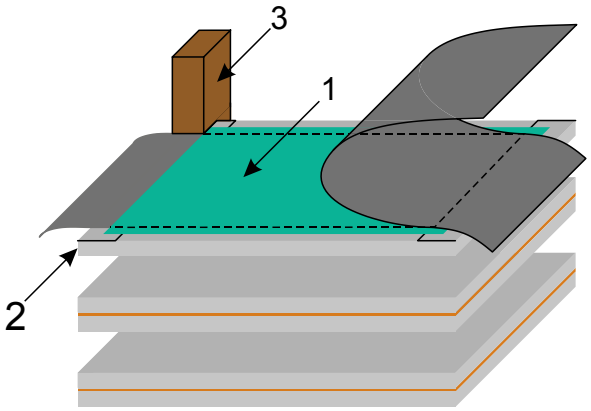

Figure 6.16. Advanced aging system utilizing combined thermoelectrical stresses. Outline: 1: Film stack consisting of test film and metallized foil electrodes, 2: Glass support plates, 3: Temperature resistant frame, milled with plate holding gaps.

The role of the antioxidants in the changes in the breakdown behavior should be verified, for example with methods mentioned in Subchapter 6.4.3. If the disappearance of the defect population was a result from the transformation of the antioxidants, controlled thermal stresses can be seen as a way to improve the properties of insulating thin films.

The previously described thermoelectric aging system utilizing large film areas would offer the industry a new and innovative way to characterize the properties of novel dielectrics. Although short-time measurements for novel types of dielectrics have been promising, the long-term properties of any would-be dielectrics needs to be verified before said materials can be regarded suitable for capacitor applications where life expectancies up to several decades are common.

7. SUMMARY

The purpose of this thesis was to review the aging of polymer thin films used in capacitor insulation systems. The research subject was approached in the form of a literature review and an empirical part. The literature review is divided into Chapters 2-4. Chapter 2 begins with the introduction to basic polymer chemistry, expanding into the multiple structural layers perceived in actual polymers. Concepts such as configuration, conformation and morphology were discussed, in addition to the manufacturing processes used to produce capacitor grade thin films. Changes in any of these structural layers may result in different dielectric properties. The electrical properties of polymers are discussed Chapter 3. Band gap theory was reviewed as the reason behind the insulating nature of polymers, and the discussion continued into the stochastic and physiological nature of dielectric breakdowns. Finally, practical capacitor applications and recent trends to develop materials with superior properties were reviewed. Chapter 4 evaluated the aging and degradation mechanisms relevant to capacitor applications. The progression of aging mechanisms limits the service lives of actual insulation systems, and both stochastic model-oriented and physiological viewpoints were considered.

The objective in the empirical part of this thesis was to conduct an accelerated thermal aging experiment for SiO_2-BOPP nanocomposite and various capacitor- and pilot-scale BOPP thin films. The experiment itself is depicted in Chapter 5. The test films were aged in a purpose tailored oven, and inert nitrogen was used to inhibit redox activity not relevant to hermetically sealed oxygen-free capacitors. The test spanned 1008 hours, during which the test films were subjected to temperatures from 50 to 110°C. 144 hour steps were used, after which the temperature was increased in 10°C increments. The breakdown behavior of the test films was measured after each step to assess the possibility of multiple temperature-dependent reactions. The DBS measurements utilized a test area of 486cm^2, made possible by a novel MultiBreak test method. By taking advantage of the self-healing capability of metallized film electrodes, and with the help of a two-phase discharge energy and incremental voltage -based selection criteria, an average of 90 breakdowns was recorded from each material after every step. The amount of breakdowns recorded was substantially higher that what is common for traditional small-area breakdown measurements.

Weibull statistical analysis was used to assess the breakdown data. To reach a visually and mathematically best fit one- or two-subpopulation Weibull distributions were applied, based on which the 5%, 63.2% and 95% percentiles were calculated. Statistical analysis revealed the formation of a distinct defect subpopulation in all pure

PP materials after 50…70°C. Based on literature sources the defect population was suggested result from locally occurring aging. On the other hand, no defect population was measured in case of the SiO_2-nanocomposite, but instead an increased scatter in the breakdown voltages was measured towards higher temperatures. Based on literature sources this was suggested to be a sign of different aging mechanisms, as aging of nanocomposites is suggested to occur in the nanoparticle-polymer interface which spans throughout the material. The behavior of the pure PP materials changed drastically after being subjected to 100…110°C, as after that no weak spots were measured.

The apparent disappearance of the weak spot subpopulation was reckoned to result from either the stochastic nature of breakdown phenomena, or from a separate process presumably activated by the higher temperatures. A number of possible explanations were given, such as antioxidant conversion and morphological changes linked to relaxation of built-in stresses. Antioxidant conversion has been linked with increased dielectric breakdown strength [26], and the relationship between morphological changes and breakdown behavior is well-founded, but additional research is needed to clarify to issue. Moreover it was considered probable that even in if the disappearance of the weak spots was a result from a high temperature process, the improvement would be temporary, and especially in case of antioxidant conversion the positive effect would end as soon as its supply of reactants was depleted. In this case a continuing exposure to high temperatures may accelerate other aging reactions. This was considered as one possible reason behind the appearance of individual weak spots diverting from the Weibull probability line measured after the films were subjected to high temperatures.

The implications of the thesis are that first of all any accelerated aging experiments utilizing traditional BOPP films should be conducted at moderate temperatures, preferably in the range of 60…65°C. This is to limit the mechanisms to those relevant to practical capacitor applications, as the measurement results hinted towards different mechanisms at higher temperatures. SiO_2-BOPP nanocomposites in turn may be evaluated at higher temperatures, since the breakdown behavior followed the trend set at the lower temperatures. Moreover the possibility of reactant-dependent mechanisms should be verified. If such mechanisms exist, they may affect the aging progression at first by slowing down the initial aging reactions. If such reactions are ignored, the predicted insulation lifetimes may be overly optimistic. Finally, it may be possible improve the dielectric breakdown strength of BOPP thin films by controlled heat treatment after manufacturing. If so, the already existing forming cycles may be improved, or additional heat treatment should be considered as means to gain improved dielectric breakdown strength with relatively minor investments.

Based on the results it was suggested that further research work should be conducted to verify the factors behind the measured disappearance of weak spots. Moreover given that practical capacitor insulation systems are subjected to combined thermoelectric stresses, its long-term effects especially on novel dielectrics, such as nanocomposites, should be examined in greater detail. Moreover the long-term properties of processing

additives and antioxidants are relatively unknown, and further research is needed to verify their effects.

REFERENCES

[1] J. K. Nelson, *Dielectric Polymer Nanocomposites*. Springer US, 2010.

[2] H. Ranta, I. Rytöluoto, K. Lahti, M. Karttunen, H. Joki, T. Munter, M. Koponen, M. Pettersson, S. Virtanen, and E. Arola, "Novel Polymer Nanocomposites for Power Capacitors (NANOPOWER), Final Report," 2014.

[3] K. G. Harutun, Ed., *Handbook of Polypropylene and Polypropylene Composites, Revised and Expanded*. CRC Press, 2003.

[4] S. W. Rowe, "Electrical Ageing of Composites: An Industrial Perspective," in *Solid Dielectrics, 2007. ICSD '07. IEEE International Conference on*, 2007, pp. 401–406.

[5] D. Cangialosi, V. M. Boucher, A. Alegría, and J. Colmenero, "Enhanced physical aging of polymer nanocomposites: The key role of the area to volume ratio," *Polymer (Guildf).*, vol. 53, no. 6, pp. 1362–1372, Mar. 2012.

[6] V. M. Boucher, D. Cangialosi, A. Alegrìa, J. Colmenero, J. González-Irun, and L. M. Liz-Marzan, "Physical aging in PMMA/silica nanocomposites: Enthalpy and dielectric relaxation," *J. Non. Cryst. Solids*, vol. 357, no. 2, pp. 605–609, Jan. 2011.

[7] R. Peetz, J. A. Manson, T. J. Romack, and J. M. DeSimone, "'Polymerization.' AccessScience. McGraw-Hill Education," 2014. [Online]. Available: http://www.accessscience.com/content/polymerization/535300. [Accessed: 16-Sep-2014].

[8] A. Rudin, *Elements of Polymer Science and Engineering*, Second Edi. Elsevier, 1999.

[9] M. Chanda and S. K. Roy, *Plastics technology handbook*. CRC Press, 2006.

[10] "American Chemical Society National Historic Chemical Landmarks. Foundations of Polymer Science: Wallace Carothers and the Development of Nylon." [Online]. Available: http://www.acs.org/content/acs/en/education/whatischemistry/landmarks/carotherspolymers.html . [Accessed: 09-Nov-2014].

[11] L. H. Sperling, *Introduction of Physical Polymer Science*, Fourth Edi. Hoboken, New Jersey: Wiley-Interscience, 2006.

[12] H. D. Young and R. A. Freedman, *University Physics with Modern Physics 11th edition*, 11th ed. San Francisco, CA: Pearson Addison-Wesley, 2003.

[13] Dynalab Corp, "Plastic Properties of Acrylonitrile Butadiene Styrene (ABS)." [Online]. Available: http://www.dynalabcorp.com/technical_info_abs.asp. [Accessed: 09-Nov-2014].

[14] T. L. Richardson and E. Lokensgard, *Industrial Plastics: Theory and Applications*. Thomson Delmar Learning, 2004.

[15] J. Seppälä, *Polymeeriteknologian perusteet*. Helsinki: Otatieto, 2005.

[16] L. Dissado and J. C. Fothergill, *Electrical degradation and breakdown in polymers*. Peter Peregrinus Ltd., 1992.

[17] K. Ziegler, "Consequences and development of an invention*." Nobelprize.org. Nobel Media AB 2014., 1963.

[18] A. . Vaughan, Y. Zhao, L. . Barré, S. . Sutton, and S. . Swingler, "On additives, morphological evolution and dielectric breakdown in low density polyethylene," *Eur. Polym. J.*, vol. 39, no. 2, pp. 355–365, Feb. 2003.

[19] S. N. Kolesov, "The Influence of Morphology on the Electric Strength of Polymer Insulation," *Electrical Insulation, IEEE Transactions on*, vol. EI-15, no. 5. pp. 382–388, 1980.

[20] M. Yanagiwara, F. Z. Huai, and N. Yoshimura, "Effect of spherulites on water-tree in polypropylene," in *Properties and Applications of Dielectric Materials, 1994., Proceedings of the 4th International Conference on*, 1994, vol. 1, pp. 436–439 vol.1.

[21] A.-B. Elsayed, Ed., *Handbook of Plastic Films*. Smithers Rapra Technology, p. 2000.

[22] D. H. Gracias, D. Zhang, L. Lianos, W. Ibach, Y. R. Shen, and G. A. Somorjai, "A study of the glass transition of polypropylene surfaces by sum-frequency vibrational spectroscopy and scanning force microscopy," *Chem. Phys.*, vol. 245, no. 1–3, pp. 277–284, Jul. 1999.

[23] Tervakoski Films, "Tervakoski Film RER," 2008. [Online]. Available: http://www.tervakoskifilm.com/index.php?id=454626b5bb117. [Accessed: 16-Apr-2014].

[24] S. Talapatra and A. Kulshreshtha, "Competitive New Technologies in Polyolefin Synthesis and Materials," in *Handbook of Polyolefins*, CRC Press, 2000.

[25] J. Ho, R. Ramprasad, and S. Boggs, "Effect of alteration of antioxidant by UV treatment on the dielectric strength of BOPP capacitor film," *IEEE Trans. Dielectr. Electr. Insul.*, vol. 14, no. 5, pp. 1295–1301, 2007.

[26] J. Ho and S. Boggs, "Effect of UV treatment on the dielectric strength of BOPP capacitor film," in *Electrical Insulation, 2006. Conference Record of the 2006 IEEE International Symposium on*, 2006, pp. 314–317.

[27] J. Ho and T. R. Jow, "Effect of crystallinity and morphology on dielectric properties of PEEK at elevated temperature," in *Solid Dielectrics (ICSD), 2013 IEEE International Conference on*, 2013, pp. 385–388.

[28] T. Blythe and D. Bloor, *Electrical Properties of Polymers*. New York: Cambridge University Press, 2005.

[29] F. Kremer and S. Andreas, *Broadband Dielectric Spectroscopy*. Berlin: Springer, 2003.

[30] J.-K. Tseng, S. Tang, Z. Zhou, M. Mackey, J. M. Carr, R. Mu, L. Flandin, D. E. Schuele, E. Baer, and L. Zhu, "Interfacial polarization and layer thickness effect on electrical insulation in multilayered polysulfone/poly(vinylidene fluoride) films," *Polymer (Guildf).*, vol. 55, no. 1, pp. 8–14, Jan. 2014.

[31] M. Aro, J. Elovaara, M. Karttunen, K. Nousiainen, and V. Palva, *Suurjännitetekniikka*. Jyväskylä: Otatieto, 2011.

[32] D. M. Pozar, *Microwave Engineering Fourth Edition*. Wiley, 2011.

[33] P-N Designs Inc., "Capacitors," 2012. [Online]. Available: http://www.microwaves101.com/encyclopedia/capacitors.cfm. [Accessed: 07-May-2014].

[34] G. Chen and J. Zhao, "Space charge and thickness dependent dc electrical breakdown of solid dielectrics," in *High Voltage Engineering and Application (ICHVE), 2012 International Conference on*, 2012, pp. 12–15.

[35] W. J. Sarjeant, "Capacitor fundamentals," in *Electrical Electronics Insulation Conference, 1989. Chicago '89 EEIC/ICWA Exposition., Proceedings of the 19th*, 1989, pp. 1–51.

[36] S. Ul-Haq and G. R. G. Raju, "Weibull statistical analysis of area effect on the breakdown strength in polymer films," *Annu. Rep. Conf. Electr. Insul. Dielectr. Phenom.*, pp. 518–521, 2002.

[37] IEC, "International standard IEC 60243-1, Part 1: Tests at power frequencies. Edition 3.0." 2013.

[38] J. Kotiniitty, "Discussion," 2014.

[39] IEC, "International standard IEC 60243-2 Part 2, Electric strength of insulating materials – Test methods – Part 2: Additional requirements for tests using direct voltage, Second edition." 2001.

[40] IEC, "CEI IEC TS 60871-2 Technical Spesification,Shunt capacitors for a.c. power systems having a rated voltage above 1 000 V – Part 2: Endurance testing." 1999.

[41] "IEC/IEEE Guide for the Statistical Analysis of Electrical Insulation Breakdown Data (Adoption of IEEE Std 930-2004)," *IEC 62539 First Edition 2007-07 IEEE 930*. pp. 1–53, 2007.

[42] M. A. Schneider, J. R. MacDonald, M. C. Schalnat, and J. B. Ennis, “Electrical breakdown in capacitor dielectric films: Scaling laws and the role of self-healing,” in *Power Modulator and High Voltage Conference (IPMHVC), 2012 IEEE International*, 2012, pp. 284–287.

[43] S. J. Laihonen, U. Gafvert, T. Schutte, and U. W. Gedde, “Influence of electrode area on dielectric breakdown strength of thin poly(ethylene terephthalate) films [power capacitor applications],” in *Electrical Insulation and Dielectric Phenomena, 2004. CEIDP ’04. 2004 Annual Report Conference on*, 2004, pp. 563–567.

[44] I. Rytöluoto, K. Lahti, M. Karttunen, and M. Koponen, “Large-Area Dielectric Breakdown Performance of Polymer Films – Part I: Measurement Method Evaluation and Statistical Considerations on Area-Dependence,” *[Under Rev.*, 2014.

[45] I. Rytöluoto, K. Lahti, M. Karttunen, and M. Koponen, “Large-Area Dielectric Breakdown Performance of Polymer Films – Part II: Interdependence of Filler Content, Processing and Breakdown Performance in Polypropylene-Silica Nanocomposites,” *[Under Rev.*, 2014.

[46] *Springer Handbook of Engineering Statistics*. Würzburg: Springer London, 2006.

[47] S. J. Laihonen, A. Gustafsson, U. Gafvert, T. Sch??tte, and U. W. Gedde, “Area dependence of breakdown strength of polymer films: Automatic measurement method,” *IEEE Trans. Dielectr. Electr. Insul.*, vol. 14, no. 2, pp. 263–274, 2007.

[48] R. Ross, “Graphical methods for plotting and evaluating Weibull distributed data,” in *Proceedings of 1994 4th International Conference on Properties and Applications of Dielectric Materials (ICPADM)*, 1994, vol. 1, pp. 250–253.

[49] ReliaSoft Corporation, “Life Data Analysis Reference Book.” [Online]. Available: http://reliawiki.org/index.php/Life_Data_Analysis_Reference_Book. [Accessed: 26-Mar-2014].

[50] W. R. Blischke and D. N. P. Murthy, *Reliability: Modeling, Prediction, and Optimization*. Wiley, 2011.

[51] W. Hauschild and W. Moss, *Statistic Techniques for High Voltage Engineering*. London: Peter Peregrinus Ltd., 1992.

[52] C. Xu, J. Ho, and S. A. Boggs, “Automatic breakdown voltage measurement of polymer films,” *IEEE Electr. Insul. Mag.*, vol. 24, no. 6, pp. 30–34, 2008.

[53] S. J. Laihonen, U. Gafvert, T. Schutte, and U. W. Gedde, “DC breakdown strength of polypropylene films: Area dependence and statistical behavior,” *IEEE Trans. Dielectr. Electr. Insul.*, vol. 14, no. 2, pp. 275–286, 2007.

[54] S. Diaham, S. Zelmat, M. L. Locatelli, S. Dinculescu, M. Decup, and T. Lebey, “Dielectric breakdown of polyimide films: Area, thickness and temperature

dependence," *IEEE Trans. Dielectr. Electr. Insul.*, vol. 17, no. 1, pp. 18–27, 2010.

[55] I. Rytoluoto and K. Lahti, "New approach to evaluate area-dependent breakdown characteristics of dielectric polymer films," *Dielectr. Electr. Insul. IEEE Trans.*, vol. 20, no. 3, pp. 937–946, 2013.

[56] Nichicon, "Electric double layer capacitors 'EVerCAP®,'" 2014. [Online]. Available: http://fi.mouser.com/Nichicon/. [Accessed: 26-Jun-2014].

[57] M. Rabuffi and G. Picci, "Status quo and future prospects for metallized polypropylene energy storage capacitors," *IEEE Trans. Plasma Sci.*, vol. 30, no. 5 I, pp. 1939–1942, 2002.

[58] Murata, "The Effect of Non ideal Capacitors." [Online]. Available: http://www.murata.com/products/emc/knowhow/pdf/12to14.pdf. [Accessed: 03-Jun-2014].

[59] A. Nishino, "Capacitors: operating principles, current market and technical trends," *J. Power Sources*, vol. 60, no. 2, pp. 137–147, Jun. 1996.

[60] J. Ho, T. R. Jow, and S. Boggs, "Historical introduction to capacitor technology," *IEEE Electr. Insul. Mag.*, vol. 26, no. 1, pp. 20–25, 2010.

[61] S. A. Boggs, J. Ho, and T. R. Jow, "Overview of laminar dielectric capacitors," *IEEE Electr. Insul. Mag.*, vol. 26, no. 2, pp. 7–13, 2010.

[62] H. Ranta, "Interview with M.Sc. researcher at ex Nokian Capacitors," 2014.

[63] D. Shaw, S. Cichanowski, and A. Yializis, "A Changing Capacitor Technology - Failure Mechanisms and Design Innovations," *IEEE Trans. Electr. Insul.*, vol. EI-16, no. 5, pp. 399–413, 1981.

[64] C. W. Reed and S. W. Cichanowski, "Fundamentals of aging in HV polymer-film capacitors," *IEEE Trans. Dielectr. Electr. Insul.*, vol. 1, no. 5, pp. 904–922, 1994.

[65] B. Drugge, H. Fuhrmann, S. Laihonen, and J. Mood, "DryQ –Dry and silent." ABB.

[66] X. Qi and S. Boggs, "Analysis of the effects of end connection quality on the dielectric loss of metallized film capacitors," *Dielectr. Electr. Insul. IEEE Trans.*, vol. 11, no. 6, pp. 990–994, 2004.

[67] E. Kuffel, W. . Zaengl, and J. Kuffel, *High Voltage Engineering Fundamentals*. Elsevier, 2000, p. 534.

[68] Y. Chen, H. Li, F. Lin, F. Lv, M. Zhang, Z. Li, and D. Liu, "Study on Self-Healing and Lifetime Characteristics of Metallized-Film Capacitor Under High Electric Field," *Plasma Sci. IEEE Trans.*, vol. 40, no. 8, pp. 2014–2019, 2012.

[69] S. Krisna, *Handbook of Thin Film Deposition Processes and Techniques (Second Edition)*. San Jose: Elsevier, 2001.

[70] D. K. Schroder, *Semiconductor Material and Device Characterization: Third Edition*. John Wiley and Sons, 2005, pp. 1–779.

[71] R. J. Flanagan, R. G. Conners, and R. C. Merrill, "Partially impregnated capacitor," 3,987,348, 1976.

[72] J. H. Tortai, A. Denat, and N. Bonifaci, "Self-healing of capacitors with metalized film technology: Experimental observations and theoretical model," *J. Electrostat.*, vol. 53, no. 2, pp. 159–169, 2001.

[73] S. Qin, S. Ma, and S. A. Boggs, "The mechanism of clearing in metalized film capacitors," in *Electrical Insulation (ISEI), Conference Record of the 2012 IEEE International Symposium on*, 2012, pp. 592–595.

[74] W. J. Sarjeant, I. W. Clelland, and R. A. Price, "Capacitive components for power electronics," in *Proceedings of the IEEE*, 2001, vol. 89, no. 6, pp. 846–855.

[75] I. Rytöluoto, "Discussion with doctoral student and researcher in Tampere University of Technology." 2014.

[76] T. Rinne, "Metalloitujen ohutkalvokondensaattoreide ominaisuudet tasajännitteellä," Tampere University of Technology, 2011.

[77] A. Schneuwly, P. Gröning, and L. Schlapbach, "Uncoupling behaviour of current gates in self healing capacitors," *Mater. Sci. Eng. B*, vol. 55, no. 3, pp. 210–220, Sep. 1998.

[78] I. Rytoluoto and K. Lahti, "Effect of inter-layer pressure on dielectric breakdown characteristics of metallized polymer films for capacitor applications," in *Solid Dielectrics (ICSD), 2013 IEEE International Conference on*, 2013, pp. 682–687.

[79] Y. Wang, X. Zhou, Q. Chen, B. Chu, and Q. Zhang, "Recent development of high energy density polymers for dielectric capacitors," *Dielectr. Electr. Insul. IEEE Trans.*, vol. 17, no. 4, pp. 1036–1042, 2010.

[80] C. C. Wang, G. Pilania, S. A. Boggs, S. Kumar, C. Breneman, and R. Ramprasad, "Computational strategies for polymer dielectrics design," *Polymer (Guildf).*, vol. 55, no. 4, pp. 979–988, Feb. 2014.

[81] H. Ranta, I. Rytöluoto, K. Kannus, M. Karttunen, H. Joki, T. Munter, M. Koponen, M. Petterson, S. Virtanen, and E. Arola, "Novel Polymer Nanocomposites for Power Capacitors (NANOPOWER), Progess Report II," Tampere.

[82] H. Ranta, I. Rytöluoto, K. Kannus, M. Karttunen, H. Joki, T. Munter, M. Koponen, M. Pettersson, S. Virtanen, and E. Arola, "Novel Polymer

Nanocomposites for Power Capacitors (NANOPOWER), Progess Report III," Tampere, 2012.

[83] H. Ranta, I. Rytöluoto, K. Kannus, M. Karttunen, M. Koponen, S. Virtanen, and E. Arola, "Novel Polymer Nanocomposites for Power Capacitors (NANOPOWER), Progess Report IV," Tampere, 2013.

[84] C. J. Cramer, *Essentials of Computational Chemistry: Theories and Models*, vol. 2004. Wiley, 2004, p. 618.

[85] H. Ruuska, E. Arola, K. Kannus, T. T. Rantala, and S. Valkealahti, "Feasibility of density functional methods to predict dielectric properties of polymers," *J. Chem. Phys.*, vol. 128, no. 6, 2008.

[86] C. Green and A. Vaughan, "Nanodielectrics - How much do we really understand?," *IEEE Electr. Insul. Mag.*, vol. 24, no. 4, pp. 6–16, 2008.

[87] T. Tanaka, "Dielectric nanocomposites with insulating properties," in *IEEE Transactions on Dielectrics and Electrical Insulation*, 2005, vol. 12, no. 5, pp. 914–928.

[88] I. Rytöluoto, "Application of polypropylene nanocomposites in metallized film capacitors under DC voltage," Tampere University of Technology, 2011.

[89] D. M. Rock, X. Tan, N. Bowler, and M. R. Kessler, "Dielectric and mechanical properties of polyimide-barium titanate nanocomposites," in *Electrical Insulation and Dielectric Phenomena (CEIDP), 2012 Annual Report Conference on*, 2012, pp. 912–915.

[90] T. J. Lewis, "Nanometric dielectrics," *Dielectr. Electr. Insul. IEEE Trans.*, vol. 1, no. 5, pp. 812–825, 1994.

[91] T. Tanaka, M. Kozako, N. Fuse, and Y. Ohki, "Proposal of a multi-core model for polymer nanocomposite dielectrics," *IEEE Trans. Dielectr. Electr. Insul.*, vol. 12, no. 4, pp. 669–681, 2005.

[92] M. Takala, "Electrical Insulation Materials towards Nanodielectrics," Tampere University of Technology, 2010.

[93] J. C. Fothergill, "Ageing, Space Charge and Nanodielectrics: Ten Things We Don't Know About Dielectrics," in *Solid Dielectrics, 2007. ICSD '07. IEEE International Conference on*, 2007, pp. 1–10.

[94] J. Lu, "High Dielectric Constant Polymer Nanocomposites for Embedded Capacitor Applications," Georgia Institute of Technology, 2008.

[95] G. C. Montanari and L. Simoni, "Aging phenomenology and modeling," *Electr. Insul. IEEE Trans.*, vol. 28, no. 5, pp. 755–776, 1993.

[96] H. Ranta, “Long-term electrical properties of polypropylene nanocomposites for high voltage capacitor applications,” Tampere University of Technology, 2008.

[97] G. Mazzanti, G. C. Montanari, and L. A. Dissado, “Elemental strain and trapped space charge in thermoelectrical aging of insulating materials: life modeling,” *Dielectr. Electr. Insul. IEEE Trans.*, vol. 8, no. 6, pp. 966–971, 2001.

[98] J. P. Jones, J. P. Llewellyn, and T. J. Lewis, “The contribution of field-induced morphological change to the electrical aging and breakdown of polyethylene,” *Dielectr. Electr. Insul. IEEE Trans.*, vol. 12, no. 5, pp. 951–966, 2005.

[99] J.-P. Crine, C. Dang, and J.-L. Parpal, “Electrical aging of extruded dielectric cables: a physical model,” in *Electrical Insulation, 1996., Conference Record of the 1996 IEEE International Symposium on*, 1996, vol. 2, pp. 646–649 vol.2.

[100] D. B. E. Bowler, D. W. R. Ellis Jr., D. H. B. Gray, and D. T. J. Meade, “Electron-transfer reaction.” [Online]. Available: http://www.accessscience.com/content/electron-transfer-reaction/224950. [Accessed: 16-Jul-2014].

[101] D. J. Vaya and D. L. Packer, “Antioxidant.” [Online]. Available: http://www.accessscience.com/content/antioxidant/041500. [Accessed: 16-Jul-2014].

[102] A. Andreyev, M. Jevtić, and N. Zhuravleva, “Ageing of impregnating liquids with different chemical structure for polypropylene capacitor dielectric,” *Electr. Eng.*, vol. 85, no. 2, pp. 83–85, 2003.

[103] ReliaSoft Corporation, “Accelerated Life Testing Data Analysis Reference,” 2014. [Online]. Available: http://reliawiki.com/index.php/Accelerated_Life_Testing_Data_Analysis_Reference. [Accessed: 26-Mar-2014].

[104] V. M. Montsinger, “Loading Transformers By Temperature,” *Am. Inst. Electr. Eng. Trans.*, vol. 49, no. 2, pp. 776–790, 1930.

[105] M. Celina, K. T. Gillen, and R. A. Assink, “Accelerated aging and lifetime prediction: Review of non-Arrhenius behaviour due to two competing processes,” *Polym. Degrad. Stab.*, vol. 90, no. 3, pp. 395–404, Dec. 2005.

[106] P. Richters, “Initiation Process in the Oxidation of Polypropylene,” *Macromolecules*, vol. 3, no. 2, pp. 262–264, Mar. 1970.

[107] F. Gugumus, “Effect of temperature on the lifetime of stabilized and unstabilized PP films,” *Polym. Degrad. Stab.*, vol. 63, no. 1, pp. 41–52, Jan. 1999.

[108] Aerosil, “AEROSIL ® R 812 S Hydrophobic fumed silica Product Information,” 2014. [Online]. Available: https://www.aerosil.com/lpa-productfinder/page/productsbytext/detail.html?pid=1832. [Accessed: 09-Sep-2014].

[109] Borealis, "Borclean™ HC318BF," 2007. [Online]. Available: http://www.borealisgroup.com/en/polyolefins/products/Borclean/Borclean-HC318BF/. [Accessed: 09-Sep-3025].

[110] BASF, "Technical Information, Plastic Additives: Irganox ® 1010," 2010. [Online]. Available: http://www.telko.com/files/images/telko/ru/basf/termostabilizator/irganox_1010_tds.pdf. [Accessed: 09-Sep-2014].

[111] Ciba Inc, "Ciba ® IRGAFOS ® 168," 2009. [Online]. Available: http://www.telko.com/files/images/telko/ru/basf/termostabilizator/irgafos_168_tds.pdf. [Accessed: 09-Sep-2014].

[112] Tervakoski Films, "Tervakoski Film RERS," 2008. [Online]. Available: http://www.tervakoskifilm.com/index.php?id=45463086a517c&lang=en. [Accessed: 11-Sep-2014].

[113] I. Rytöluoto and K. Lahti, "Effect of Film Thickness and Electrode Area on the Dielectric Breakdown Characteristics of Metallized Capacitor Films," in *Nordic Insulation Symposium*, 2013, pp. 33–38.

[114] Folex, "X-10.0 Product Datasheet," 2014. [Online]. Available: http://www.folex.com/htm/580/en/X-10-0.htm?Article=47670. [Accessed: 10-Sep-2014].

[115] Tervakoski Films, "Tervakoski Film PSX," 2007. [Online]. Available: http://www.tervakoskifilm.com/index.php?id=45464991918ff&lang=en. [Accessed: 11-Sep-2014].

[116] MeasureItAll, "LE1000-1 Bench Top Contact Thickness Gauge." [Online]. Available: http://www.measureitall.com/overview/le1/index.html. [Accessed: 25-Sep-2014].

[117] Spellman High Voltage Electronics Corporation, "Spellman SL Series High Voltage Power Supply Instruction Manual." 2013.

[118] Maxim Integrated, "DS18B20 Programmable Resolution 1-Wire Digital Thermometer, datasheet," 2011. [Online]. Available: http://www.maximintegrated.com/en/products/analog/sensors-and-sensor-interface/DS18B20.html. [Accessed: 23-Sep-2014].

[119] H. H. Sisler, "'Nitrogen.' AccessScience. McGraw-Hill Education,."[Online]. Available: http://www.accessscience.com/content/nitrogen/453700. [Accessed: 22-Sep-2014].

[120] E. Valtanen, *Koneenrakentajan taulukkokirja*. Jyväskylä: Teknolit OY, 1994.

APPENDIX A: TEST OVEN

Figure A.1. Test oven used for the aging experiment. The tempered double glass window was used to monitor the condition of the samples during aging.

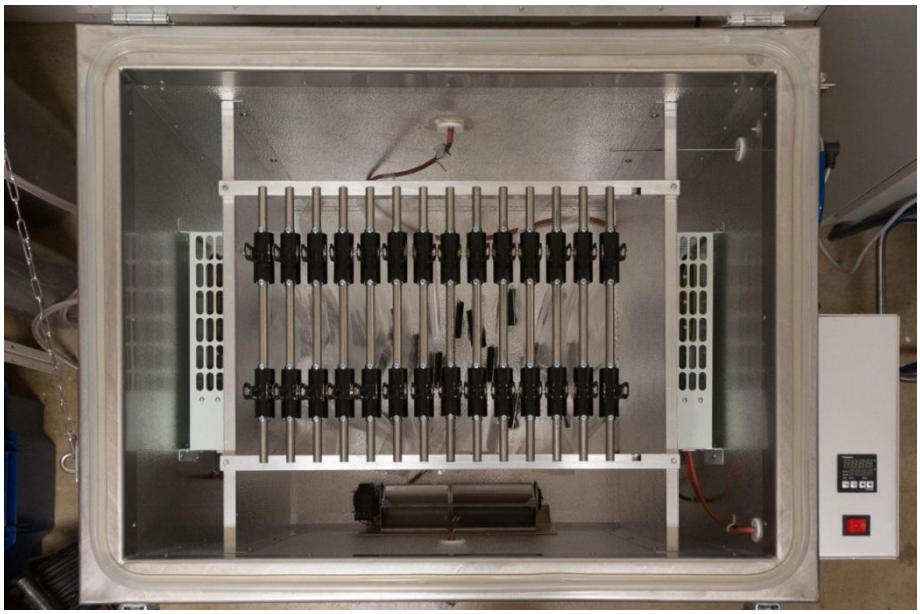

Figure A.2. Top view of the test oven moments before the actual test cycle began. The lid is still open and the 14 sample holders with film samples are visible. The fan speed was adjusted to prevent excessive fluttering.

APPENDIX B: MULTIBREAK MEASUREMENT

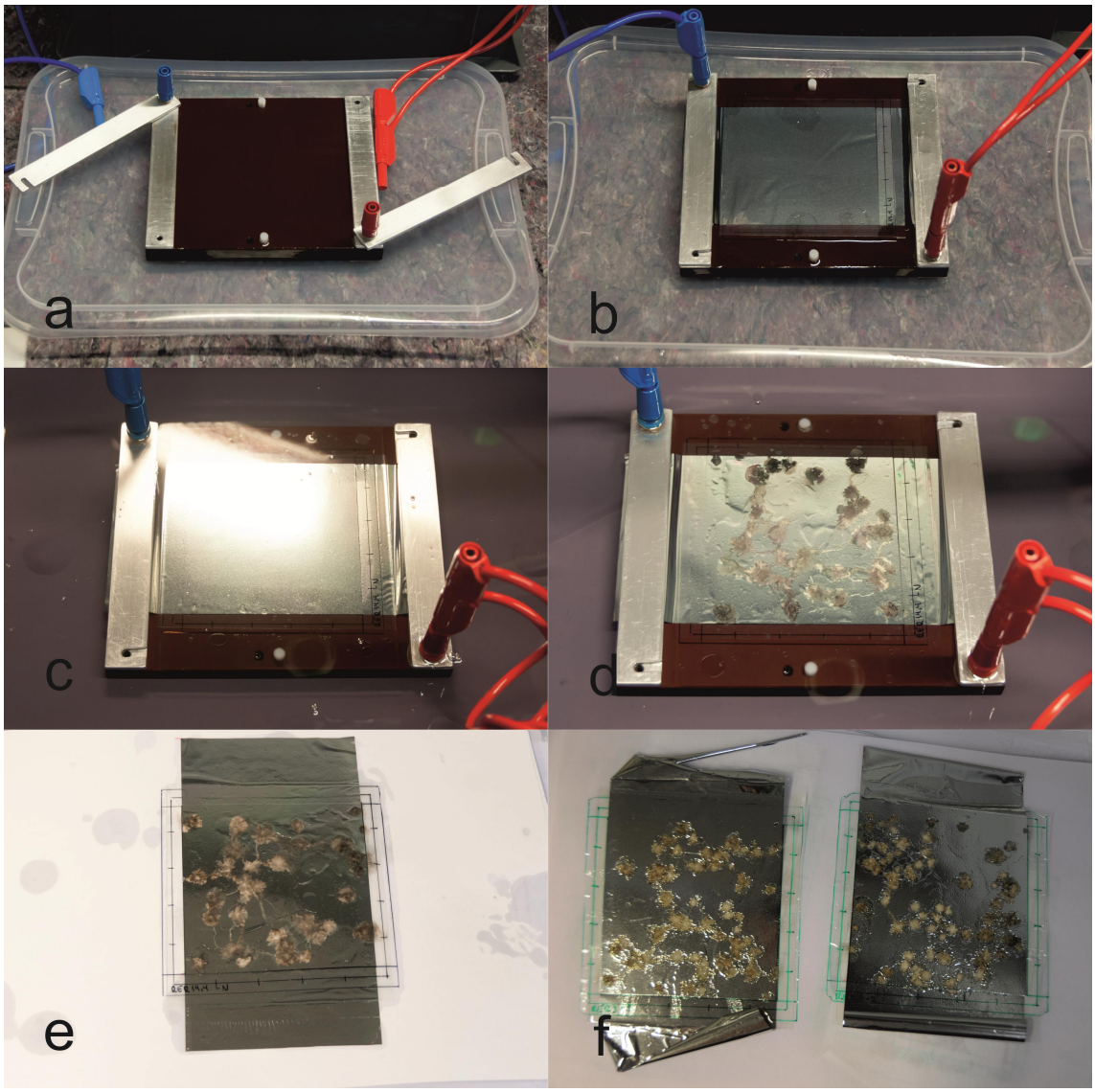

Figure B.1. Visual description of the MultiBreak measurement method. (a) Test bench with acrylic top plate removed, (b) ready for pre-ramp; test bench with sample in place, (c) ready for actual measurement; test bench (top cover in place) submerged in dielectric oil, (d) after measurement; the test films has experienced multiple self-healing breakdowns, (e) film removed from test bench, (f) additional examples of test films from MultiBreak measurements.